Consequences of the '*Legs at odd angles*' mutation within the motor protein dynein and its possible implications in neurological disease

Caroline Alice Garrett

Doctor of Philosophy in Biochemistry

University of Sussex

August 2012

Dedicated to my parents

Acknowledgements

There are four people that have played distinctly different, yet essential roles towards the completion of this thesis and these are the people I would like to thank wholeheartedly.

Majid Hafezparast is the person who offered me the fantastic opportunity to work under his supervision. From him I have learnt so much – practically, academically and personally. He has encouraged me to expand my ideas and has given me the freedom to do so. His support, time and trust have been unequivocal and for that I will be forever grateful.

The support given to me un-reservedly and un-conditionally from my parents is truly remarkable. They support me in every walk of my life, every day and by every means possible. I know that they would be pleased with any path I chose to take so long as I am happy, but I hope that this is a path for which they can be very proud.

Christopher Reeve (1952-2004) will never know the part he played in my life as he is not someone I ever met personally and sadly never will. He was a person that despite adversity, had optimism and belief in science that never wavered. It was Christopher who drew me to the fascinating world of scientific research, a world with many frustrations and uncertainties but one that is fascinating, awe-inspiring, enjoyable and challenging.

Thank you!

Work in this thesis was generously funded by the
Biotechnology and Biological Sciences Research Council

Chapter 1: Introduction Page

Publications

Deng W, **Garrett C**, Dombert B, Soura V, Banks G, Fisher EM, van der Brug MP & Hafezparast, M. (2010). Neurodegenerative mutation in cytoplasmic dynein alters its organization and dynein-dynactin and dynein-kinesin interactions. *J Biol Chem* 285, 39922-34

Crossley L, **Garrett CA,** Hafezparast M, Madzvamuse A (2012). From the cell membrane to the nucleus: Unearthing transport mechanisms for dynein. *Bull Math Biol* 74, 2032-2061

List of figures and tables **Page**

Figures

Tables

Abbreviations

AAA+	ATPases associatied with diverse cellular activity
AD	Alzheimer's disease
ADP	Adenosine diphosphate
ALS	Amyotrophic lateral sclerosis
AMP-PNP	Adenylyl-imidodiphosphate
ANOVA	Analysis of variance
AP	Adaptor or adaptin protein
AP	Alkaline phosphatase
AP-1	Activator protein 1
Arf6	ADP ribosylation factor 6
Arg	Arginine
Arl	*Abnormal rear legs*
ARP1	Actin related protein 1
ASK1	Apoptotic signal related kinase
Atg	Autophagy related genes
ATP	Adenosine triphosphate
ATPases	Adenosine triphosphatases
A-β	β-amyloid
Bar	Bin-amphiphysin-Rvs
Bcl2	B-cell lymphoma 2
BDNF	Brain derived neurotrophic factor
Bim	Bcl2 interacting mediator of cell death
BrdU	5-bromo-2'-deoxyuridine
BSA	Bovine serum albumin
$Ca2^{+}$	Calcium
CALM	Clathrin assembly lymphoid myeloid leukaemia protein
Cav 1, 2 3	Caveolin 1, 2 ,3
CCV	Clathrin coated vesicle

CLIC/GEEC	Clathrin-independent carrier/GPI-enriched endocytic compartment
CMA	Chaperone mediated autophagy
CMT	Charcot-Marie-Tooth
CNTF	Ciliary neurotrophic factor
CORVET	Class C core vacuole/endosome tethering complex
Cra1	*Cramping 1*
CT	Cycle threshold
C-terminus	Carboxy-terminal
Cu	Copper
Cys	Cysteine
DEPTOR	DEP domain-containing mTOR-interacting protein
DHC	Dynein heavy chain (*Dync1h1*)
DIC	Differential interference contrast
DIC	Dynein intermediate chain
DLC	Dynein light chain
DLIC	Dynein light intermediate chain
DRG	Dorsal root ganglia
DUSP	Dual specificity (serine/threonine/tyrosine) phosphatases
E	Embryonic day
E	Glutamic acid
EE	Early endosome
EGF	Epidermal growth factor
EGFR	EGF receptor
eIF4E	eukaryotic initiation factor 4E
eIF4E-BP	eIF4E-binding protein 1
ELK1	$p62^{TCF}$
ENU	N-ethyl-N-nitrosourea
ERK	Extracellular signal related kinase
ESCRT	Endosomal sorting complexes required for transport

F	Phenylalanine
FIP200	Family interacting protein
FIP3	Rab11 family interacting protein
FoxO	Forkhead box transcription factor
GAP	GTPase accelerating protein
GDF	GDI-displacement factors
GDI	GDP-dissociation inhibitor
GDNF	Glial cell derived neurotrophic factor
GEF	Guanine nucleotide exchange factor
GF	Growth factor
GFP	Green fluorescent protein
GGT	Geranylgeranyl transferase
Gly	Glycine
GRB2	Growth factor receptor-bound protein 2
GTP	Guanosine triphosphate
GβL	G-protein beta like
Hb9	Homeobox gene 9
HD	Huntington’s disease
HEPTP	Hematopoietic PTP
His	Histidine
hnulp	Human nulp (TCF25)
HOPS	Homotypic fusion and vacuole protein sorting
Hrs	Hepatocyte growth factor regulated tyrosine kinase
Hsp70	Heat shock protein 70
ID	Intellectual disability
IEG	Immediate early gene
IL2Rβ	Interleukin-2 receptor β
Ile	Isoleucine
ILV	Intraluminal vesicles

IMP	Impedes mitogenic signal propagation
JNK	c-Jun N-terminal kinase
K	Lysine
kDa	KiloDalton
KHC	Kinesin heavy chain
KLC	Kinesin light chain
KSR	Kinase suppressor of Ras
LBPA	Lysobisphosphatidic acid
LE	Late endosome
Leu	Leucine
LIS1	Protein of platelet-activating factor acetylhydrolase 1B α-subunit (*Pafah1b1)*
Loa	*Legs at odd angles*
Lys	Lysine
MAP	Mitogen activated protein
MAP2	Microtubule associated protein 2
MAP2K	MAP kinase kinase
MAP3K	MAP kinase kinase kinase
MAP4K	MAP kinase kinase kinase kinase
MAPK	MAP kinase
MDA	MegaDalton
MEK4	Stress activated protein kinase/extracellular signal related kinase kinase 1
MKP	MAPK phosphatase
MLST8	Mammalian lethal with SEC13 protein 8
MP1	MEK partner-1
MT	Microtubules
MTBD	MT binding domain
mTOR	Mammaliam target of rapamycin
MVB	Multivesicular bodies

Myb	Myeloblastosis family of transcription factors
NGF	Nerve growth factor
NTC	No template control
N-terminus	Amino-terminus
NUDE	Nuclear distribution protein E
NUDEL	NUDE-like
O/N	Overnight
$p75^{NTR}$	p75 Neurotrophic receptor
Pafah1b1	Platelet-activating acetylhydrolase 1B α subunit
PC12	Pheochromocytoma cells from a rat neuroendocrine tumour
PD	Parkinson's disease
p-ERK	Phospho-ERK
Phe	Phenylalanine
PI3K	Phosphatidylinositol 3-kinase
PIKK	Phosphatidylinositol kinase-related kinase
PKB	Protein kinase B
pN	PicoNewtons
PP2	Protein phosphatase 2
PRAS40	Proline-rich Akt substrate of 40 kDa
Pro	Proline
PRR5/Protor-1	Proline-rich repeat protein 5
PtdIns3P	Phosphatidylinositol-3-phosphate
PTP	Protein tyrosine phosphatases
PTRF	Polymerase 1 and transcript release factor
Q	Glutamine
qPCR	Quantitative real-time polymerase chain reaction
R	Arginine
R/T	Room temperature
RabGGT	Geranylgeranyl transferase

raptor	Regulatory associated protein of TOR
REP	Rab escort protein
Rheb	Ras homolog enriched in brain
rictor	Rapamycin-insensitive companion of mTOR
RILP	Rab7 interacting lysosomal protein
ROS	Reactive oxygen species
RSK	90K ribosomal S6 kinase
RTK	Receptor tyrosine kinase
S6K	S6 kinase beta-1
SAPK	Stress activating protein kinase
SDPR	Serum deprivation protein response
SEM	Standard error of the mean
Ser	Serine
SFK	Src family kinase
Sin1	SAPK-interacting protein-1
SiRNA	Small interfering RNA
SMA	Spinal muscular atrophy
SMA-LED	SMA with lower extremity predominance
SNARE	Soluble N-ethylmaleimide-sensitive factor attachment protein receptors
SOD1	Superoxide dismutase
SPRY	Sprouty
SRF	$p67^{SRF}$
STEP	Striatum-enriched PTP
Swl	*Sprawling*
TCF25	Transcription factor 25 (nulp1)
TDP43	Transactive response DNA-binding protein 43
TeNT H_c	Fluorescent fragment of the tetanus toxin
TGFα	Transforming growth factor α
Thr	Threonine

TPR	Tetratricopeptide repeats
TrkB	Tropomyosin-related kinase receptor type B
Trp	Tryptophan
Tyr	Tyrosine
ULK	Unc-51-like kinase
VAMP	Vesicle-associated membrane protein
VPS	Vacuole protein sorting
Zn	Zinc
λ-PP	λ-protein phosphatase

Abstract

Cytoplasmic dynein is a retrograde motor protein complex that carries cargo such as organelles and growth factors along microtubules from the cell periphery towards the peri-nuclear region.

The cytoplasmic dynein complex is centred around two homodimerised heavy chains, within which multiple mutations have been identified in human neurological diseases.

The ‘Legs at odd angles’ (*Loa*) mouse has a missense ‘T’ to ‘A’ point mutation in the cytoplasmic dynein heavy chain gene (*Dync1h1*), resulting in a phenylalanine to tyrosine substitution at position 580. Mice homozygous for this mutation die within 24 hours of birth whilst heterozygote’s manifest an age-related and progressive neurodegeneration.

Fixed and live-cell microscopy shows aberrant movement of endocytosed growth factors in *Loa.* Retrograde speed is reduced with a distinct lack of the fastest moving carriers. Moreover, the overall pattern of movement is altered with increased anterograde and side-steps occurring in *Loa.*

Impaired endosomal trafficking of growth factors for degradation prolongs the activation of extracellular signal related kinases 1 and 2 (ERK 1/2) and increases the expression of the immediate early gene *c-Fos* in mouse embryonic fibroblasts. Motor neurons also show increased levels c-Fos however this can be induced by starvation, indicating their enhanced susceptibility to stress.

The light chain (KLC) of dynein’s opposing motor - kinesin is one of many genes differentially expressed in *Loa* compared to wild-type. In addition, associations of KLC with the dynein complex is altered in *Loa*.

Similarities between human neurological diseases and *Loa* both at the organism and cellular level make *Loa* a valuable tool towards understanding cellular mechanisms fundamental to the process of disease. Through understanding comes advancement towards therapeutic targets to improve the lives of thousands of people worldwide.

Chapter 1

Introduction

1.1.1 Motor proteins

Efficient intracellular transport of organelles, endosomes and other vesicular structures is fundamental to morphogenesis as well as the everyday function and survival of the cell. There are three families of motor proteins that work co-operatively to achieve and maintain cellular homeostasis. Kinesins and Dyneins bind microtubules (MT) s and move mainly towards the plus end (anterograde) or minus end (retrograde) of microtubules respectively. Myosins bind actin and move predominantly in an anterograde direction.

1.1.2 Dynein families

Two families of dynein exist; cytoplasmic and axonemal. There are distinct differences between the two. Axonemal dynein is structurally based around 1, 2 or 3 non-identical heavy chains and is responsible for cilia and flagella beating. Cytoplasmic dynein on the other hand is formed around a core of two identical homodimerised heavy chains and is involved in retrograde transport of membrane-bound structures, centrosome assembly and cell cycle progression (through associations with kinetochores) [1].

1.1.3 Cytoplasmic dynein

Two forms of cytoplasmic dynein exist; 1 and 2. They function as complexes centred around heavy chains 1 or 2 (encoded by *Dync1h1* or *Dync2h1* respectively). Dynein 1, is abundantly found in all cells containing MTs and is a complex formed of dynein heavy chain 1 (DYNC1H1; referred to as DHC from this point onward), intermediate (DYNC1I1 AND DYNC1I2; referred to as DICs), light intermediate (DYNC1LI1 AND DYNC1LI2; referred to as DLIC), light chains (DYNLT1, DYNLT3, DYN1RB1, DYN1RB2, DYNLL1 and DYNLL2; referred to as DLCs) and numerous accessory proteins [2]. In contrast dynein 2 is distributed similarly to axonemal dynein in cilia and flagella and is a complex formed of dynein heavy chain 2, solely in association with light intermediate chains [1-4]. Dynein 1 complex is the topic of this thesis and will be the complex discussed from this point on.

1.1.4 Dynein heavy chains

Seventy eight exons encode the two ~530 kDa DHCs that homodimerise to form the cytoplasmic dynein complex and account for the majority of the1.2 MDa complex mass [2, 5, 6]. At the carboxy (C) -terminal is a large, 12 nm globular ‘head’ consisting of a hexameric ring of adenosine triphosphatases (ATPases) associated with diverse cellular activity (AAA+), which are responsible for the approximate 350 kDa of each heavy chain mass. AAA+ domains (AAA) 1-4 have recognisable Walker A, or P-Loops, required for binding ATP. However, only AAA1 and AAA3 have the necessary Walker B loop for ATP hydrolysis to occur, thereby generating energy to propel the motor along the MTs. Release of ATP from AAA1 is thought to be the predominant and essential driver of dynein’s power stroke, however domain 3 has been shown to be essential for dynein motility as ATP-induction at this site releases dynein from associated MTs [6-9]. AAA2 and AAA4 aid specificity for MT binding whilst domains 5 and 6 lack the P-Loop required for ATP binding and are considered to have a more structural role [8] and King, S. *Dyneins*. 2011, page 148. C-terminal to AAA6 is a C-sequence with unknown but essential motor function. It is thought to interact with AAA4, 5 and/or 6 [10].

Protruding, ~180 amino acids downstream of AAA4 are two α-helices that have recently been identified as extensions of AAA4 itself. One α-helix runs from AAA4 to a small globular ATP sensitive MT binding domain (MTBD) whilst the second originates at the MTBD and terminates back at AAA4, Figure 1.1 [11, 12].

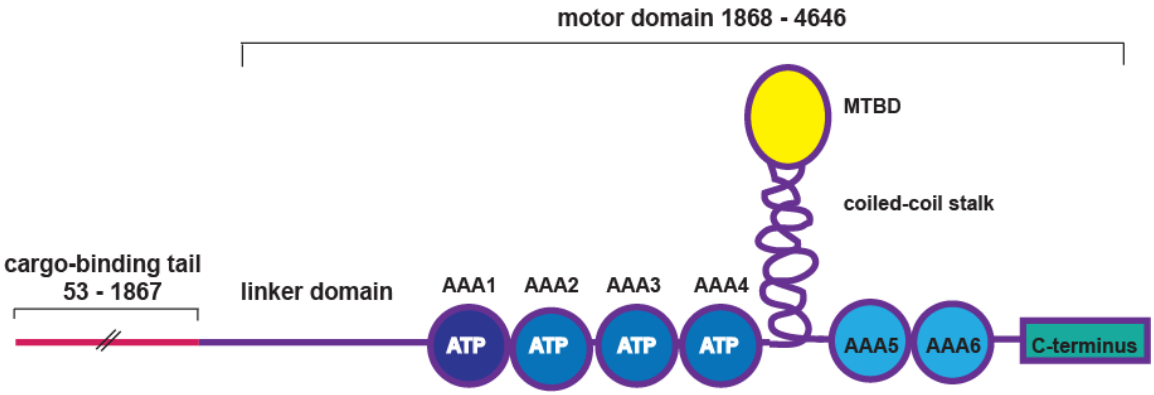

Figure 1.1: Schematic diagram of the dynein motor domain. Linear representation of the six AAA+ modules, the MTBD, the linker, and the C-terminus sequence. The region including AAA1 to the C-terminus folds into a ring-shaped motor core. DIC, DLIC, DLC and accessory proteins bind at the cargo-binding tail (adapted from : King, S. *Dyneins*. 2011 and [14].

ATP-dependent movement between the α-helices results in altered structural alignment so that straight and kinked conformations are possible and may contribute to the motility of the complex [11]. This 'stalk' is measured at <15nm in length and ~2 nm in diameter [10, 12]. Recent X-ray structural analysis identified a second coiled-coil, thought to be an extension of AAA5 which acts as a support 'strut' to the stalk but with some flexibility to enable functionality in both the straight and kinked conformations of the stalk [11].

Opposite the stalk, amino (N)-terminal to AAA1 is a 10 nm linker domain that connects the dynein head to the stem or 'tail' region [12, 13]. This linker domain spans the face of the head from AAA1 where it originates to AAA4 in an un-primed, post-powerstroke (no ATP bound) state. The primed, pre-powerstroke state finds the linker associated with AAA2. Alternative docking positions of the linker, likely produce the predominant movement to account for the dynein power stroke [8, 12].

The N-terminal 'tail' is the location of DHC homodimerisation and association with DIC, DLIC, DLC and accessory proteins.

1.1.5 Dynein power stroke

As described in 1.1.4, when un-primed or in the post-power stroke state, the linker domain of DHC spans the face of the hexameric AAA ring from AAA 1 to 4. At this time there is a strong affinity between the MTBD and MTs. ATP binding releases the MTBD and primes DHC so that the linker domain moves near to AAA2, a distance of ~ 17 nm. During this stage MTBD moves further along the MT and a weak MT association is made. The release of ADP + Pi causes the power stroke in which the linker returns back to its original position and the MTBD associates strongly once again with MTs [13, 15], Figure 1.2.

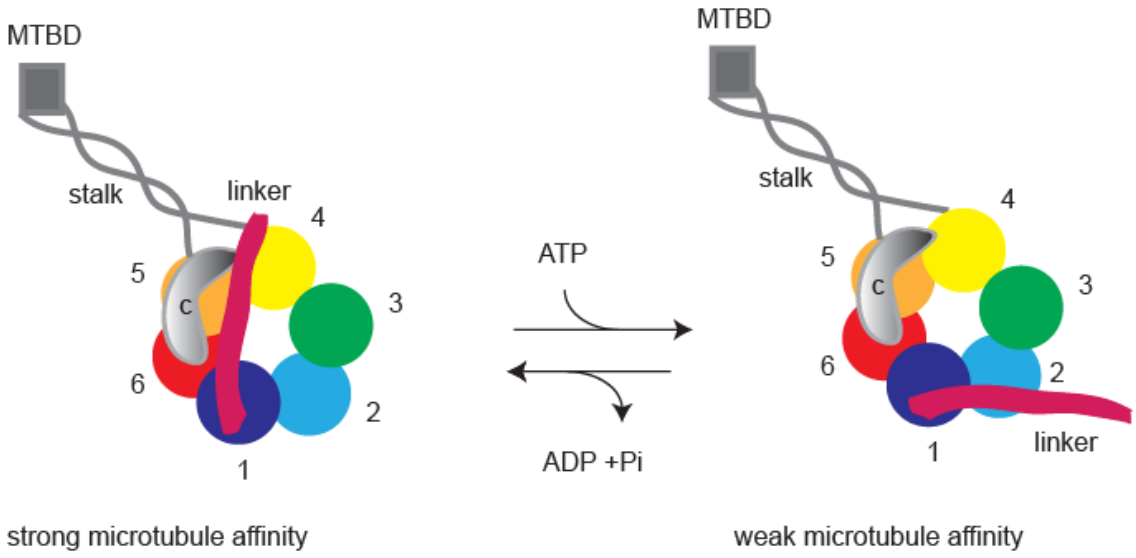

Figure 1.2: A model of the structure and priming stroke of dynein. Six ATPases associated with diverse cellular activity AAA+ form a hexamieric ring at the C-terminus of dynein heavy chain. The C-sequence 'C' interacts with AAA4, AAA5 and AAA6. The linker connects the motor domain to the 'tail' region and spans the hexameric ring from AAA1 to AAA4 in the ADP-bound, unprimed state. When ATP is bound the linker moves to a 'primed' position near AAA2, a distance of ~17nm. Dynein is strongly or weakly associated with microtubules in the ADP or ATP states respectively, Figure adapted from King, *Dyneins*, 2011, page 148.

Dynein motility is processive, that is, it can take multiple 'steps' along a MT without detaching. In order to achieve this one head of the motor must remain attached to the MT whilst the other moves forward [5]. Average step size has

been repeatedly recorded as 8 nm, however considerable variation has been observed [5, 16, 17]. Stepping can be coordinated (steps of the same size) or uncoordinated (irregular step sizes) although coordination seems to develop with larger steps [5,17]. Recent observations using fluorophores to independently label the two dynein heads showed that the two motors can pass each other alternately in a' head over head' fashion but more often will not pass, instead one head will take the lead and the second will play 'catch up' in what has been described as a side-stepping shuffle along the MT. In addition to this, asymmetry was detected within the dimerised proteins which indicated that the 'right' head was more likely to lead the 'left' which, would constitute the lagging head [17].

Dynein requires two motor heads but not the tail region to establish processivity [16] and is thus suggestive of 'gating' mechanisms in which one motor head can influence the action of the other. Two gating mechanisms have been proposed; a 'polymer gate' dependent on the rate of MTs association/dissociation and/or a 'nucleotide gate' controlled by a mechanochemical aspect of the ATP cycle [18]. Intramolecular tension has been implicated in polymeric gating as in the absence of ATP dynein still moves in a minus end direction along MTs under constant force [19]. That a pulling force detaches the rear head before forward movement occurs implies that both heads are bound to MTs whilst tension is applied and that the force on the rear head is greater than that of the leading head, propelling the motor forward. Force applied to the dynein motor can influence the directional movement. Under low loads <1 pN dynein has been shown to take mainly 8 nm steps in a minus-end direction however, as load increases to ~7 pN, step size increases although there is an increased likelihood of plus-end movement, resulting in net movement that fails to advance dynein in a retrograde direction. The co-operation of multiple motors to move large cargos likely overcomes this phenomenon [19, 20]. The size of the dynein ring (13-15 nm) and stalk (10-15 nm) imply some constraint to result in the most frequent 8 nm step. A compact formation in which the AAA rings overlap has been suggested as a restraint that can be released into a splayed conformation for larger steps to occur [18]. Evidence for these theories are

increased force producing larger steps and shortening of the linker region connecting the two motor domains results in smaller steps [16, 18, 19].

Side steps and backward movements relative to the direction of dynein travel have been observed in several studies but are far less frequent and smaller in distance than those of the forward movements [5, 17, 20-22]. These alternative step movements may be a result of regulation by the opposing motor kinesin as there is some evidence that both kinesin and dynein require opposing motors to activate one another and that multiple dynein and kinesin motors are bound to membranous vesicles at the same time [23]. Although described as a 'tug of war' between the two motors, it may be better described as co-operative regulation by two opposing motors to optimise directional movement through a crowded cytoplasm.

1.1.6 Dynein subunits

The N-terminal, tail domain of DHC associates with numerous subunits, which help stabilise and modulate the complex, interact with accessory proteins and confer specificity to cargo.

The largest of the dynein subunits; DIC is encoded by two genes; *Dync1i1* and *Dync1i2*, and in contrast to DHC's single isoform has many splice variants that can be developmental and/or tissue specific [24-26]. For example; tropomyosin-related kinase receptor B (TrkB) signalling endosomes are transported by neuron-specific DIC isoform 1B and not by the ubiquitous DIC 2C [27]. DICs are ~ 74 kDa, forming both homo and hetrodimers, which bind DHC tail through WD40 repeats at DIC C-terminal [24, 27]. The N-terminus binds membranous cargo and the regulatory complex dynactin in close proximity. Steric interference of the N-terminal cargo-binding domain eliminates membranous cargo transport and associations with dynactin [28].

The LICs DYNC1LI1 and DYNC1LI2 are estimated to be ~ 53-59 kDa [2] . Four bind DHC directly at sites overlapping those of DIC-DHC interactions however, there is thought to be no direct interaction between the DIC and DLICs [29]. Their location infers a role in cargo binding, which was indeed confirmed by

DLIC1 and DLIC2 siRNA experiments in which severe disruption to the late endocytic pathway was observed [30].

DLCs are encoded by at least six genes *Dynlt1* and *Dynlt3* (formerly identified as *Tctex1*) *Dyn1rb1* and *Dyn1rb2* (formerly roadblock) and *Dynll1* and *Dynll2* (formerly LC8) [2, 31]. DLCs homo and heterodimeise but only the homodimers bind the dynein complex and this occurs via DIC [32]. DLC are ~ 8-20 kDa and are reported to participate in cargo attachment by binding intermediate adaptor proteins [33-35].

In addition to isoform and splice variations within the subunits described, phosphorylation also acts as a method for determining cargo associations. For example; hyperphosphorylation of DLIC1 during metaphase is thought to reduce membrane-bound organelle movement whilst the phosphorylation status of DIC affects dynein-kinetochore and DIC-dynactin interactions [36-38].

1.1.7 Dynein accessory and regulatory proteins

The dynein complex has multiple regulators and associates, however the most relevant to this thesis are dynactin and LIS1 and thus these are the two I will describe briefly.

With a mass of ~1 MDa and 11 subunits, the dynactin complex is the largest and essential regulator of dynein function [39, 40].

The actin-related protein 1 (ARP1) forms the central support to which the subunits associate. Subunits range in size from 22-150 kDa, the largest of which; p150 (sometimes referred to as $p150^{Glued}$, due to the Drosphila homologue) is the associate of dynein. The association is via DIC and facilitates the association of the dynein complex with cargos [41, 42].

Dynamitin, the p50 subunit of dynactin interacts with p150 and appears to stabilise dynactin structure to enable association with dynein. Over-expression of p50 results in disassembly of the dynactin complex, impaired dynein association and inhibits retrograde movement [43, 44]. In addition, p50 has a role in binding intermediates such as Bicaudal to enable, through rab6, the binding of Golgi vesicles as cargo [45].

A further example of dynactin-dynein cargo binding is in the late endocytic pathway where Rab7-interacting lysosomal protein (RILP) acts as an intermediate (perhaps indirectly) to bind Rab7 coated late endosomes to the dynein-dynactin complex [46].

Dynactin can work independently of dynein to organise and stabilise MTs, particularly during cell cycle progression, however more often dynactin works to regulate dynein, for example by directing dynein to MT plus ends in readiness for retrograde transport, or in co-operation with dynein, for example in kinetochore and spindle organisation during mitosis and cellular transport [47, 48].

LIS1 is the protein of platelet-activating factor acetylhydrolase 1B α subunit (*Pafah1b1*) gene and along with associated nuclear distribution protein E (NUDE) and NUDE-like (NUDEL) are required for dynein activity and cellular distribution. LIS1 associates dynein with tubulin. The LIS1-dependent association of dynein with tubulin destined for anterograde transport (transport tubulin) likely allows 'transport' tubulin to act as an intermediate for kinesin-dependent transport of the LIS1-dynein complex, during which time LIS1 is considered to supresses the activity of dynein. Upon arrival of dynein at its destination NUDEL releases the inhibition of LIS1 on dynein activity however LIS1 remains associated with dynein and thus is transported back to the minus end of MTs by dynein-associated retrograde transport [49]. NUDE and NUDEL associate with the dynein complex via DHC directly or via DIC, DLC8 and dynactin (via p150) [50]. Mutations in LIS1 are linked to Lissencephaly (see section 1.2.5) in which neuronal migration defects exist. During neuronal migration the leading process extends with the centrosome ahead of the nucleus. MTs are essential for providing polarity not only for the extension of neurites but also nuclear migration toward the leading centrosome. LIS1 and dynein inhibition alter the separation between the nucleus and the centrosome, likely leading to the impaired neuronal migration observed [51]. In addition LIS1 has a role in kinetochore and spindle organisation during mitosis [52] and localisation of membranous organelles [53]. Knock-down of LIS1 has been shown to disperse the Golgi and mis-localise lysosomes from the peri-nuclear region to the cell periphery. Conversely, EEs were redistributed from the cell

periphery towards the cell centre. Knock-down of NUDE and NUDEL had a similar effect whilst individual knock-down was less severe [54].

Figure 1.3 shows schematically how dynein associates are likely to assemble.

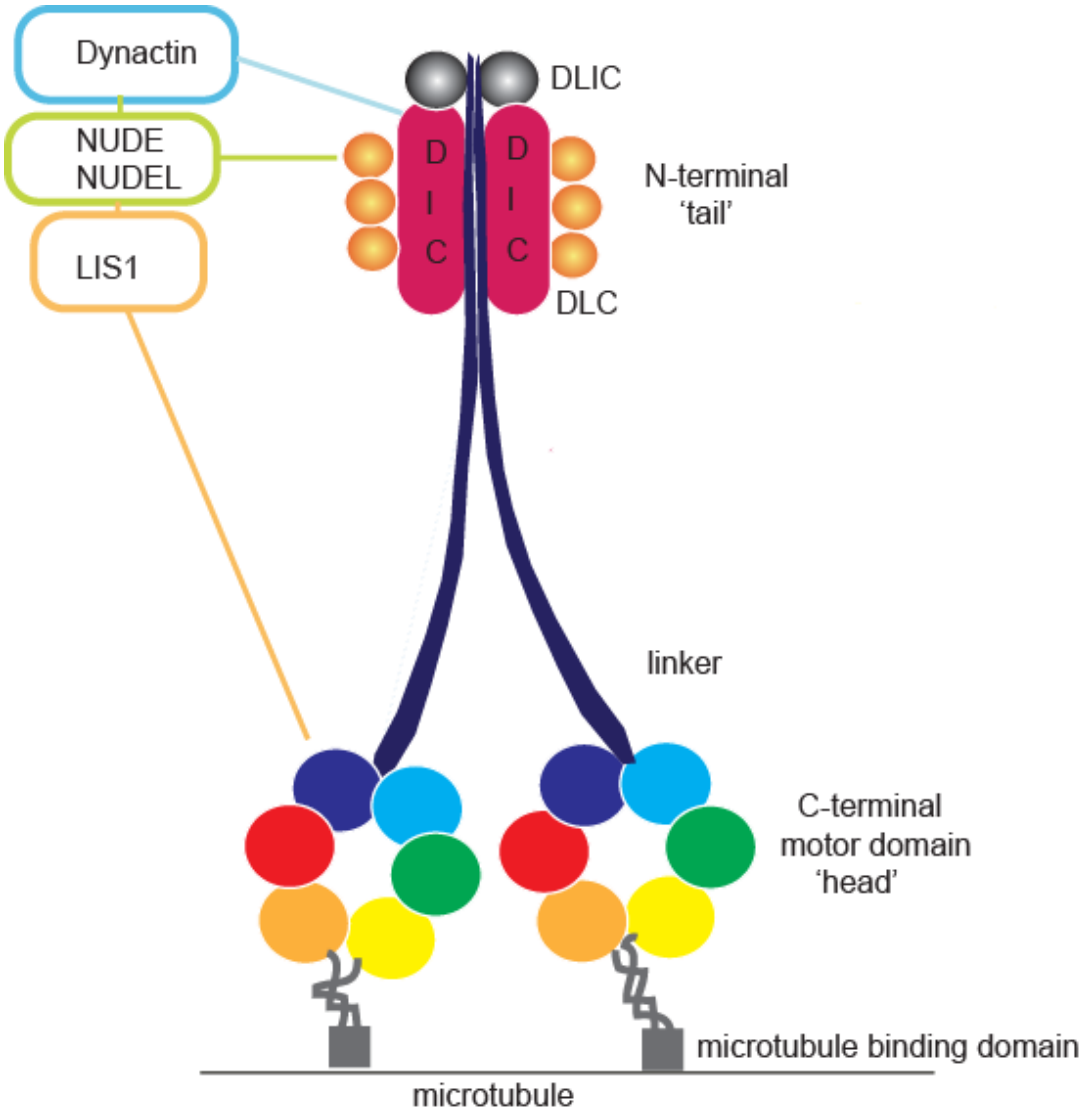

Figure 1.3: Composition and domain structure of cytoplasmic dynein (adapted from [55]). The C-terminal motor or 'head' domain is connected to the N-terminal 'tail' by a linker region which aids in the mechanics of the powerstroke. The 'tail' region is where dynein intermediate (DIC), light intermediate (DLIC) and light (DLC) chains bind, along with accessory and regulatory proteins such as dynactin, NUDE, NUDEL and LIS1.

1.1.8 Kinesin superfamily

Kinesin is a motor protein that predominantly moves in an anterograde direction, from the minus end of MTs, in the perinuclear region, towards the plus ends at the cell periphery however, there are exceptions that move in a retrograde direction.

At least 45 genes have been identified as encoding the very large kinesin superfamily however, the many alternative mRNA splice patterns mean that the number of kinesin proteins, known as KIFs, easily surpass the number of genes.

Kinesins are categorised into 15 families, although these families can be further grouped into one of three sub families, those with a motor domain at the C-terminal (C-kinesins), the N-terminal (N-kinesins) or in the middle (M-kinesins) of the heavy chain structure. The kinesins that move in an anterograde direction usually have their motor at the N-terminus, however kinesins with a C-terminal motor are more likely to move retrogradely. M-kinesins, tend to have a role in microtubule stability.

The most studied kinesin, kinesin-1, or conventional kinesin was the founding member of the kinesin superfamily tree and will be discusses further in 1.1.9. Briefly, kinesin-1 moves in an anterograde direction and has an important role in organelle, vesicle and mRNA transport. Other kinesins have roles in vesicle transport, chromosome positioning, spindle pole organisation and intraflagellar transport. The kinesin genes and families are summarised in Table 1.1, along with their cellular function, where known [56, 57] .

Gene	Family	Role
KIF5A, KIF5B, KIF5C,	kinesin-1	vesicle, organelle and mRNA transport
KIF3A, KIF3B, KIF3C, KIF17	kinesin-2	vesicle, melanosome and intraflagellar transport
KIF13B, KIF13A, KIF1C, KIF16A, KIF14, KIF16B, KIF1B, KIF1A	kinesin-3	vesicle transport
KIF27, KIF7, KIF4A, KIF4B, KIF21A, KIF21B	kinesin-4	chromosome positioning
KIF11	kinesin-5	spindle pole separation and spindle bipolarity
KIF20A, KIF20B, KIF23	kinesin-6	central spindle assembly and cytokinesis
KIF10	kinesin-7	kinetochore-microtubule attachment and chromosome congression
KIF19B, KIF19A, KIF18B KIF18A	kinesin-8	chromosome congression
KIF6, KIF9	kinesin-9	Not known
KIF22	kinesin-10	chromosome positioning
KIF26B, KIF26A	kinesin-11	Not known
KIF15, KIF12	kinesin-12	spindle pole organisation
KIF2C, KIF2B, KIF2A KIF24	kinesin-13	kinetochore-microtubule error correction and chromosome segregation
KIFC1	kinesin-14A	spindle pole organisation and cargo transport
KIFC3, KIFC2, KIF25	kinesin-14B	Not known

Table 1.1: The kinesin superfamily. The 45 known genes of the kinesin superfamily are categorised into their families with an indication of their cellular role (adapted from [56, 57]).

1.1.9 Kinesin-1

Kinesin-1 is predominantly an anterograde motor protein consisting of a hetero-tetramer of two heavy and two light chains. The heavy chains (KHC) have an N-terminal motor or ‘head’ domain and a C-terminal tail, separated by a coiled-coil region, Figure 1.4 [58].

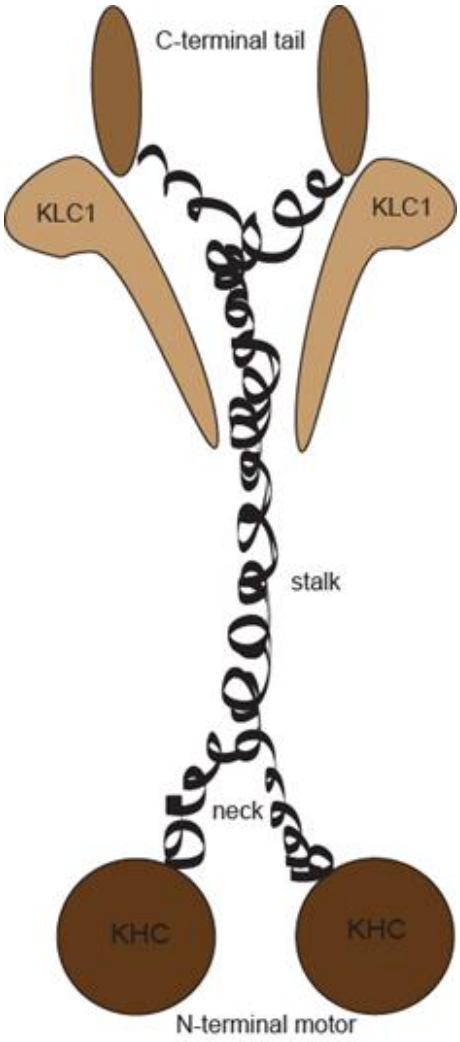

Figure 1.4: A model of kinesin structure. The two dimerised kinesin heavy chains (KHC) of kinesin-1 have an N-terminal motor domain and a C-terminal tail, separated by a coiled-coil region. Kinesin light chains (KLC) associate with KHC at the C-terminal and it is here that cargo associations are made.

ATP hydrolysis provides the energy for mobility however, when inactive kinesin is in a folded conformation whereby the tail attaches to the head inhibiting the release of ADP and interaction with MTs [58, 59]. This prevents the unnecessary expenditure of energy and enables co-ordination with other motors to maintain homeostasis of cargos within the cell. It also means that the majority of kinesin is found in the soluble cytosolic cellular fraction. KHCs have a role in cargo attachment [60].

Kinesin light chains (KLCs) are encoded in mice by multiple genes. Of these KLC-1 is primarily expressed in neuronal tissue and has many different isoforms that may play a role in cargo specificity [61, 62]. For example, KLC-1, isoform b was shown to be specific for rough endoplasmic reticulum cargo selection and KLC-1d for Golgi [63]. Dynein, through DIC may also be one of the cellular cargoes of kinesin with KLC-1 having a role in mediating the interaction between the two [63]. KLC-1 has six tetratricopeptide repeats (TPR) at the C-terminus. TPR's are structural motifs consisting of 34 amino acids, which mediate protein-protein interactions and are needed for cargo binding. The N-terminus has heptad repeats needed for binding to KHC stalk and tail regions to stabilize the inactive conformation when no cargo is bound.

Binding of cargo to kinesin may weaken the inhibition of KHC by KLC so that the KHC motor and tail domains can separate, unfolding the structure so that the motor domains of the dimer can move closer together, Figure 1.5 [59, 64-66].

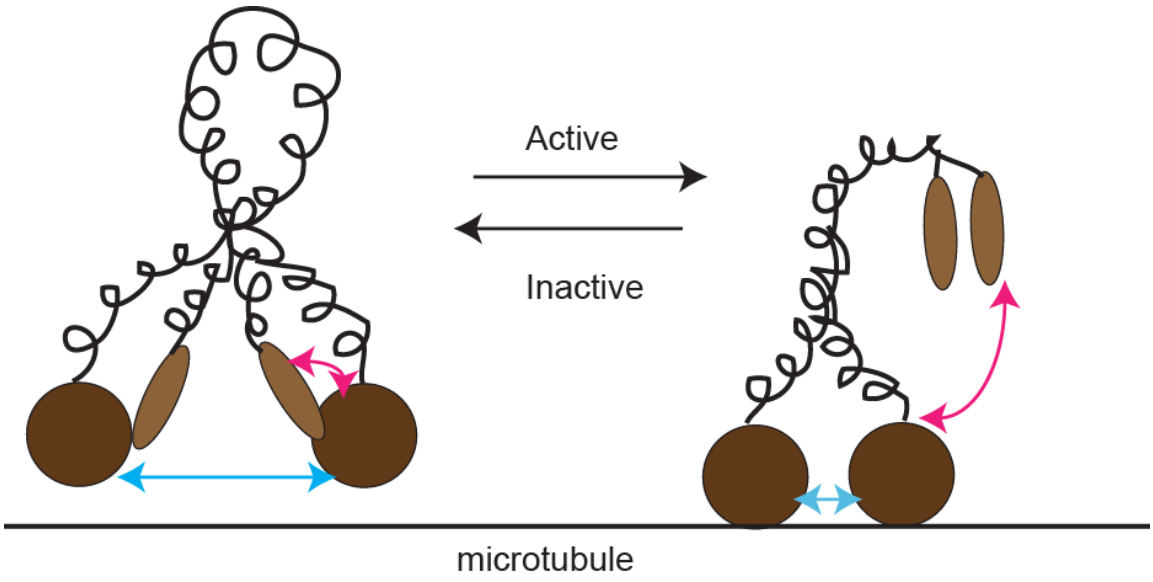

Figure 1.5: Conformation changes upon Kinesin activation. When inactive (left), Kinesin-1 is in a folded conformation with the heavy chain motor (brown circles) and tail (light brown ovals) in close proximity (pink arrow), but the motor domains are pushed apart (blue arrow). Once activated (right), the motor and tail domains are more widely separated (pink arrow), and the motor domains come closer together (blue arrow). Kinesin light chains are not depicted in this diagram. Adapted from [59].

1.2.1 Dynein mutations in human disease

Efficient intracellular transport is important in all cells however the most vulnerable are neurons, partly due to the distances involved in transporting cargo from the synapse to the perikaryon and the high energy requirement for these cells. To date there have been several mutations in either dynein itself or its protein partners that have been implicated in several forms of neurological diseases in humans.

1.2.2 Charcot-Marie-Tooth disease

Charcot-Marie-Tooth (CMT) disease is the most common neuromuscular disorder. It is a chronic polyneuropathy thus affecting both motor and sensory neurons. There are two sub-divisions to the disease; demylenating (CMT1) and axonal (CMT2), resulting from degeneration of the myelin sheath and axons respectively. Disease onset is typically during adolescence or early adulthood however symptoms can emerge later in life. Although not classified as a fatal disease CMT can be severely debilitating. Lower limbs are predominantly affected with muscle weakness and malformations, affecting gait and motility and as the disease progresses upper limbs can become affected, reducing dexterity. CMT is mainly an autosomal dominant disease, but it can also be X-linked. Numerous genes have been linked to the disease, but in the context of this thesis the most noticeable is a missense change in the homodimerisation domain of DHC: p.His306Arg (c.917A-G) in a family with CMT2 (OMIM #614228 [67]

1.2.3 Intellectual disability linked to DHC mutations

Recently, Willemsen et al reported two DHC *de novo* mutations in patients with severe intellectual disability (ID) and neuronal migration defects identified using a family based exome sequencing approach. Patient 1 (p.His3822Pro, c.11465 A-C) was a boy with developmental delay and moderately severe ID. He also had an abnormal head size and facial deformities, including a prominent forehead. He had broad shoulders, hands and feet and an altered gait. Morphologically he had reduced muscle tone and tendon reflexes.

The second patient (p.Gly1518Lys, c.4552G-A), a 51 year old woman had severe ID and had never been able to speak or walk. The lady was of a reduced height and had a small head circumference, small hands and small feet, which were clubbed. She had a flattened head and increased distance between her eyes. In addition, she had abnormal spine curvature and had developed seizures at an early age [14].

Both ID mutations and the CMT mutation within DHC cause distinctive characteristics of neurological disease with multiple overlapping phenotypes. There are however distinct differences between them, perhaps due to the location of the mutation, two within the stem domain and 1 within the motor (Figure 1.6). All three diseases are thought to be resultant of neuronal migration defects and thus highlight the importance of DHC for this function.

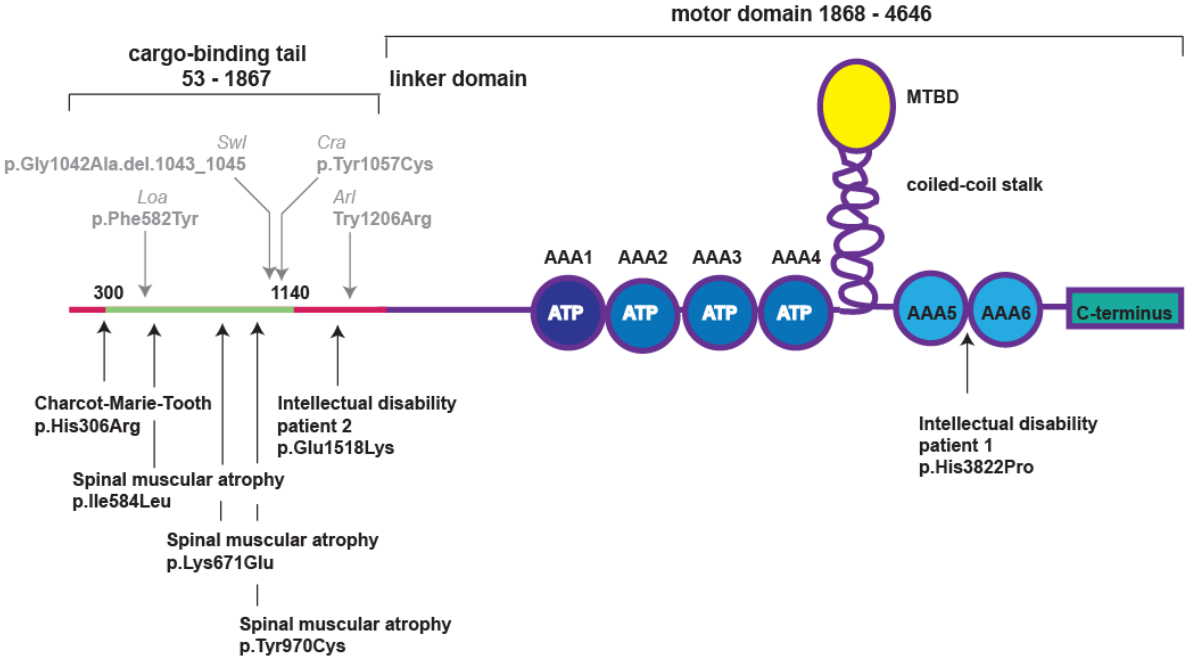

Figure1.6: Schematic representation of human DYNC1H1, indicating the location of six patient mutations. Severe intellectual disability (Patient 1 and 2) [14], a Charcot-Marie-Tooth disease [67] causing mutation and three spinal muscular atrophy mutations [68]. The location of four neurological mouse model mutations/deletions are indicated, adapted from King, S., *Dyneins,* 2011., and [14].

1.2.4 Spinal muscular atrophy

Spinal muscular atrophy (SMA) affects approximately 6000 people in the UK and is a degenerative, inherited disease in which motor neurons of the legs and trunk are primarily affected whilst sensory neurons are spared (OMIM #158600). There is a rare sub-class of SMA with lower extremity predominance (SMA-LED), where solely lower limbs are affected. Recently, target exon capture and subsequent sequencing of the 73 genes within 14q32 revealed three mutations within DHC in individuals with SMA-LED. The first identified was a c.1750 A-C transversion in exon 8 resulting in a p.Ile584Leu substitution. Interestingly this mutation is just 2 nucleotides upstream of where the p.Phe580Tyr substitution in the *Legs at odd angles* (*Loa*) mouse would be located in humans. This mouse has been used for a number of years to study neurodegenerative processes caused by impaired dynein function, see section 1.2.10 and Figure 1.6.

The other two mutations; c.2011 A-G resulting in p.Lys671Glu and c.3170 A-G changing p.Tyr970Cys were in exons 8 and 11, respectively, and all were located in the tail domain of DHC. Biochemical assays of Ile584Leu indicated a disruption of the dynein complex and reduced affinity of the complex for MTs during ATP hydrolysis [68].

In addition to DHC mutations, alterations in accessory proteins have been identified. Phenotypically there is significant overlap to DHC mutations reflecting their co-operative nature necessary for effective function.

The largest of the accessory proteins is dynactin (see section 1.1.7). A p.Gly59Ser substitution in the p150 subunit was identified in a family with slowly progressing motor neuron disease. Disease onset commenced in early adulthood and included breathing difficulties due to paralysis of the vocal folds and facial weakness. Lower limbs were affected later [69].

The mutation was located in the p150 cytoskeletal-associated protein (CAP)-Gly motif that binds MTs. Due to evidence that dynactin is essential for dynein function and has a role in directing the dynein complex to MTs it is suggestive that the p.Gly59Ser mutation in p150 disrupts dynein complex formation and

retrograde transport. Moreover, the overexpression of the p50 dynactin subunit in mice has been shown to produce a late-onset and progressive neurodegeneration due to disruption of the dynein/dynactin complex [69, 70].

1.2.5 Lissencephaly

Lissencephaly is a brain disorder caused by impaired neuronal migration. It literally means ‘smooth brain’ due to an absence of normal folds in the cerebral cortex and is often accompanied by microcephaly. Individuals affected do not survive beyond 10 years of age and have severe developmental delays. This is often accompanied by abnormal facial characteristics, mental retardation, muscle spasms, difficulty swallowing and seizures.

Deletion or mutation in the LIS1 gene accounts for a high percentage of lissencephaly cases. LIS1, in conjunction with dynein, plays an important role in the migration of developing neurons through positioning of MTs within the cell, which is disrupted in lissencephaly (OMIM #607432) [71, 72], see also section 1.1.7.

1.2.6 Dynein mouse models

There are four mouse models with alterations in DHC, chromosomal location; 12q12.55. ‘*Cramping 1’* (*Cra1),* ‘*Abnormal rear leg’* (*Arl*) (unpublished) and ‘*Legs at odd angles’* (*Loa*), have point mutations generated through *N*-ethyl-*N*-nitrosourea mutagenesis, whereas ‘*Sprawling*’ (*Swl*) has a radiation induced nine base pair deletion, Figure 1.6 [73, 74].

Cra1, *Arl* and *Swl* will be briefly described to demonstrate the severity and neuron specific nature of mutations within the DHC. *Loa* will be discussed in greater depth in the next section, as it is the mouse under investigation for this thesis.

1.2.7 ‘*Cramping 1’*

Cra1 maps to position 1055, and is within the DHC homodimerisation domain. The mutation substitutes tyrosine to cysteine (TAC to TGC) [75] .

In 2003 Hafezparast et al reported an 80% loss of anterior horn cells at embryonic day (E) 18.5 in *Cra1* homozygote (*Cra1/Cra1*) embryos and the pups were unable to survive more than 24 hours after birth, likely due to impaired migration of facial neurons resulting in an inability to suckle. They also described Lewy-like inclusions in dorsal root ganglia (DRG), similar to those seen in *Loa* (see section 1.2.10) and human forms of Amyotrophic Lateral Sclerosis, a late on-set, progressive neurodegenerative disease [75]. Moreover, Dupuis et al 2009 reported small DRGs with reduced numbers of axons per dorsal root in *Cra1* when compared to wild-type. The reduction was mainly of large (>5µm) calibre axons and is suggestive of the loss of type 1a proprioceptive axons, a phenotype also observed in *Loa* and *Swl* mice but to a greater extent 76].

1.2.8 '*Sprawling'*

The *Swl* 'GCATAGTGA' deletion from chromosome; 12q12.55 results in a substitution of residues 1040-1043 from glycine (GGC), isoleucine (ATA), valine (GTG) and threonine (ACT) to an alanine (GCT). It is within the homodimerisation and cargo binding domains of DHC. *Swl* manifests a proprioceptive sensory neuropathy with sensory loss from the DRG being much greater in the lumber region than the cervical, concurring with a hind limb phenotype. There is a 69% and 87% loss of DRG proprioceptive and muscle spindles, respectively, in heterozygous (+/*Swl*) mice by post-natal day 0.5 (P0.5), but not in E15.5 embryos, indicating that degeneration begins during the late stages of embryonic development. α-motor neurons are not altered in morphology, number or function and although a 31% loss of nociceptive neurons in 13 week +/*Swl* is observed, it is not enough to affect overall nociceptive ability and confirms that proprioceptive neurons are predominantly affected. *Swl* homozygotes (*Swl*/*Swl*) are embryonic lethal 77].

1.2.9 '*Abnormal rear leg'*

The *Arl* mouse is yet to be published but has been investigated within our lab for some time. A T-C change in DHC results in a p.Trp1206Arg substitution which is embryonic lethal before E10.5. Heterozygotes (+/*Arl*) have reduced tibialis anterior (TA) muscle strength by 1 year of age, which affects gait and

when suspended by the tail the mice twist their bodies and clench their feet, which is representative of neuromuscular defects. Examination of MNs revealed that although overall numbers were not reduced, soma size was 20% smaller in +/*Arl* than in wild-type mice. These neurons also displayed abnormal excitability patterns. Although the examination of retrograde transport, using a fluorescent fragment of the tetanus toxin (TeNT H_c), did not show any differences between heterozygotes and wild type, it has been suggested that *Arl* may affect the binding of DHC to MTs and ATP and subsequently the efficiency of the power stroke (A. Philpott, Investigations into the Biochemical and Cellular Biology of a Cytoplasmic Dynein Mutation, Abnormal Rear Leg (*Arl*), DPhil 2010).

1.2.10 '*Legs at odd angles*'

The most studied of the DHC mouse models is *Loa*, which has a T to A transversion, resulting in a substitution of phenylalanine with tyrosine (TTC to TAC) at residue 580, in the overlapping homodimerisation and DIC binding domains of DHC. The mutation is autosomal dominant and although lifespan is not significantly affected, heterozygous (+/*Loa*) adults do present with progressively weakened muscle tone and reduced mobility, as determined by SmithKline Beechman, Harwell, Imperial College, Royal London Hospital, phenotype assessment (SHIRPA) which, characterises behavioural, locomotive and cognitive phenotypes through standardised testing procedures.

The mouse was phenotypically characterised due to its clenched paws and abnormal limb flexion when suspended by the tail, which is typical of neuromuscular defects, Figure 1.7 [78].

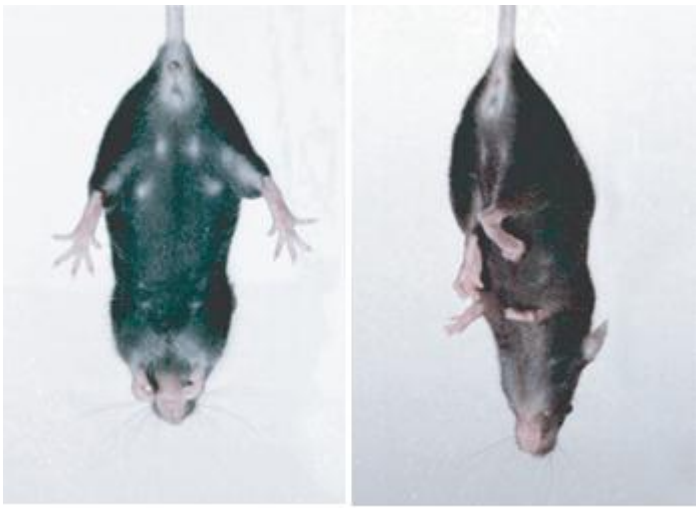

wild-type +/*Loa*

Figure 1.7: Wild-type and +/*Loa* mice suspended by the tail to show the *Loa* phenotype.

Original histopathology examination reported a ~75% loss of α-MNs in +/*Loa* adults by 19 months of age and a 50% loss of anterior horn cells in E18.5 *Loa/Loa*, moreover, Lewy-like aggregates containing superoxide dismutase 1 (SOD1), cyclin-dependent kinase-5 (CDK5), neurofilaments and ubiquitin were identified in *Loa* MNs, mirroring those seen in human ALS [75] patients. However, MN loss in *Loa* has since been disputed because, although Ilieva et al 2008 identified a 10% reduction in the total number of MNs in +/*Loa* compared to wild-type at $1^1/_2$ months of age, this loss was found to be a stable loss (no further decrease with ageing) and was identified as a loss of γ-MNs rather than α-MNs. The neuronal types are distinctly different as γ-MNs synapse with muscle spindles (to provide proprioceptive feedback regarding the length and position of the muscle), whereas α-MNs innervate skeletal muscle for locomotion. Any α-MN loss observed reflected age progression rather than being dependent on *Loa* [75, 79].

In the same study there was a clear reduction in the number of myelinated sensory axons in +/*Loa* compared to wild-type throughout the $1^1/_2$ to 22 month ages observed, although the size of the axons was not affected. In wild-type mice there was an age-dependent increase in the larger (>5μm) sensory axons however, this age-dependent shift was not observed in +/*Loa*, resulting in +/*Loa* having $^1/_4$ of the number of these larger axons compared to wild-type. +/*Loa* also have a reduction in the number of small (<5μm) axons. Parvalbumin

staining of large, type 1a proprioceptive neurons revealed substantial reductions in +/*Loa* and complete lack of these neurons in *Loa/Loa* entering the DRGs. These findings are in agreement with Chen et al 2007, who found a 42% loss of DRG in +/*Loa* at 13 weeks of age which, was specific to the lumber region, and an 86% reduction in the number of muscle spindles. Both Chen et al and Ilieva et al found a lack of the proprioceptive, Hoffman's or 'H' reflex in +/*Loa*. This test measures the time delay between stimulation of type 1a proprioceptive sensory neurons and a responding 'M' wave in the α-motor fibres. Additional testing by Ilieva showed that pain and temperature sensitivity was not affected in the +/*Loa* mice, but there were significant alterations to locomotion, gait and strength. In combination, these two studies indicate a proprioceptive deficit in the *Loa* mouse [79, 80].

Examination of neuronal migration by injecting the thymidine analogue; 5-bromo-2'-deoxyuridine (BrdU) into pregnant +/*Loa* mice revealed defective migration of cortical neurons such that instead of forming a distinct layer at the plial surface the neurons were more unevenly distributed in the *Loa/Loa* embryos and cortical lamination was severely impaired. Moreover, somal translocation and axon extension in migrating neurons was prolonged. Migration defects are also observed in the hippocampus [20, 81]. If defective neuronal migration is extended to include facial neurons it may offer explanation as to why *Loa/Loa* pups are unable to survive for more than 24 hours and their inability to suckle [75].

At the cellular level *Loa* does not affect mitotic functions but a significant reduction in high speed retrograde trafficking of membrane bound compartments has been observed [20, 75, 81]. Hafezparast et al. used TeNT H_c, which utilises the same pathway as Nerve Growth Factor (NGF) to observe this speed reduction along with an increased number of stationary pauses in *Loa/Loa* MNs when compare to wild-type. At the molecular level, using quantum dot optical trap assays a reduced run length and overall number of long runs was revealed. This is reflected in live-cell imaging of late endosome/lysosome movement. No difference in DHC step size has been observed [20]. When examining Golgi reorganisation following nocodazole treatment it was found that

the reorganisation of the Golgi was slower in *Loa/Loa,* suggesting that the cells are particularly vulnerable under stress (nocodazole depolymerizes MTs) [75].

Biochemical work identified an increased interaction between DLIC1, DLIC2, DIC and DHC in *Loa/Loa* compared to wild-type. Increased affinity between DHC and DIC subsequently increased the association of DYNLT1 *and* DYNLT3, DLCs. This altered association between the dynein subunits and subsequently, significantly reduces the interaction with p150 dynactin in *Loa/Loa* (Wenhan Deng, Caroline Garrett et al. Neurodegenerative Mutation in cytoplasmic Dynein Alters Its Organisation and Dynein-Dynactin and Dynein-Kinesin Interactions. *J.Biol.Chem.285, 39922-39934*) [82]. Altered interactions within the tail region of dynein may affect cargo and/or MT associations and is suggestive of why retrograde axonal transport is impaired in *Loa*. Moreover, there is evidence that *Loa* could also affect the motor activity of dynein. An increased affinity between DHC and MTs has been observed in +/*Loa* in the absence of ATP. Conversely, MT binding and ATPase activity in +/*Loa* is reduced in the presence of ATP, indicating a reduction in DHC force production and MT association during dynein power stroke in these mice [20].

With diseases such as SMA-LED, CMT and ID all being linked to mutations in DHC, *Loa* research has the potential to further our understanding in a broad collation of neurodegenerative diseases. Although *Loa* does not show behavioural abnormalities as seen in some human patients with DHC mutations, there is a mouse model with a mutation in DLIC1 that presents with behavioural changes such as increase anxiety [83], highlighting the collaborative potential of these mouse models to help in the understanding of debilitating and devastating neurological diseases.

1.3.1 Endocytosis overview

Endocytosis is a mechanism by which a cell can communicate between cells, adapt to intra and extracellular variations and regulate ligand receptors at the plasma membrane. Endocytic cargo varies from growth factors (GFs) and their receptors to nutrients, extracellular fluid, bacterial pathogens and some viruses (for cells of the immune system). The method of internalisation is largely dependent on the size of the cargo. Phagocytosis and macropinocytosis is generally initiated by particles >500nm, whereas clathrin-dependent and clathrin-independent endocytosis engulfs smaller cargo. Phagocytosis, macropinocytosis and clathrin-independent mechanisms will be described in brief, whilst clathrin-dependent endocytosis will be discussed in more detail. Additional endocytic mechanisms do exist. They are clathrin-independent carrier/GPI-enriched endocytic compartments (CLIC/GEEC), interleukin-2 receptor β (IL2Rβ) and ADP-ribosylation factor 6 (Arf-6) –dependent endocytic mechanisms. As yet there is far less known about the proteins and mechanics involved in these latter pathways and they will not be covered here [84].

1.3.2 Phagocytosis

Phagocytosis is predominantly initiated in macrophages, neutrophils and dendritic cells of the immune system. Pathogens, apoptotic cells or nutrients are presented to receptors in the plasma membrane, which initiate actin polymerisation and in some cases signalling cascades such as phosphoinositide 3-kinase for cellular growth. Actin polymerisation extends the plasma membrane, invaginating the cargo into a phagosome to be transported for degradation. To meet the membrane demand for engulfing very large cargos, additional membrane can be sought from recycling and late endosomes, lysosomes and endoplasmic reticulum. The phagosome proceeds through the cell to the lysosome to which it fuses to form a phagolysosome. The internal compartment of the phagolysosome is acidic, resulting in content degradation [84-86].

1.3.3 Macropinocytosis

Macropinocytosis or ‘cell drinking’ can occur both on the macro and micro (pinocytosis) scales. Both involve the internalisation of extracellular fluid as a result of membrane ruffling. Motile cells extend their plasma membrane by actin polymerisation and if no substrate is contacted the extension is recycled back into the cell, often with the addition of extracellular fluids. Membrane ruffling is controlled by the G-protein Rac and can be in response to external GFs, such as epidermal growth factor (EGF) or internal activation of Src family kinase (SFK), a non-receptor tyrosine kinase. There is evidence that some membrane proteins can be regulated by macropinocytotic depletion [84, 85, 87].

1.3.4 Clathrin-independent endocytosis.

The most studied of the clathrin-independent endocytic mechanisms is that of the integral membrane protein caveolin. There are three caveolin proteins; 1, 2 and 3 (Cav-1, Cav-2 and Cav-3, respectively). Cav-1 was the first to be identified and is expressed predominantly in post-mitotic cells. Cav-2 requires Cav-1 for correct function and Cav-3 is expressed mainly in muscle cells.

The association of caveolin proteins to membrane cholesterol results in the formation of flask-shaped structures; caveolae, or ‘little caves’ 50-100nm in size. Taking up approximately a third of the plasma membrane, they are important for the internalisation of proteins, toxins and viruses. Polymerase 1 and transcript release factor (PTRF or cavin), and serum deprivation protein response (SDPR) have recently been identified as being necessary structural proteins for caveolae formation and coat structure [88-90].

1.3.5 Clathrin-dependent endocytosis

Clathrin was first discovered in 1975 by Barbara Pearse [91]. It has three heavy chains of ~180 kDa and each associates with light chains of ~25 kDa to form a triskelion structure. These triskelions (with regulation from the light chains) [92, 93] are able to form extensive pentagonal and hexagonal formations, building lattices that encapsulate proteins and lipids from the plasma membrane into internalised compartments. They also form to shuttle proteins from the trans-Golgi network to the endosome. Clathrin cannot bind directly to membranes and

thus adaptor or adaptin proteins (AP) are required to bind clathrin and either plasma membrane lipid or protein to initiate clathrin coated pit formation [91, 94, 95].

There are four major tetrameric mammalian AP complexes; AP-1, AP-2, AP-3 and AP-4 that have localisation and recognition sequences to bind clathrin and other APs, and help confer cargo specificity. Their roles include Golgi vesicle trafficking (AP-1 and AP-4), endocytosis of receptors such as transferrin and epidermal growth factor (EGFR) from the plasma membrane (AP-2), and synaptic vesicle formation (AP-3) [96-98]. Monomeric APs include AP180 and CALM (clathrin assembly lymphoid myeloid leukaemia protein), important for endocytosis of synaptic vesicles and clathrin coat formation respectively [99]. Overexpression of the C-terminal, clathrin-binding domain of AP180 inhibits association with PtdIns(4,5)P_2 (or PIP_2) in the plasma membrane inhibiting clathrin coated vesicle (CCV) formation [99]. The AP family is not solitary in its role, there are many other adaptor and associate proteins including epsin and amphiphysin which assists membrane curvature and recruits the GTPase dynamin for scission from the membrane.

A CCV takes <1 min to assemble and once formed can have an outside diameter of ≥ 600 to ≥ 2000 Å (60-200 nm). It is estimated that in cultured fibroblasts ~2500 CCVs leave the plasma membrane every minute, resulting in a high turnover of plasma membrane components.

Following CCV internalisation from the plasma membrane, the clathrin associate- auxilin binds. Auxillin has binding sites for clathrin, dynamin and AP-2. In addition, auxillin recruits heat shock protein 70 (Hsp70), an ATP-dependent enzyme shown to disassemble clathrin coats. Loss of the clathrin coat is rapid, ~5 sec after internalisation. The vesicle is now an early endosome (EE), Figure 1.8 [99-103].

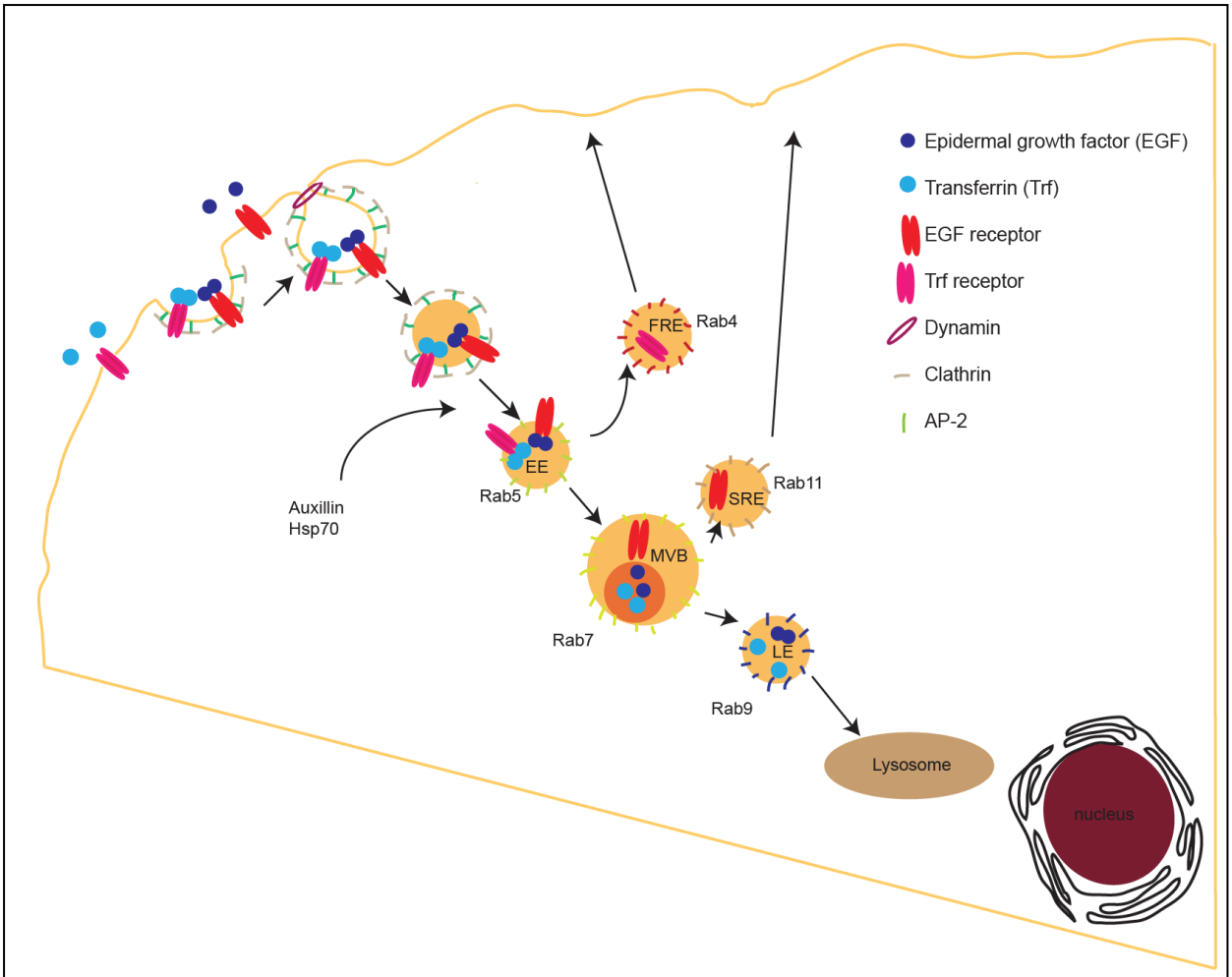

Figure 1.8: Clathrin-dependent endocytosis. Following ligand binding, receptors such as epidermal growth factor (EGF) and transferrin (Trf) are encapsulated into a clathrin coated pit with the aid of adaptor proteins such as AP-2. The GTPase dynamin pinches off the vesicle from the cell membrane and very quickly the clathrin associated protein, auxillin recruits heat shock protein 70 to dissociate the clathrin coat. The vesicle is now an early endosome (EE), directed onto cytoskeletal motors by small Rab GTPase (Rab) 5. Sorting of some receptor-ligand complexes enables fast recycling endosomes (FRE) containing receptors such as Trf receptor to be quickly directed back to the plasma membrane by Rab4. Ubiquitinated contents is sorted into intraluminal vesicles which, changes the EE to multivesicular bodies (MVB) coated in Rab7. Cargo directed back to the plasma membrane in slow recycling endosomes (SRE) are directed by Rab11 and remaining contents are sent via a late endosome (LE) to the lysosome by Rab9, for degradation.

1.3.6 Rab-directed endosomes

Endosome fate is directed by members of the Ras superfamily; small Rab GTPases of which at least 60 have been identified in humans [104]. Rabs bind the cytosolic surface of intracellular membranes and in the presence of GTP co-locate effector proteins to enable actin or tubulin based transport to occur [105].

Rabs are post-translationally modified by the addition of 1-2 geranylgeranyl lipid groups to cysteine residues in their C-terminus, a process is carried out by geranylgeranyl transferase (RabGGT) having been recruited via Rab escort proteins (REPs). The prenylation produces a lipid anchor for membrane insertion [106]. Rabs are held in their 'inactive' GDP-bound state by GDP-dissociation inhibitor (GDI). It is GDI-displacement factors (GDFs) that identify specific Rab-GDP-GDI complexes from the cytosol and initiate the release of the GDI from Rab-GDP for insertion into the membrane [107]. Guanine nucleotide exchange factors (GEF) activate Rabs by exchanging GDP for GTP. This facilitates interactions with effector proteins such as molecular motors, kinases, phosphatases, coat and tethering proteins, and soluble N-ethylmaleimide –sensitive factor attachment protein receptors (SNAREs).

The interactions between Rabs and the dynein complex are plentiful. Examples include Rab 4a on the EE that interacts with DLIC1 [108]. Rab7 on the late endosome (LE) through RILP associates with $p150^{Glued}$ subunit of dynactin [109] and Rab11a on the slow recycling endosome interacts with DLIC1 and DLIC2 through the Rab11effector protein FIP3 [107, 110]. These interactions target endosomes to the dynein complex for transport to occur.

Hydrolysis of Rab-bound GTP to GDP by GTPase accelerating protein (GAP) deactivates the Rab once its role has been fulfilled and it is removed from the membrane by GDI.

The transition from one Rab to the next likely occurs as a highly organise sequence of events in which the recruited Rab (for example; Rab A) is activated by its respective GEF (GEF A), Rab A activation recruits the GEF (GEF B) of the sequential Rab (Rab B) which, upon activation recruits GAP to the upstream

Rab (GAP A) whilst recruiting the GEF (GEF C) for the next Rab downstream, Figure 1.9.

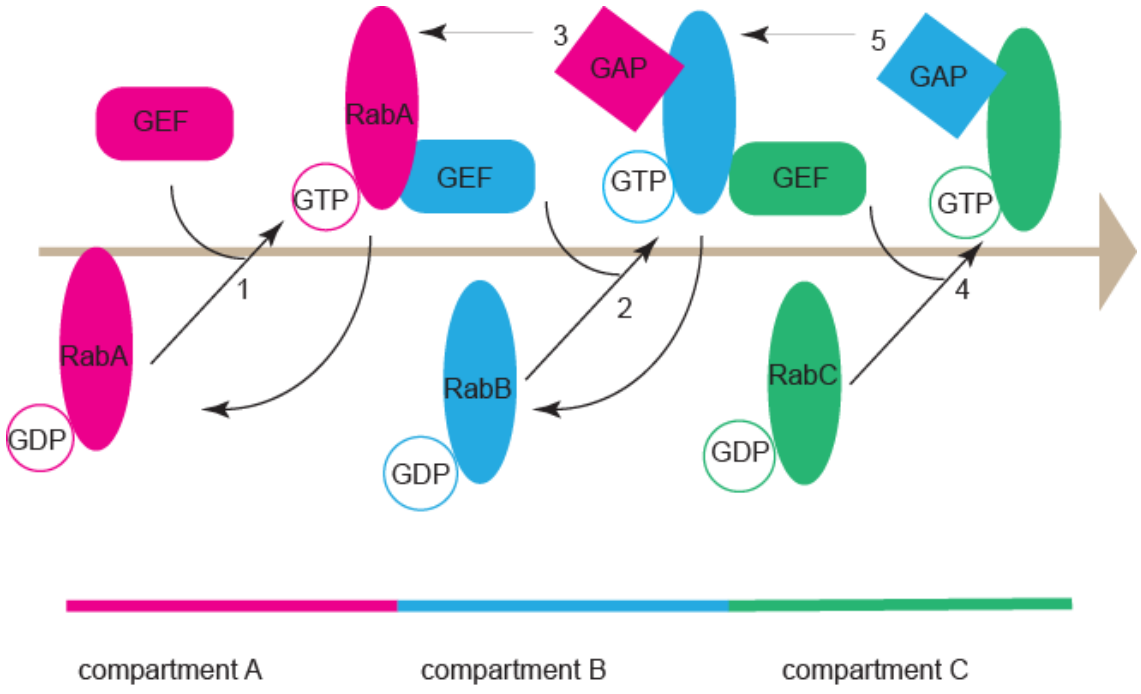

Figure 1.9: The Rab GEF and GAP cascade. Once RabA is attached to the membrane it is activated by its respective GEF (step 1). Active RabA recruits the GEF for activation of it's sequential Rab, RabB (step 2). RabB recruits GAP for RabA deactivation (step 3) and the GEF for RabC activation (step 4). RabC activation recruits GAP for RabB (step 5). Adapted from [110].

EEs are coated with Rab5 which activates the Rab effector protein EEA1 (early endosome antigen-1 to enable EE fusion. EEA1 is localised to the cytosolic face of the EE membrane after the removal of the clathrin coat. EEA1 is highly specific to the EE and is thought to have a role in EE targeting and docking [111]. EEs have an internal pH of ~6.4 which is acidic enough to dissociate some ligand-receptor complexes, such as the nutrient receptor transferrin, to allow fast receptor recycling, directed by Rab4, back to the plasma membrane [112]. After activation EGFR is ubiquitinated on its cytosolic surface to mark the receptor degradation. Further sorting and compartmentalisation of endosomal contents is dependent on endosomal sorting complexes required for transport (ESCRT) which, recognise ubiquitin tags on the cytosolic surface of EGFR. Hepatocyte growth factor regulated tyrosine kinase substrate (Hrs) (ESCRT 0)

sequentially recruits ESCRT I, II and III to the endosomal membrane to invaginate proteins destined for degradation into intraluminal vesicles (ILV). The formation of the multivesicular body (MVB) is concurrent with a change to Rab7 coat [113]. The phospho-lipid; lysobisphosphatidic acid (LBPA) which is abundant in LE membranes associates with ESCRT machinery via Alix to facilitate formation of MVBs [114] whilst the calcium and phospho-lipid binding protein annexin-1 is thought to have an essential and specific role down-stream of ESCRT for EGFR vesiculation [115]. ESCRT III and the AAA-ATPase vacuolar protein sorting-associated (VPS) 4 is recruited to detach the ILV from the membrane. Cargo that is not enclosed within the ILV is localised into tubular structures that will be slowly recycled back to the plasma membrane, a path directed by Rab11 [116, 117]. This process can occur in as little as 4-30 min post ligand stimulation [118, 119]. The mature MVB/late endosomes (LE) now solely containing particles destined for degradation is directed toward the lysosome in the peri-nuclear region by Rab9. The exchange of contents between LE and the lysosome is likely through either fusion and/or transient "kiss and run" mechanisms [120]. To enable LE/lysosomal fusion events, tethering of the two organelles is required. Tethering complexes include the homotypic fusion and vacuole protein sorting (HOPS) complex which interacts with Rab7, and class C core vacuole /endosome tethering (CORVET) complex. HOPS and CORVET have been shown to interconvert by exchange of subunits [121]. Following tethering four SNAREs form a trans-SNARE or four-helix 'bridge' in which an arginine (R), and 3 glutamine (Q) residues are contributed by each of the; R-SNARE, Qa (syntaxin 7), Qb (VTI1b) and Qc (syntaxin 8) SNAREs, respectively. The R-SNARE vesicle-associated membrane protein (VAMP) 7 is required for LE/lysosome fusion whereas VAMP8 is associated with LE fusion events. Ca^{2+} and calmodulin are thought to be responsible for the final stages of LE/lysosomal fusion to form a hybrid organelle in which degradative events take place. Further mechanisms exist to restore the lysosome to its original state [122]. LE acidity is ~6.0-5.0 but in the lysosome acidity reaches 5.0-4.5 for effective degradation to occur [112,123]. The whole process is complete in ~60 min post internalisation [124].

Figure 1.8 shows Rab directed endocytosis from the plasma membrane.

1.3.7 Dynein and endocytosis

Dynein is required for efficient transport of endosomes from the cell periphery to the peri-nuclear region and efficient sorting of receptors such as EGFR and transferrin in the EE [125]. Defects in the latter are a likely consequence of altered subcellular location which, in co-operation with kinesin and using directional cues from Rabs, enables bidirectionality for efficient delivery of recycling endosomes back to the plasma membrane and degradative cargos to the lysosome [125, 127].

Causal disruptions to dynein integrity may involve impaired physical movement of the cargo due to DHC mutation or may involve altered associations with cargo. As discussed in 1.1.6 and 1.1.7 DIC, DLIC, DLC and dynactin either bind directly to membranous cargo such as endosomes or bind through additional proteins, or in the case of dynactin facilitate binding. Any mutations in either DHC itself or any of its associated subunits and accessory proteins may alter protein-protein affinities or cause steric interference, leading to severe disruption to the endocytic process. Motor processivity may also be affected.

One of the consequences of disrupted endocytic trafficking is altered intracellular signalling.

1.4.1 Intracellular signalling

In the last section I discussed how, through endocytosis a cell can internalise information from its extracellular environment. The information can be in the form of a direct signal from another cell or a change in nutrient or fluid composition of its environment. I will now look specifically at how the cell responds to GF stimulation for survival and proliferation.

1.4.2 Growth factors

GFs as their name suggests are important for cellular growth. In addition they aid in determining differentiation, development, cell migration, mitosis, regeneration and morphology [128 -131]. Impaired GF regulation can result in oncogenesis, particularly in proliferative cells, but may also play a role in cellular degeneration and/or death in post-mitotic cells such as neurons.

1.4.3 EGF signalling cascade

EGFR is one of four members of the ErbB receptor tyrosine kinase (RTK) family. RTKs span the plasma membrane and upon ligand binding are endocytosed. Signalling from the receptor continues within the cell until the receptor is recycled or degraded in the lysosome [132-136]. EGFR ligands include amphiregulin, transforming growth factor-α (TGF-α) and EGF.

EGF binds EGFR in highly proliferative cells such as endo and epithelium. Ligand binding initiates autophosphorylation of the receptor followed by endocytosis of the ligand-receptor complex. EGF/EGFR is internalised in a clathrin-dependent or clathrin-independent manner at low or high levels of EGF, respectively [137]. Once receptor activation has occurred the growth factor receptor-bound protein 2 (GRB2) is recruited through its SH2 domain. GRB2 is a member of the Src-homology 2 adaptor proteins and thus has both SH2 and SH3 domains. Through its SH3 domains, GRB2 binds to the guanine nucleotide exchange factor (GEF) SOS. The GEF activity of SOS promotes the dissociation of guanosine diphosphate (GDP) from inactive G-protein Ras, so that Ras can bind guanosine triphosphate (GTP) to become active. Ras activates RAF, a mitogen-activated protein (MAP) kinase kinase kinase (MAP3K) which phosphorylates to activate Mek (MAP2K). Mek subsequently

phosphorylates extracellular signal-related kinase (ERK) 1 (or MAPK3) on Thr 202/Tyr 204 and ERK 2 (MAPK2) on Thr 15/Tyr 187 [138, 139]. Phosphorylated ERK 1/2 (pERK 1/2) activates downstream transcription factors such as Elk1, which binds immediate early gene (IEG) promoters to initiate transcription of genes such as *c-Fos*, *c-Jun* and *c-Myc* for a rapid survival response to GF stimulation [140], Figure 1.10.

EGF activation of ERK 1/2 is transient in nature with active, pERK 1/2 levels remaining in the cytosol, reducing by 30 min post stimulation and returning to basal levels by 60 min [141].

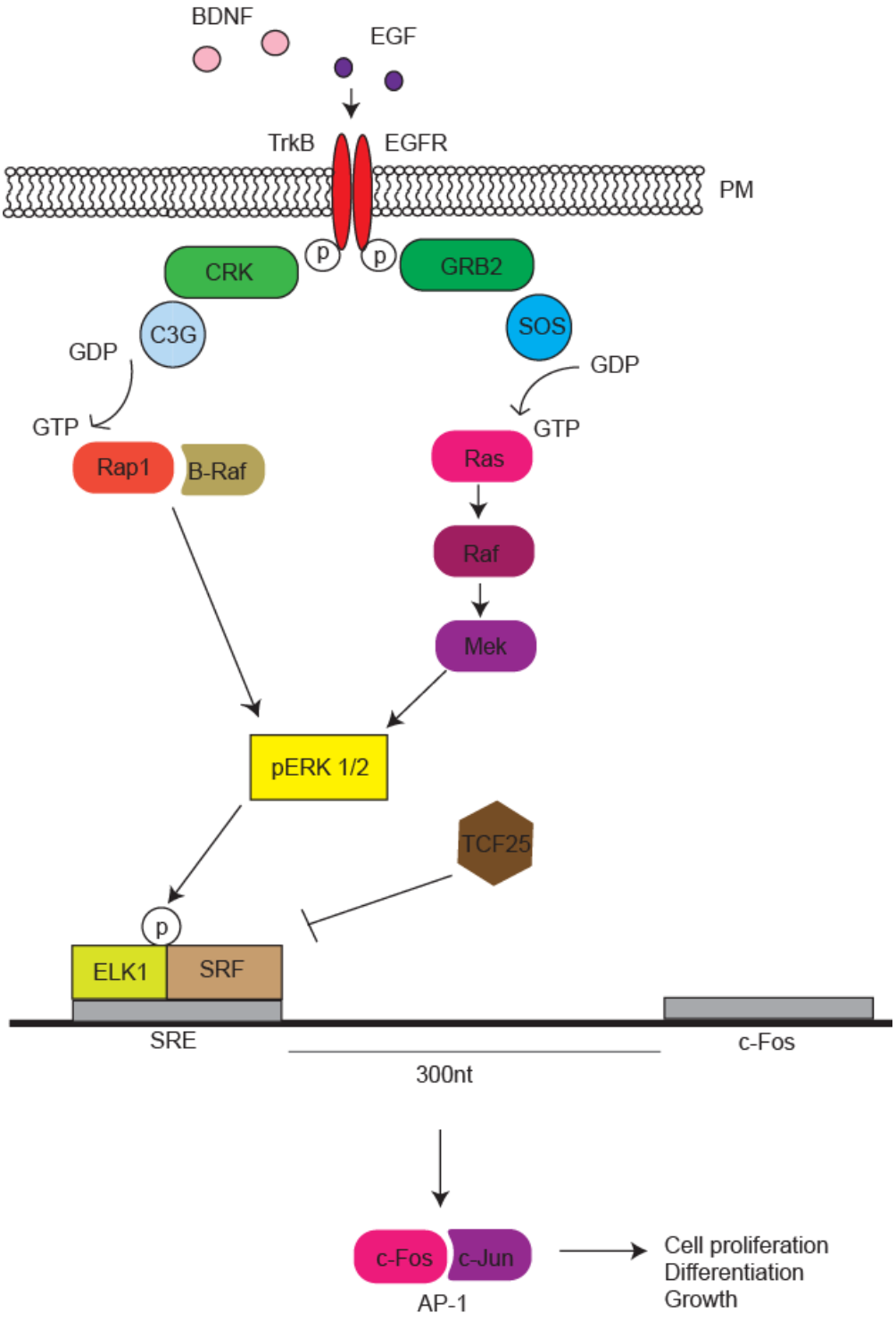

Figure 1.10: Extracellular signal related kinase activated by epidermal growth factor (EGF) or brain derived neurotrophic factor (BDNF). EGF or BDNF activate receptor tyrosine kinases; EGFR and TrkB, respectively. EGF initiates the Ras pathway resulting in transient activation of ERK 1/2 (pERK 1/2), whereas in neuronal cells a sustained activation of ERK 1/2 is achieved by initiating Rap1. pERK 1/2 phosphorylates ELK1, which binds the serum response element (SRE) of the c-Fos promoter when serum response factor (SRF) is bound. Transcription factor 25 (TCF25) is a negative regulator of c-Fos expression.

1.4.4 Brain-derived neurotrophic factor

Brain-derived neurotrophic factor (BDNF) is a member of the nerve growth factor (NGF) family. BDNF binds TrkB and p75-neurotrophic receptor ($p75^{NTR}$), a member of the tumour necrosis factor family of receptors. The BDNF receptors have different effects; TrkB activation aids differentiation and survival, whereas $p75^{NTR}$ can induce survival or apoptosis. Receptor expression and ligand-receptor affinity regulates this process [128-130]. TrkB, like the EGFR is a RTK. Two other Trk receptors; TrkA and TrkC exist, however they are specific to other members of the NGF family; NGF and neurotrophin-3 respectively.

BDNF activation of TrkB activates the ERK 1/2 pathway described above. In this pathway, however, Crk is also activated [142]. Crk, like GRB2 is a member of the Src-homology 2 adaptor proteins and thus has both SH2 and SH3 domains. Crk SH3 domain nucleotide exchanger (C3G), which acts as a GEF for Rap1 binds Crk for activation and subsequent activation of Rap1 by GDP-GTP exchange. Rap1 forms a complex with B-Raf to activate ERK 1/2 for sustained activity. Thus, acute or gradual GF stimulation may trigger transient or sustained activation of ERK1/2, respectively, Figure 1.10 [131, 143-145].

1.4.5 Linking ERK 1/2 to IEG expression

Activation of ERK 1/2 via the transient Ras or sustained Rap1 pathways described above has a profound effect on the ultimate cellular response. In both instances, however, ERK 1/2 phosphorylates to activate ELK1 ($p62^{TCF)}$, which is vital for transcription of the IEG c-Fos.

c-Fos was one of the first IEGs to be identified. Defined as rapid response genes that produce a fast and transient response to growth factors, IEGs are important not only in cell growth and proliferation, but also as proto-oncogenes in tumourigenesis [146]. The c-fos enhancer region is located around 300nt upstream of the transcription initiation site and contains a serum response element (SRE) with a 20bp dyad symmetry element [147], to which the 67kDa serum response factor (SRF) binds in conjunction with ELK1, to initiate transcription of c-Fos [147-149] (Figure 1.10). ELK1 is encoded by *Elk-1*, *Sap1* or *Sap2*, which are all ETS-related genes; those containing an ETS DNA-

binding motif, a SRF interaction domain and a mitogen activated protein kinase (MAPK) transcription activation domain [150, 151]. ELK1 forms a ternary complex with SRE and SRF to initiate transcription. Binding of SRF to SRE is essential for binding of ELK1 [146]. Following transcription c-fos is phosphorylated by pERK 1/2 and RSK (90K-ribosomal S6 kinase) on Ser 374 and Ser 362, respectively. c-Fos dimerises with c-jun, itself activated by c-Jun N-terminal kinase (JNK) phosphorylation on Ser 63 and Ser 73. Together they form activator protein-1 (AP-1) to enhance the transcription of genes involved in cell proliferation [152-154].

Phosphorylation of c-Fos on Ser 374 is a result of transient ERK 1/2 activation, which returns to basal levels before further phosphorylation can occur. In this state c-Fos is highly unstable. This initial phosphorylation does however prime c-Fos for further phosphorylation by exposing an ERK docking, DEF domain such that subsequent phosphorylation can occur on Thr 325 and Thr 331, if ERK 1/2 activity is sustained, resulting in a hyperphosphorylated, stable c-Fos [154].

Such variation in signal duration is a way in which cells use a single pathway to communicate alternate cellular fates. For example, sustained ERK 1/2 activation causes entry into S-phase in fibroblasts and causes differentiation into sympathetic-like neurons in PC12 cells. Moreover, fast and slow delivery of GFs can induce transient or sustained responses. Ji et al. reported that fast delivery increased both the number of neurites and neurite length in acutely activated rat hippocampal neurons, but increased branch points when BDNF was delivered gradually [141, 155, 156]. Such differences in morphology and mitotic nature highlight the importance of regulating signal duration.

1.4.6 Regulating signal duration

Efficient localisation, degradation or recycling of receptor-ligand complexes through endocytosis is vital for regulating signal duration. Although receptor activation is initiated at the plasma membrane, there is evidence that receptors can continue to activate signalling cascades as they are transported along MTs in a dynein-dependent manner thus acting as ‘signalling endosomes’. Any impairment to the transport process may result in aberrant signal duration of multiple pathways [157, 158].

The use of scaffold proteins to tether signalling molecules to distinct subcellular compartments enables alterations in amplitude and length of signalling. Bringing together multiple signalling partners into close proximity allows rapid transmission of signal and likely prevents cross-talk between pathways (reviewed in [159]). The kinase suppressor of Ras (KSR) and MEK partner-1 (MP1) are two scaffold proteins important in MAPK signal duration, that are mobilised in response to RTK signalling. In quiescent cells KSR interacts with MEK1/2 and protein phosphatase 2 (PP2) and is held in the cytosol by the molecular regulator 14-3-3 and the Ras-sensitive ubiquitin ligase impedes mitogenic signal propagation (IMP). GF activation of Ras results in the release of KSR-MEK from PP2 and IMP which, is then free to move to the plasma membrane to assemble up and downstream effectors Raf and ERK 1/2, respectively [159]. In the case of MP1, regulation of ERK is via MP1-MEK1 interactions. The adaptor protein p14 associates MP1 with LEs and is essential for efficient EGF-stimulated ERK signalling [160]. The membrane protein caveolin is an additional scaffold protein that can associate with EGFR, G-protein coupled receptors, G-proteins, kinases and the ‘sprouty’ family of proteins. Sprouty proteins are encoded by the Spry2 gene and have been shown to inhibit ERK activity through binding GRB2 and inhibiting the recruitment of SOS. Following GF stimulation SPRY1 and SPRY2 translocate to the plasma membrane where they are tyrosine phosphorylated within approximately 5 min following GF stimulation however maximal phosphorylation occurs by 15 min. That Spry can be increased through RTK activity indicates a negative feedback for these pathways however post translational modification allows precise control. Caveolin may have a role in enhancing the activity of

SPRY as SPRY phosphorylation and signal inhibition occur at the plasma membrane [161].

Phosphatases are more specific regulators of intracellular signalling. The MAPK phosphatase (MKP) family responsible for dephosphorylation of MAPK are split into three groups; those that dephosphorylate tyrosine (phosphotyrosine-specific protein tyrosine phosphatases [PTP]), including PTP-SL, striatum-enriched PTP (STEP) and hematopoietic PTP (HEPTP), the serine/threonine phosphatases; PP2A and PP2C and the serine/threonine and tyrosine (dual specificity phosphatases [DUSP]) of which there are >30 and at least 13 of which are dual specific MKPs. Interestingly MKP transcription is initiated by MAPK signalling, causing dephosphorylation within the p.ThrXp.Tyr activation loop of MAPK and acting as a negative feedback loop for MAPK regulation [162]. Increased or decreased phosphatase activity leads to reduced or enhanced duration of ERK 1/2, respectively [157,163]

In addition to the wide-scale regulation through endocytosis and phosphatase regulation described above, there is the additional regulatory mechanism of altered gene expression. An example of this is transcription factor 25 (TCF25/nulp1).

TCF25 is a regulator of c-Fos expression. It belongs to the basic helix-loop-helix family but contains a novel DUF654 domain with enhanced transcriptional suppressive activities. There is evidence that the repressive activity of human nulp1 (hnulp1) occurs through recruitment of histone deacetylases and that the DUF654 domain is important for this function. Furthermore expression of hnulp1 significantly reduced the transcriptional activities of SRF, thus suggesting an inhibitory mechanism for prolonged ERK activation as reduced SRF-SRE binding would inhibit ELK1 binding and c-Fos expression [164, 165].

1.5.1 Autophagy

There are three major autophagic pathways; macroautophagy, microautophagy and chaperone mediated autophagy (CMA). Macroautophagy, from here on referred to as autophagy, is a catabolic process in which cytosolic proteins and organelles are sequestered into double-membrane bound vesicles (autophagosomes), originating from phagophores or isolation membranes, to be transported and fused with lysosomes (autophagolysosomes). The contents of autophagolysosomes are degraded in preparation for nutrient recycling when the cell is under extreme stress such as starvation, UV irradiation and heat shock. Microautophagy facilitates general housekeeping functions through the degradation of old or damaged organelles and along with pinocytosis is active throughout cellular resting states. CMA selectively degrades soluble cytosolic peptides with distinctive KFERQ pentapeptide motifs (present in ~25-30% of cell proteins), recognised by heat shock cognate 70 (hsc70) chaperone and co-chaperones for transport to the lysosome for degradation.

The ~30 autophagy-related genes (Atg) were first identified in *Saccharomyces cerevisiae,* although homologues in other organisms have since been identified. Knockdown of many Atgs have been shown to cause cell death in *Saccharomyces cerevisiae* when deprived of nutrients [166, 167].

Autophagy and cell growth are tightly coupled such that nutrient or growth factor deprivation induces the former and reduces the latter. The serine/threonine kinase, mammalian target of rapamycin (mTOR) is a member of the phosphatidylinositol kinase-related kinase (PIKK) family and is the major regulator of autophagy whilst being coupled to control of cell growth. To illustrate this point, mutation of mTOR or inhibition by rapamycin can induce autophagy even in nutrient rich conditions [168].

mTOR forms two complexes mTORC1 and mTORC2. mTORC1 is formed of the regulatory associated protein of TOR (raptor), mTOR associated protein LST8 (MLST8), also known as G-protein beta subunit like (GβL), proline-rich Akt substrate of 40 kDa (PRAS40) and DEP domain-containing mTOR-interacting protein (DEPTOR). mTORC1 requires association with the small GTPase; Ras homolog enriched in brain (Rheb) on intracellular membranes for

activity and is inhibited by the tuberous sclerosis complex (TSC 1/2) which, by acting as a GAP for Rheb inactivates Rheb by GDP association [169]. mTORC2 is formed of rapamycin-insensitive companion of mTOR (rictor), MLST8/GβL, stress activating protein kinase (SAPK)-interacting protein-1 (Sin1), proline-rich repeat protein 5 (PRR5/Protor-1) and DEPTOR [170].

mTORC1 is responsible for regulating autophagy in response to nutrient and growth factor deprivation, and stress. In favourable conditions mTOR associates with and phosphorylates the autophagy-related proteins ATG13 and serine/threonine Unc-51-like kinase1 and 2 (ULK1 and ULK 2, the mammalian homologues of Atg1), which, inhibits the kinase activity of ULK1 and thus phosphorylation of downstream effector; focal adhesion kinase family-interacting protein (FIP200) and therefore autophagy. mTORC via raptor, recruits S6 kinase beta-1(S6K) and eukaryotic initiation factor 4E(eIF4E) inhibitor; eIF4E-binding protein 1 (4E-BP1) to regulate protein synthesis and cell growth. S6K is also a regulator and inhibitor of autophagy. The activation of S6K and 4E-BP1 is through MAP4K3 in reponse to amino acids and although not directly affected by rapamycin, is affected by rapamycin treatment indicitaing that MAP4K3 likely works downstream of mTOR [169, 171].

Autophagic suppression and activation of S6K1 are through distinct mTOR pathways as unlike inhibition of mTOR, inhibition of S6K1 does not induce autophagy under nutrient conditions. Moreover, S6K1 is essential for autophagy to occur [172]. Whilst mTOR can inhibit autophagy independently of S6K1 it may be that the positive regulatory effects of S6K1 and the negative regulation from mTOR provide a balance between the initiation of autophagy to promote cell survival and extended autophagy leading to autophagy-induced cell death [173-175].

Amino acid (particularly leucine and arginine) or GF deprivation results in a reduced cytosolic pool of available amino acids which may affect Rheb-GTP levels and thus the activity of mTORC. In addition amino acid deprivation inhibits the activity of the endosome associated class III phosphatidylinositol 3-kinase (PI3K)/VPS34 thereby inhibiting mTOR. Subsequently, ATG13 mediates the interaction between ULK1/2 and FIP200 to form two complexes of ATG13-

FIP200-ULK1 and ATG13-FIP200-ULK2, the latter of which can only form in the presence of FIP200 (Figure 1.11). ULK 1 and 2 autophosphorylate as well as phosphorylating both FIP200 and ATG13, inducing autophagy. The existence of two complexes with differing binding affinities is indicative of distinct roles in autophagy, perhaps in the formation of autophagosomes [176, 177].

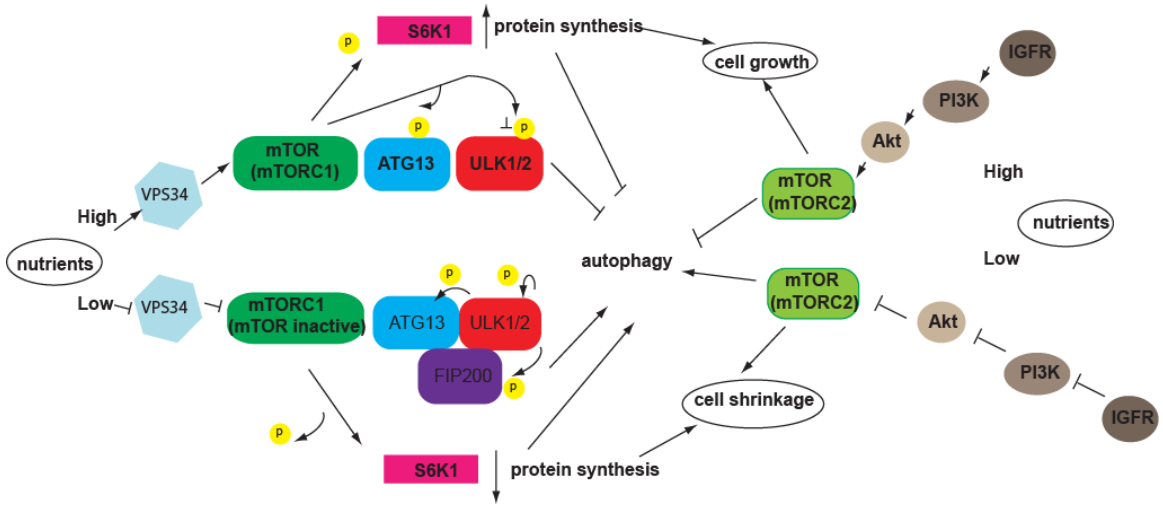

Figure 1.11: mTOR regulation of autophagy. During nutrient rich conditions mTOR actively phosphorylates ATG13 and ULK 1 and 2 to inhibit autophagy. However amino acid deprivation results in inhibition of VPS34 and subsequently mTOR. When mTOR is inactive the inhibition of ULK 1/2 is released, allowing autophosphorylation. In addition ULK 1/2 phosphorylates ATG13 and FIP200 which, complex to initiate autophagosome formation. S6K1 is downstream of mTOR and is both an inhibitor of autophagy and essential for its occurrence. mTORC2 regulation of autophagy is via the IGF receptor (IGFR) and follows the pattern of inhibiting or inducing autophagy when nutrients are high or low respectively.

mTORC2 has been shown to regulate autophagy via the insulin receptor, class I, PI3K and protein kinase B(PKB)/Akt. This pathway is a positive regulator of mTOR and thus a negative regulator of autophagy. Akt also phosphorylates FoxO to inhibit the transcription of autophagy-related genes [168, 178].

1.5.2 c-Jun N-terminal kinase

The major kinases activated in response to stress are c-jun N-terminal kinase (JNK), also known as stress activated protein kinase (SAPK) and p38 kinase. Of these, I would like to take a closer look at JNK.

JNK is encoded by 3 genes; *JNK1*, *JNK2* and *JNK3* which produce 10 mammalian splice variants consisting of 4 from *JNK1*, 4 from *JNK2* and 2 from *JNK3*, *JNK3* isoforms being specific to the brain.

Like ERK, JNK can be activated by cytokines and mitogens. Whereas ERK is activated through RAF, the JNK pathway is divergent at the level of Ras, which binds and activates MEKK1 (a MAPK subgroup, distinct from Raf) and subsequently SEK and then JNK [179, 180]. JNK primarily phosphorylates c-Jun but also ELK1, a transcription factor up-stream of c-Fos. Together, c-Fos and c-Jun form the AP-1 complex and initiate transcription of IEGs for cell proliferation and growth.

JNK is more widely recognised for its activation in response to stress and is capable of activating a programme of cell death. This will be looked at in the following section along with reports that JNK activation is linked to the formation of autophagosomes. Autophagy is often initiated as a mechanism of cell survival during times of stress. However, autophagy can also terminate in an alternative pathway of cell death.

1.5.3 JNK initiation of autophagy and cell death

JNK phosphorylates Bcl2. Bcl2 has been shown to associate with and inhibit pro-apoptotic Bax, and pro-autophagy, Beclin1. Following nutrient deprivation limited phosphorylation of Bcl2 by JNK releases the inhibitory effect on Beclin1, enabling autophagy to be utilised for nutrient recycling. Bcl2 inhibition of Bax remains. However, following sustained starvation JNK phosphorylation of Bcl2 becomes sufficient to disrupt the Bcl2/Bax association so that the cell moves into a program of caspase-activated cell death [181, 182].

In contrast to this there are reports that in response to nutrient or growth factor deprivation, JNK has a suppressive role in autophagy and instead, activates

FoxO and effector Bcl2 interacting mediator of cell death (Bim) to initiate cell death [183, 184]. A similar response has been observed following UV-induced cell stress. During favourable conditions Bim is sequestered by DLC and myosin V however, phosphorylation-dependent release by JNK activates the Bax-dependent mitochondria apoptotic pathway [185]. Moreover, there are interesting reports that the inhibition of Bax can ameliorate SMA symptoms in a mouse model of the disease [186]. Activation of Bim is dependent on cooperative binding of c-Jun, FoxO and Mybs transcription factors, perhaps enabling the utilisation of each pathway independently but also ensuring a definitive signal for cell death [183].

Interestingly, up -regulation of c-Fos and c-Jun in lymphoid cell lines, 60-120 min post nutrient starvation has been observed in cells undergoing programmed cell death and inhibition of c-Fos and/or c-Jun is reported to be sufficient to increase cell survival in nutrient-deprived cells [187]. c-Fos levels are likely to increase simultaneously to c-Jun as JNK phosphorylates ELK1, upstream to c-Fos.

From the data discussed here it would seem that JNK is very important in the determination of cell fate. There is evidence that JNK activated autophagy may promote cell survival yet it may also be an alternative and distinct method of class II, autophagic cell death. It is clear that JNK is involved in an intricately regulated pathway that has a narrow margin between the ability to save a cell under stressful conditions or proceed down a pathway of cell death. The ultimate trigger determining cell fate is not clear however, autophagy appears to have a clear influence whether as cause or consequence and is implicated in the pathology of several neurodegenerative diseases (see section 1.5.4).

1.5.4 Autophagy in neurological disease

Autophagosome formation has been observed in several neurological diseases such as Alzheimer's disease (AD), Amyotrophic Lateral Sclerosis (ALS), Parkinson's disease (PD) and Huntington's disease (HD) [188].

In AD and PD the hallmark pathological features are the accumulation of β-amyloid (Aβ) peptides, produced by the cleavage of amyloid precursor protein, or α-synuclein in Lewy-like aggregates, respectively. In HD toxicity arises from a >35 CAG trinucleotide repeat expansion in the Huntingtin (*HTT*) gene which produces an expanded polyglutamine tract at the N-terminus of the protein. All of these proteins have been shown to be degraded via autophagy [188, 189].

In ALS, transactive response DNA-binding protein 43 (TDP43) and Cu, Zn superoxide dismutase (SOD1) are two further proteins degraded through autophagy. Both TDP43 and SOD1 mutations and aggregates have been identified in familial cases of ALS while mouse models overexpressing TDP43 or transgenic $SOD1^{Gly93Ala}$ have linked such degradation to the autophagic pathway. Moreover, inhibition of autophagy results in increased accumulation of TDP43 and SOD1 in the respective mouse models, which correlate with increased toxicity and cell death [190-192].

These findings indicate a neuroprotective effect of autophagy and a potential therapeutic target for several neurodegenerative diseases. However, autophagosomes have also been identified as a major source of Aβ production in AD, resulting in an increased and toxic soluble source of Aβ and subsequently disease [189].

Together, this suggests beneficial effects of autophagy that have the potential to be utilised, however due to the distal origination of autophagosomes and their spatial dependency for maturation [193], any deficiencies in autophagy transport may tip the balance from one of neuroprotection to one of autophagy-induced cell death.

1.5.5 Dynein and autophagy

Microinjection of anti-DIC antibody into Hela cells has been shown to virtually abolish the rapid retrograde movement of autophagosomes and overexpression of the p50/dynamitin subunit of dynactin resulted in significant reductions in autophagic trafficking [194]. In addition, DLC1 is required for autophagy clearance of protein aggregates and for mediation of autophagy-induced cell death in Drosophila salivary cells [195].

Loa DHC mutation has been shown to impair autophagy processing of toxic protein aggregates in a Ross/Borchelt mouse model of Huntington's disease. In this model mice express Huntington residues 1-171, including 82 glutamine repeats. When crossed with +/*Loa*, disease progression was enhanced, including early onset of muscle tremors and more severe gait abnormalities. This coincided with increased toxic aggregates compared to control mice either heterozygous for *Loa* or toxic HD repeats [196].

These results are suggestive that mutations within DHC, now determined in several neurological diseases may well be a major determinant of the neuronal autophagy stress response and implicate autophagy as causal in many neurodegenerative diseases. The associated signalling pathways, particularly JNK likely play a vital role in determining cell fate.

1.6.1 Research

Although previous reports of reduced retrograde transport had been reported in *Loa* there had been little evaluation of multidirectional transport kinetics, which is important due to cooperation with kinesin. I hypothesised that overall track patterns would be markedly different from those of wild-type, perhaps including an alteration in number or speed of anterograde movements. Moreover, that such impairment would manifest substantial alterations to cell signalling, due to the role of dynein in transporting receptor-ligand complexes for degradation. This, in turn would have global effects on gene expression. The staggering size and non-proliferative nature of neuronal cells, particularly MNs render them more vulnerable to defective transport. I therefore predicted responses to such defects would be far more severe than in the robust fibroblast cells on which many experiments would be established.

Chapter 2

Methods

2.1 Genotyping

E13 tails were digested overnight in 100 mM Tris-HCl pH 8.0, 5 mM EDTA, 0.2% SDS, 200 mM NaCl and 20 µg Proteinase K (New England Biolabs), at 55°C. Samples were vortexed before centrifugation at 13,000 rpm for 10 min and supernatant collected. Qiagen HotStar Taq master mix was used for PCR as per manufacturer's instructions and 0.5 µM of each forward and reverse primer; TGCTGTGTGCTCTCCTGTTT and TTTTACAAGCTTGGCTTTGC, respectively, added. The PCR cycle was set to denature for 15 min at 95°C before 35 cycles of PCR at 95°C for 30 sec denaturation, 62°C for 30 sec annealing and 72°C for 1 min elongation, followed by a final elongation at 72°C for 10 min. The T to A transversion in *Loa* introduces an additional *Rsa1* restriction site within the fragment of *Dync1h1* amplified by PCR products and thus PCR products were digested with *Rsa1* (New England Biolabs) for 2 hours at 37°C. Products were run on a 2% agarose gel to identify the genotypes. Product sizes and a representative gel are shown in Figure 2.1.

a

	672bp	537bp	135bp	24bp
wild-type	+			+
Loa/Loa		+	+	+
+/*Loa*	+	+	+	+

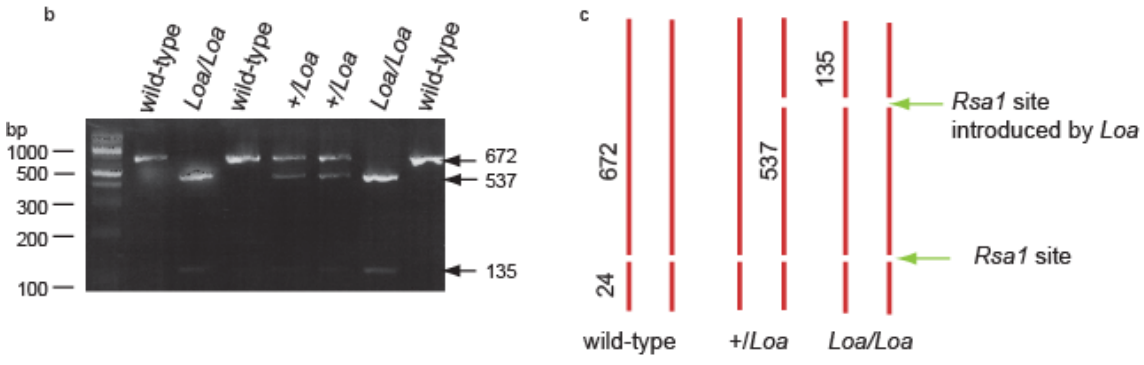

Figure 2.1: Genotyping the *Loa* mouse. a and c) *Loa* introduces a second *Rsa1* restriction site to the partial *Dync1h1* PCR product. Wild-type mice have PCR products of 672 and 24 bp, +/*Loa* have 672, 537, 135 and 24 bp products and *Loa/Loa* have 537, 135 and 24 bp products. b) A representative gel showing the digested PCR products for the three genotypes. Because of their small size, the 24 bp products are not visible on the agarose gel.

2.2 Dissection, cell culture and cell assays

2.2.1 Motor neuron dissection, dissociation and culture

All cell culture media was purchased from Gibco and chemicals from Sigma, unless otherwise stated.

E13 embryos were removed from the uterine horn on ice and in Dulbecco's phosphate buffered saline without calcium or magnesium ($DPBS^{-}$) and supplemented with 1% penicillin/streptomycin (Figure 2.2a). The brain and tails were removed and snap frozen in liquid nitrogen for further analysis or genotyping respectively (see section 2.1 for genotyping protocol).

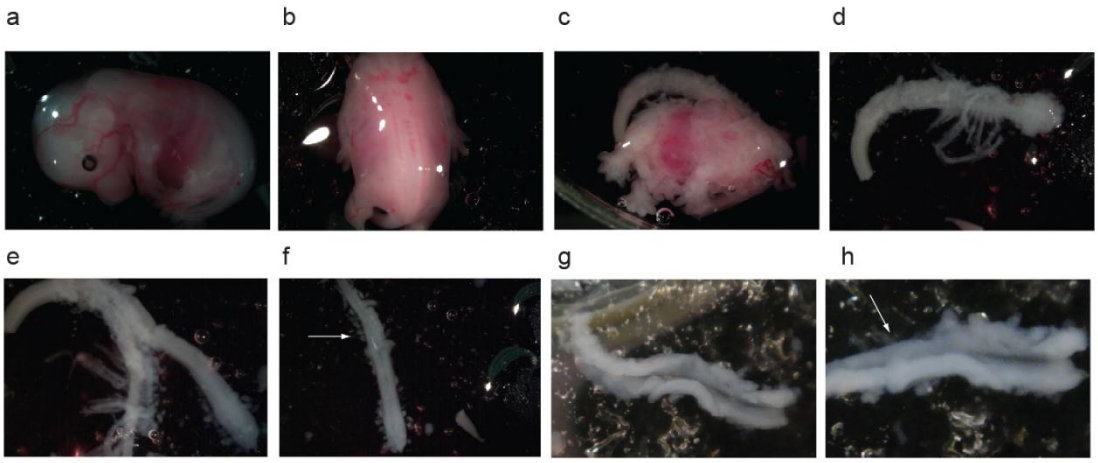

Figure 2.2: Motor neuron dissection from E13 mice embryos. a) An E13 embryo removed from its embryonic sac. b) Embryos were placed on their sternum to visualise the spinal column. c) Skin was removed and the spinal column dissected away from the remaining embryo. d) Spinal column with ribcage and vertebrae clearly visible. e) The spinal cord was removed from the vertebrae. f) Extracted spinal cord. Arrow indicates dorsal root ganglia (DRG). g) Opening of the spinal cord to reveal the MNs along the midline. h) Removal of DRG. Arrow indicates a section where DRG have been cut away.

The body was placed on its sternum with dorsal side uppermost, using the limbs to stabilise (Figure 2.2b). The spinal column was clearly visible. Skin overlying the spinal column was removed and careful dissection resulted in removal of the spinal column from the surrounding tissues (Figure 2.2c-d). The column was turned on its side to separate the spinal cord from the vertebrae (Figure 2.2e),

before orientating the spinal cord, dorsal side uppermost (Figure 2.2f) to open up the spinal cord for removal of DRGs (Figure 2.2g-h). The ventral root containing the anterior horn cells was transferred to a 15ml falcon tube containing fresh $DPBS^-$ with antibiotics and kept on ice while the remaining embryos were dissected.

Following dissection, $DPBS^-$ was removed from the spinal tissue and replaced with 1 ml HBSS, 1% penicillin/streptomycin and 0.025% trypsin. Samples were incubated at 37ºC for 10 minutes with occasional agitation. The solution was then removed and 1 ml of complete L-15 media (L-15 media containing 1% glucose, 1% penicillin/streptomycin, 20 µM progesterone, 5 µg/ml insulin, 100mM/ml putrescine, 100 µg/ml coalbumin, 30nM/ml sodium selenite, 2% horse serum) with 0.4% bovine serum albumin (BSA) and 100µg DNaseI (Sigma #DN25) was added. The tissue was dissociated by pipetting 8 times and then allowed to settle for 2 min before the supernatant containing the cells was collected and transferred to a fresh tube. 1ml complete L-15 media with 0.4% BSA and 20 µg DNase was added to the pellet and triturated a further 8 times, allowed to settle, supernatant removed and added to the previous collection. 900µl complete L-15 media was added to the remaining tissue and a final dissociation carried out before removal of the supernatant and disposal of the remaining pellet.

The pooled supernatants were spun through a 1ml 4% BSA cushion at room temperature for 5 min at 390 xg. The supernatant was discarded and the pellet resuspended in 600 µl MN culture media (Neurobasal media plus 1x B27 supplement, 0.25% glutamine, 0.1% β-mercaptoethanol, 2% horse serum, 0.1% fungizone, 1% penicillin/streptomycin). Cells were added to Lab-Tek II chamber slides (Fisher #155379) or coverslips, pre-coated with poly-D-lysine (Sigma #P7280) and motor neuron culture media was added to make a final volume appropriate for the culture vessel. Media was supplemented with 0.1 ng/ml GDNF (R & D systems), 0.5 ng/ml CNTF and 0.1 ng/ml BDNF (Invitrogen) and cells were incubated at 37ºC in 5% CO_2.

After 24 hours half media was removed and replenished with fresh. The cells were then left undisturbed until day three when 7µM Cytosine β-D-

arabinofuranoside hydrochloride (Sigma #C6645) was added to the culture. MNs were left to mature for at least 1 week, but not more than 10 days before experimental data was obtained.

2.2.2 Establishment and culture of Mouse embryonic fibroblasts

E13 embryos were dissected from the uterus of a culled +/*Loa* female, and placed in ice-cold $DPBS^{-}$. Following complete removal of the placenta, the brain and red organs were removed. The remaining tissue was minced using a scalpel blade and subsequently digested in 2 ml trypsin-EDTA (0.05% trypsin and 0.53 mM EDTA 4Na) for 15 min, with occasional agitation. An equal volume of complete Dulbecco's Modified Eagles Medium (DMEM) supplemented with 15% Hyclone (Fisher), 1% Penicillin/Streptomycin and 1% L-Glutamine was added to neutralise the trypsin and the cells were centrifuged for 5 min at 390xg. Cells were resuspended in complete DMEM and cultured in a 37°C incubator with 3% O_2 and 5% CO_2.

2.2.3 Cell assays

Starvation of MEFs and MNs was for 2 hours using MN culture media without the addition of horse serum (MN starvation media) or complete DMEM without the addition of bovine serum (DMEM starvation media) for MNs or MEFs, respectively.

BDNF at a concentration of 5ng/ml was used for MN stimulation and this was applied either as a 10 min 'pulse' for live-cell imaging or left *in situ* as 'continuous' stimulation for cell signalling assays. 40µg/ml pHrodo-dextran (Invitrogen) was simultaneously applied for live-cell imaging.

EGF was used for stimulation of MEFs at a concentration of 20 ng/ml and was applied either as a pulse for cell fractionation or continuous stimulation for other biochemical analysis. Stimulation for microscopy was a 10 min pulse of EGF-AlexaFluor546 (Molecular Probes) for Live-cell imaging, or EGF-AlexaFluor555 (Invitrogen) for fixed-cell imaging (to prevent bleed through with other fluorophores used, see section 2.5).

For live-cell imaging MNs and MEFs were rinsed and replenished with warmed MN and MEF starvation media respectively, however the neurobasal media or DMEM was replaced in both instances with Leibovitz L-15 CO_2-independent media. Imaging was undertaken at 37°C.

2.3 Biochemistry

All chemicals and reagents were from Sigma unless otherwise stated.

2.3.1 Cell lysis and tissue homogenisation

For whole cell lysates or homogenisation of E13 brain tissue, where extraction of nuclear contents was important, lysis was in 25 mM tris-HCl, pH 7.4, 150 mM NaCl, 1 mM EDTA, 1% NP-40, 5% Glycerol, 1x protease inhibitors and 10 µl/ml phosphatase inhibitors 1 and 2 (Sigma). For brain homogenisation in which nuclear disruption was not essential, brains were homogenized in a Dounce homogeniser with $DPBS^{-}$, protease and phosphatase inhibitors as above. A volume 9x weight of tissue was used. All lysates were incubated on ice for 15 min before being vortexed and centrifuged at 13,000 rpm in a table top Eppendorf microcentrifuge, set at 4°C. Supernatants were collected and, where possible, protein concentrations were determined using a Pierce BCA Protein Assay Kit. In situations of very low protein or small sample volume, equal volumes were loaded onto electrophoresis gels.

Subcellular Cell fractionation was carried out using the Calbiochem Proteoextract Subcellular Proteome Extraction Kit, as per the manufacturer's instructions.

2.3.2 λ-Protein phosphatase treatment

λ-Protein phosphatase (New England Biolabs) treatment of cell lysates was carried out as per manufacturer's instructions and incubated at 30°C for 30 min.

2.3.3 Immunoprecipitation

Immunopreciptiation was carried out at 4°C with ice cold buffers throughout.

Protein A-Sepharose beads (Zymed Laboratories Inc.) were washed twice in ice-cold PBS- and centrifuged at 3,000 rpm for 2 min to collect the beads.

Beads were then washed with $DPBS^-$ containing 1x protease inhibitors and 10 µl/ml phosphatase inhibitors before being incubated for 2 hours with 0.05 µg/ml mouse anti-dynein cytoplasmic 74.1 kDa monoclonal antibody (a generous gift from Dr Kevin Pfister, University of Virginia) or mouse IgG (Millipore #PP54) control under gentle agitation. Meanwhile brain homogenates were pre-cleared by incubating with washed beads and gently agitating for 1 hour. Brains were homogenised using a Dounce homogeniser in buffer without detergent or high salt concentration. This would enable identification of altered protein-protein interactions which otherwise could be substantially altered by detergent and salt [82].

Antibody bound beads were collected by 2 min centrifugation at 3,000 rpm and were then washed in $DPBS^-$ to remove any free antibody. Cleared brain homogenates were separated from the beads by 5 min centrifugation at 13,000 rpm and equal amounts of brain extract from *Loa/Loa* and wild type were added to the antibody beads for incubation overnight, with gentle shaking. Beads were collected by centrifugation at 2,000 rpm for 2 min and washed three times in $DPBS^-$. They were then washed for 10 min in H_2O by rocking and finally spun at 13,000 rpm for 5 min to collect the beads. Proteins were re-suspended into SDS-PAGE sample loading buffer (0.125 M Tris-Cl, 4% sodium dodecyl sulfate, 20% v/v glycerol, 0.2 M dithiothreitol (DTT), 0.02% bromophenol blue, pH 6.8, made up in double distilled H_2O) by boiling for 5 min, and equal volumes were loaded onto a gel for westernblot analysis.

2.3.4 Immunoblotting and analysis

Precast NuPage 4-12% density gradient gels (Invitrogen) were used for all westerns other than those of KLC-1, for which homemade 10% SDS page gels were used. Proteins were transferred to a Hybond-LFP PVDF membrane (Amersham Bioscience) at 110 V, for 75 min at 4°C. Membranes were blocked in wash buffer (PBS – 0.2% Tween 20) supplemented with 5% non-fat milk for > 60 min and then rinsed in wash buffer before the application of the primary antibody in appropriate wash buffer and incubation period (Table 2.1). Membranes were then washed once in wash buffer for 15min at room temperature and then 3 times for 5 min each with rinses in between washes before appropriate secondary antibodies (Table 2.1), were applied for 45 min at

room temperature. Repeat washes were applied and either Western Lighting Enhanced Chemiluminescent Luminal Reagent or CDP-Star chemiluminescent substrate (Sigma) was applied appropriately to allow detection on film.

primary antibody	**dilution and incubation buffer**	**incubation time and temp**	**secondary antibody, dilution and incubation buffer**
phospho-p44/42 MAPK (ERK 1/2) Thr 202/Tyr 204 (New England Biolabs #4377S)	1:1,000 WB+ 5% BSA	O/N 4°C	anti-rabbit HRP (GE Healthcare)1:10,000 WB+ 5% non-fat milk
c-Fos (Santa Cruz Biotechnology sc-52)	1:400 WB+ 5% BSA	O/N 4°C	anti-rabbit HRP 1:10,000 WB+ 5% non-fat milk
phospho-SAPK/JNK T183/Y185 (Cell Signalling #9251S)	1:1,000 WB+ 3% BSA	O/N 4°C	anti-rabbit HRP 1:10,000 WB+ 5% non-fat milk
β-actin (Sigma A5316)	1:15,000 WB	60 min R/T	anti-mouse HRP (Dako Cytomation)1:30,000 WB
Phospho-XRCC1S485/T488 (Bethyl Laboratories S461)	1:3,000 WB	60 min R/T	anti-rabbit HRP 1:10,000 WB
KLC1 (Santa Cruz Biotechnology sc-25735)	1:200 WB	60 min R/T	anti-rabbit HRP 1:10,000 WB
DIC (gift from Dr Kevin Pfister)	1:1,000 WB	60 min R/T	anti-mouse AP (Sigma)1:10,000 WB
Calnexin (Santa Cruz Biotechnology sc-6465)	1:1,000 WB+ 5% BSA	O/N 4°C	anti-goat AP (Sigma)1:10,000 WB
α-tubulin (Upstate 05-829)	1:2,000 WB	60 min R/T	anti-mouse HRP 1:10,000 WB
TCF25 (Sigma AV47624)	1:400 WB+ 5% BSA	O/N 4°C	anti-rabbit HRP 1:10,000 WB + 5% non-fat milk

Table 2.1: Antibodies for immunoblotting. WB = wash buffer, O/N = overnight, R/T = room temperature, HRP = Horse radish peroxidase, BSA = Bovine serum albumin, AP = Alkaline phosphatase. All secondary antibodies were applied for 45 min at R/T.

For the blocking peptide assay the c-Fos blocking peptide (Santa Cruz sc-52) was incubated at room temperature for 30 min with the c-Fos antibody at a final concentration of 1µg/ml, before being added to the protein-bound membrane and protocol continuation as for c-Fos immunoblotting outlined above. An immunoblot without the blocking peptide was run in parallel to determine the specificity of the antibody.

Films were scanned using an Epson Perfection 4990 Photo scanner and Quantified using ImageJ gel analysis software. Data was transferred to Excel, GraphPad and Adobe Illustrator for data representation and statistical analysis.

2.4 Immunocytochemistry

All reagents and antibodies were diluted in DPBS- and all washes carried out using DPBS-. Cells were washed twice and fixed in 4% paraformaldehyde for 15 min. Then, 0.1% Triton X-100 was applied for 5 min to permeabilise the cells, which were then blocked for 60 min in 2% BSA. The cells were then stained with anti-α-tubulin (Upstate) at 1:2000, Islet1 and Hb9 at 1:200 (generated by Dr Wenhan Deng from hybridoma cells obtained from the developmental studies hybridoma bank), or MAP2 (Chemicon International) at 1:500 dilution, where applicable, for 30min at room temperature before being washed three times and applying AlexaFluor 488 conjugate anti-mouse (Molecular Probes) at 1:200 for 30min. Coverslips were then washed three times and either mounted using Prolong gold anti-fade reagent with DAPI (Invitrogen) or incubated with Draq5 (Cell Signalling) at 1:1,000 dilution for 5 min before being rinsed and mounted using Prolong gold anti-fade reagent (Invitrogen).

2.5 Image acquisition and microscopy analysis

Live-cell images were collected at 10 min and 30 min post removal of growth factor and tracks measured required an overall net retrograde migration to be included in the analysis. EGF-AlexaFluor546 images were captured with a 100X objective, using a TRITC filter (ex. 490/20, em. 528/38) from a 0.2 sec exposure at 100% transmission and a time-lapse of 2 sec for 1 min duration. The MN images were acquired with a 100X objective using a 0.08 sec DIC exposure at

100% transmission and 1 sec exposure, 100% transmission for TRITC with a 3 sec time-lapse for 2 min using an Applied Precision personal Delta Vision microscope. The Image J 'Manual Tracking' plugin (Fabrice P.Cordelieres) was used to gather track information.

For EGF assays fixed-cell images were obtained using FITC (ex.490/20 em.528/38), Cy5 (ex. 640/20 em. 685/46) and DAPI (ex. 360/40 em.457/50) filters and a 60X objective, on an Applied Precision Core Deltavision microscope. Exposures were 0.025 sec, 5 sec and 0.05 sec respectively at 100% transmission. Exposures were uniform for all images.

Deconvolved images were analysed with the aid of standard image J programs. For this; images were converted to 8-bit and following subtraction of background fluorescence, a standard threshold was set for all images analysed such that particles over the threshold were counted. The polygon drawing tool was utilised to measure the area of the cells, visualised using FITC to capture α-tubulin staining.

Both live-cell imaging and EGF assays were analysed with the assistance of Excel and GraphPad. A Mann-Whitney U test was applied to determine significance.

Kymographs were produced using software from the MacBiophotonics ImageJ for microscopy users. Adobe Illustrator was utilised for data representation.

2.6 RNA extraction, reverse transcription and qRT-PCR

For qRT-PCR, RNA was extracted using the NucleoSpin II RNA extraction kit, and cDNA was generated using the Promega reverse transcription system. Gene sequences were found in the National Centre for Biotechnology Information (NCBI ID no's:TCF25:66855, KLC1:16593, 18S:19791) data base and were cross-referenced using a Basic Local Alignment Search Tool (BLAST) to those found on the Protein Knowledgebase UniProtKB) data base. Primers were designed from this information using the Invitrogen primer design tool. qRT-PCR was carried out by adding 2x QuantiTect SYBR Green PCR master mix (Qiagen) to 1 mM each of forward and reverse primers in Table 2.2.

Gene	forward Primer	reverse Primer
18S	gccgctagaggtgaaattctt	cattcttggcaaatgctttcg
KLC1	tcttcccaaatgacgaggac	ctgtacaccagggccaagat
Tcf25	cctgatacagcaggcactca	tgacctccccaggtacagac

Table 2.2: qRT-PCR primers. Primers for the two genes of interest, KLC1 and TCF25 along with the 18S control.

1.5 µg cDNA was required per reaction and the overall reaction volume was made up to 30 µl with RNase free water. A Stratagene Mx4000 qPCR machine was set to denature at 95ºC for 15 min before 40 cycles of 94ºC denaturation for 30 sec, annealing at 56ºC for 30 sec and elongation at 72ºC for 30 sec. A dissociation curve followed each real-time cycle.

All data sets were collected from at least three brains for each genotype. Each qRT-PCR reaction was carried out in triplicate with at least three reactions for each gene. For analysis the mean CT of the 18S triplicates were calculated for each genotype and the means were subtracted from each genotypes individual triplicate CT for the gene of interest to give a calibrated ΔCT. The mean ΔCT of the wild-type was then subtracted from the ΔCT of each genotypes gene of interest ΔCT to give a comparative ΔΔCT. To calculate a fold change, the ΔCT of the wild-type gene of interest triplicates was divided by the mean ΔCT of the wild-type resulting in a mean value of 1. A fold change for the other genotypes was calculated by $2^{-\Delta\Delta CT}$ for each triplicate. Fold change significance was analysed across the experiments using GraphPad Prism [82].

Chapter 3

Endosome trafficking is aberrant in *Loa*.

3.1 Introduction

Dynein is an essential retrograde motor protein. The p.Phe580Tyr mutation in the *Loa* mouse produces a significant neurodegenerative phenotype with many similarities to human disease. Although the precise sequence of events leading to neuronal migration defects and neurodegeneration are yet to be determined, we can use multiple tools to observe intracellular events that likely contribute to the disease process.

The aim for this chapter was to determine whether the *Loa* mutation would affect the intracellular transport of endocytosed GF-bound receptors. To this end, I have used a cohort of fixed and live cell microscopy to analyse endosome movements in wild-type and *Loa* MEFs and primary MNs.

3.2 EGF time course in MEFs

Using fluorescently conjugated epidermal growth factor (EGF-Alexa Fluor555), it was possible to compare the localisation of endocytosed receptor-ligand complexes in wild-type and *Loa/Loa* MEFs. Cells were starved for 2 hours before being stimulated with 20ng/ml EGF-Alexa Fluor555 for 10 min. The cells were then rinsed and fixed for imaging at 0, 10, 30 and 60 min chase using an Applied Precision Core DeltaVision microscope (exact parameters for imaging can be found in section 2.5). Cells were stained for α-tubulin to determine the outer boundaries of the cells and 15 cells per genotype and time point were analysed (Fig. 3.1).

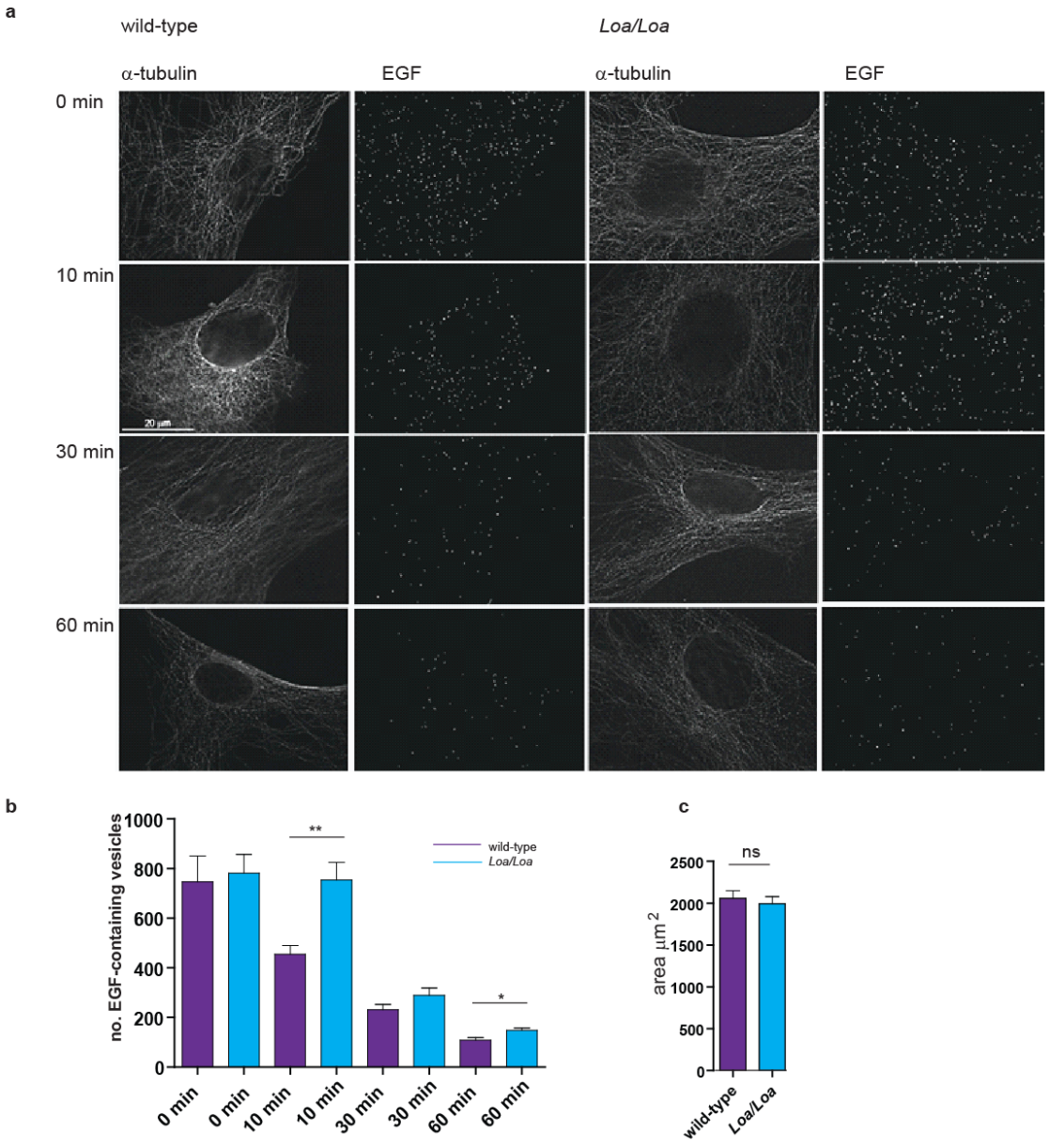

Figure 3.1: EGF-Alexafluor555 processing is altered in *Loa* MEFs. a) Representative images of EGF-Alexafluor555 in wild-type and *Loa/Loa* MEFs following a 10 min pulse. Images taken at 0, 10, 30 and 60 min chase show increased numbers of EGF-containing vesicles in *Loa/Loa* compared to wild-type over time. b) Quantification of the number of EGF-Alexafluor555 vesicles remaining at each chase time n=15. c) Average area analysed for vesicle counting was the same in wild-type and *Loa/Loa*, n = 37.

At 0 min chase both wild-type and *Loa/Loa* had similar numbers of EGF-containing vesicles: 746.9±103.8 and 781.9±74.89 respectively (all deviations are given as standard error of the mean (SEM) unless otherwise indicated) (Fig. 3.1a-b). However by 10 min chase there were significantly more EGF-Alexafluor555 containing vesicles remaining in *Loa/Loa* when compared to wild-type (wild-type = 454.6±34.6, *Loa/Loa* = 753.5±71.2 and P = 0.0014**).

By 30 min a distinct reduction in particle numbers in both genotypes was apparent, although, quantification remained higher in *Loa/Loa* than in wild-type (289.5±29.3 and 231.529.3± 26.9, respectively). The 60 min chase highlighted significance once again with wild-type particles having reduced to 108±10.1 and *Loa/Loa* to only 148.*1*±9.9 (P = 0.0152*). This may indicate a delay in EGF-AlexaFluor546 degradation however, due to the prominent difference at 10 min chase these findings may indicate a delay in EE fusion and MVB formation (Figure 3.2a-b).

To ensure that the number of particles was not simply a measure of the area analysed, 37 cells from each genotype were measures to check that the average area used for analysis was the same for each genotype. No significant difference was found (wild-type = 2057μm^2±89.29 and *Loa/Loa* = 1992μm^2±86.72) (Figure 3.2c).

3.3 Live-Cell Imaging of EGF in MEFs

To gain further insight into vesicular movement during trafficking, live-cell imaging was carried out.

The same protocol as in 3.2 was implemented, but instead of fixing the cells, they were rinsed and left in warmed CO_2-independent DMEM starvation media for imaging at 10 min and 30 min chase (exact imaging parameters can be found in section 2.5). EGF-Alexafluor546 movement was tracked using Image J manual tracking plugin (Fabrice P.Cordelieres) (Figure 3.2a-c.)

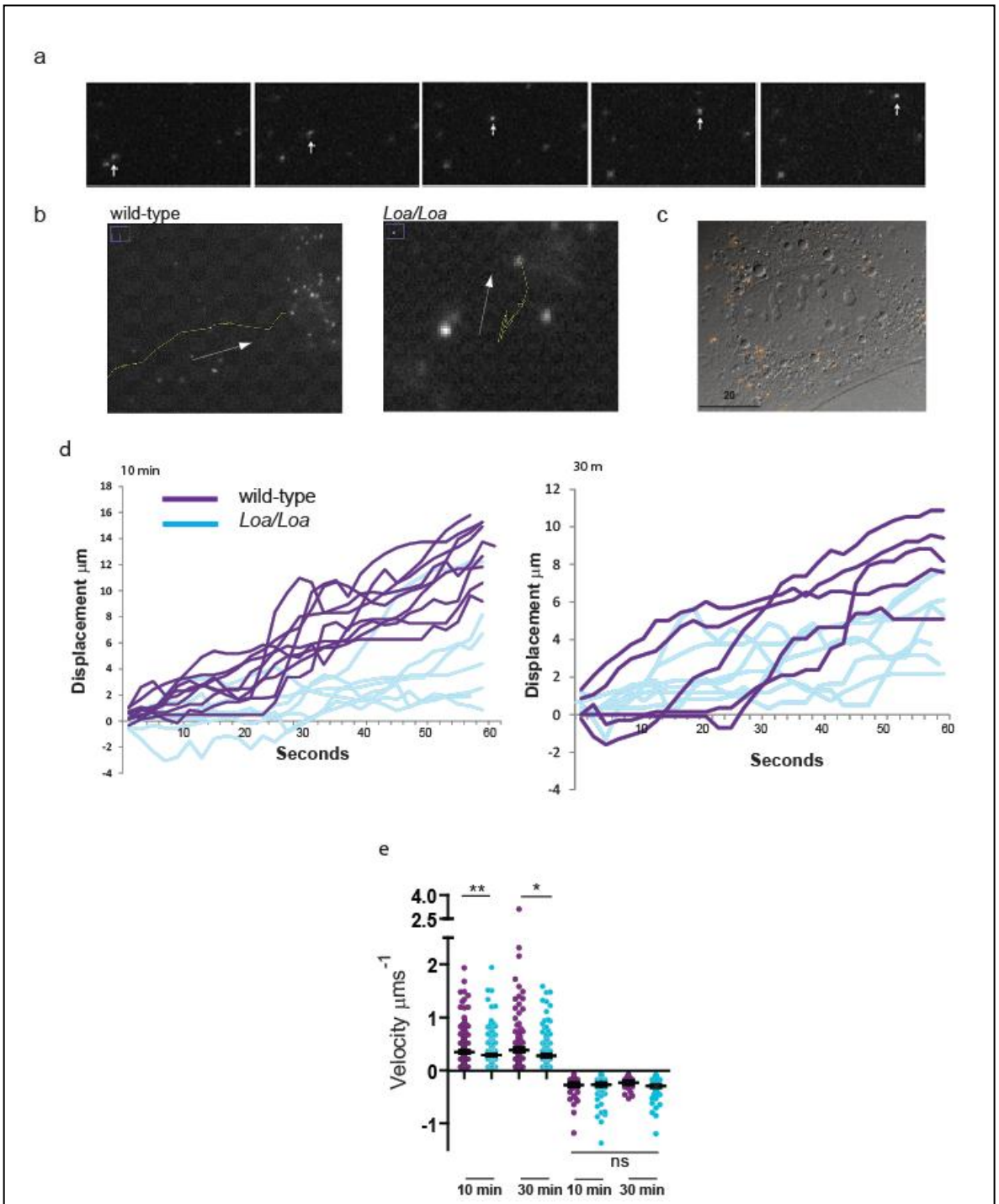

Figure 3.2: Endosome trafficking is aberrant in *Loa.* a) Frame sequence of EGF-Alexafluor546 movement in a wild-type MEF. b) Representative tracks from wild-type and *Loa/Loa* MEFs. The *Loa/Loa* path appears shorter and more ambiguous than in wild-type. c) DIC image overlaid with fluorescence from EGF-Alexafluor546. d) Representative track displacements in wild-type and *Loa/Loa* at 10 and 30 min chase. *Loa/Loa* tracks are shorter and displacement is slower than in wild-type. e) Retrograde velocity (positive values) is reduced in *Loa*/*Loa* at 10 and 30 min chase. Anterograde velocity (negative values) is not significantly different across the genotypes.

All data analysed is from sample sizes of; n = 349 movements for wild-type from 13 tracks (4 cells) and 419 movements from 15 tracks (5 cells), for *Loa*/*Loa,* at 10 min. At 30 min; n = 232 movements for wild-type from 8 tracks (5 cells) and 337 movements for *Loa*/*Loa* from 12 tracks (6 cells).

Retrograde velocity was measured as positive movements towards the nucleus whereas anterograde velocity is represented as negative values.

Initial observations identified a distinct lack of the fastest carriers, moving at velocities above 2 μms^{-1} in *Loa/Loa*, and 60% less moving at velocities above 1 μms^{-1} at both time points) (Figure 3.2d-e).

In both genotypes examined the majority of displacement occurred at speeds between 0 and 0.25 μms^{-1}. This was not surprising as we, like others observed many endosomes 'rolling' around for several seconds before longer movements were made [20,125]. For this reason these readings are more accurately a mixture of tiny retrograde, anterograde and side-wards steps than they are of distinct retrograde displacement.

Analysis of dynein-dependent retrograde velocities highlighted a significant shift towards slower velocity in *Loa/Loa* at 10 and 30 min chase (P = 0.0025** at 10 min and P = 0.0177* at 30 min) (Figure 3.2e). Table 3.1 shows the minimum, median and maximum retrograde velocities for both genotypes. At 10 min chase anterograde, stationary and retrograde movements were ~11%, ~13% and ~77% respectively for wild-type and ~22%, ~15% and 63% for *Loa*/Loa, indicating a shift towards reduced retrograde movements and increased stationary pauses and anterograde movements in *Loa/Loa*. By 30 min chase the trend remained clear with anterograde, stationary and retrograde movements being ~10%, ~27% and ~63% respectively in wild-type and 18%, ~25% and ~58% in *Loa/Loa.* Anterograde velocities were not significantly different across the time points or genotypes (Figure 3.2e).

	minimum	median	maximum
wild-type	0.07	0.27	1.95
Loa/Loa	0.07	0.21	1.95
wild-type	0.07	0.23	3.16
Loa/Loa	0.07	0.17	1.60

Table 3.1: Minimum, median and maximum retrograde velocities in wild-type and *Loa/Loa* MEFs. 10 min (dark pink) and 30 min (pink) chase. Units = μms^{-1}.

To determine whether the altered dynamics of *Loa/Loa* velocities compared to wild-type was sufficient to affected overall displacement, I analysed all tracks (76% of total tracks measured) that remained in focus for at least 96% of frames. Displacement in *Loa*/*Loa* was significantly reduced when compared to wild-type at 10 min chase (P = 0.0020**). Track length ranged from 9.2 µm to 15.8 µm (median 13.4 µm) in wild-type and 0.90 µm to 12.2 µm (median 4.4 µm) in *Loa/Loa.* This trend remained at 30 min, with wild-type total displacement ranging from 5.1 µm to 42.3 µm (median 8.2 µm) and 2.2 µm to 9.2 µm (median 5.3 µm) in *Loa/Loa*. The reduced displacement measurements in wild-type across the time points was found to be significantly different (P = 0.0442*) (Figure 3.3).

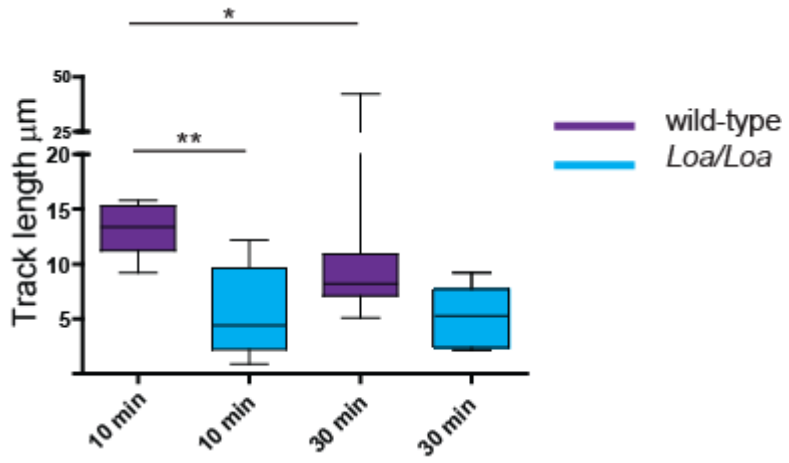

Figure 3.3: Overall track length is reduced in *Loa/Loa* compared to wild-type. 10 and 30 min chase.

During analysis, movements were observed that were neither retrograde nor anterograde, but were distinct sideward movements relative to the directional movement to which the endosome was originally travelling. ~5% of wild-type movements across both chase points were classed as side steps whereas in *Loa/Loa* the number was increased to ~7%. When measuring the velocity and distance of these sideward movements it was found that in *Loa/Loa* the velocity was significantly slower (medians of 0.31 μms^{-1} and 0.17 μms^{-1} for wild-type and *Loa/Loa* respectively, P = 0.0003***) and movement was over shorter distances (0.90 µm and 0.42 µm for wild-type and *Loa/Loa,* respectively, P = 0.0003***) (Figure 3.4 a-b).

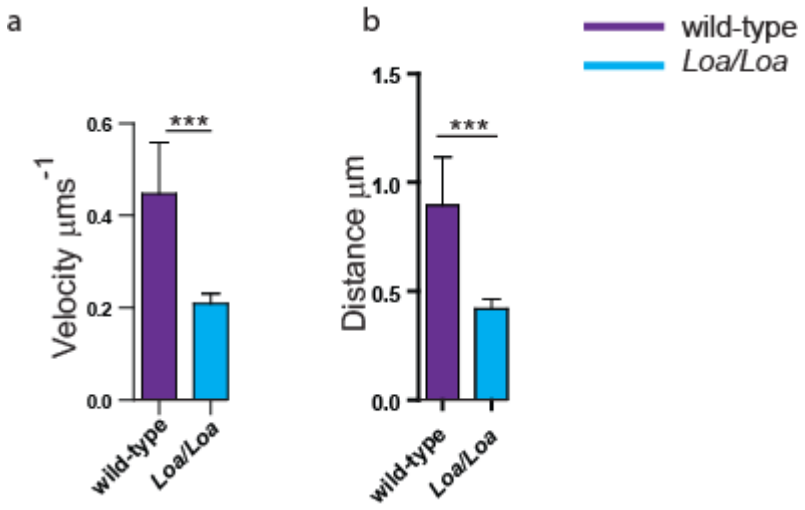

Figure 3.4: Altered side-stepping in *Loa/Loa.* a) Side stepping velocity is reduced in *Loa/Loa* compared to wild-type. b) Distance travelled during side stepping is reduced in *Loa/Loa*. For side stepping velocity and distance analysis, measurements from 10 min and 30 min chase were pooled together.

3.4 Live-cell tracking in motor neurons

As dynein mutations have been linked to several neurological diseases, it was important to collect data from neuronal cells. Although both sensory and MN defects have been identified in the *Loa* mouse, I chose to examine the cellular processes within MNs, to advance the original work by Hafezparast et al; 2003, which identified an impairment in retrograde axonal transport in this cell type. A further consideration was the knowledge that the dynein mutations discussed in the introductory sections 1.2.2-1.2.5, highlight the dominant nature of dynein mutations in neurological disease. For this reason the use of *+/Loa* MNs were deemed to be more representative of human disease than *Loa/Loa* and were thus used for MN experiments.

MNs were dissected at E13 and cultured to maturity for 1 week. MN status was determined by morphological comparison of MNs from the *Loa* mouse colony and those from a colony expressing green fluorescent protein (GFP) under the MN specific transcription factor, Homoeobox gene 9 (Hb9). Characteristics included; large cell bodies with several dendritic processes extending to form extensive branching patterns, and a single axon (Figure 3.5 a-b). Figure 3.5c shows light microscopy images of MNs cultured at day 1 and day 7, to demonstrate the extensive and elaborate branching patterns that are achieved by the time the MNs have matured.

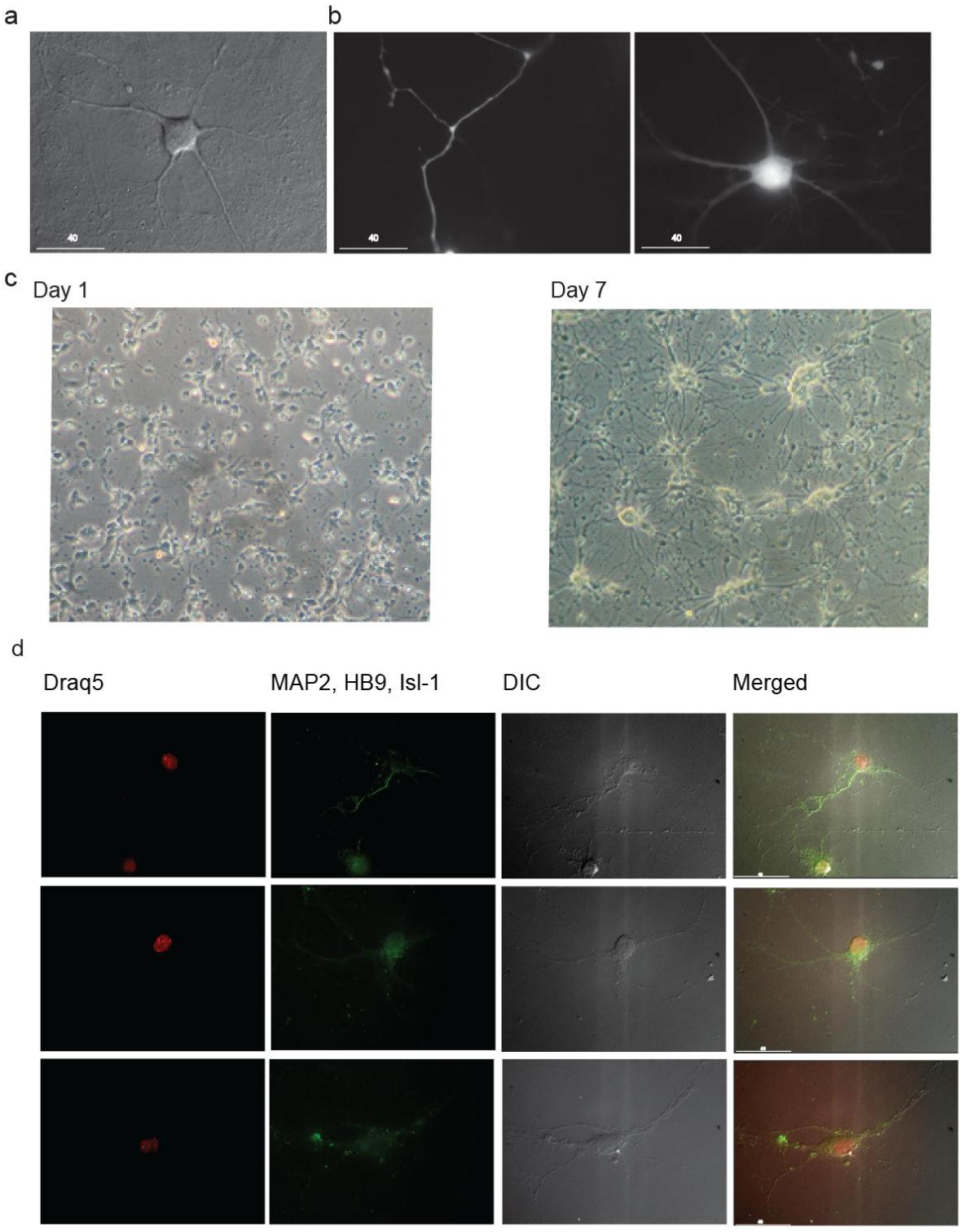

Figure 3.5: Confirmation of MN cultures a) DIC image of a MN from the *Loa* colony, showing the same morphology as MNs expressing GFP under the Hb9 promoter (b). c) Light microscopy images of MNs at day 1 and day 7 in culture, showing the extensive branching that has occurred by day 7. d) MNs stained (green) for MAP2, Hb9 and Islet1 (Isl-1) in top, middle and lower panels respectively. Draq5 (red) stains DNA in the nucleus.

In addition, MNs were stained for Hb9, Islet1, which is expressed early in MN differentiation and MT associating protein 2 (MAP2), which is expressed predominantly in dendrites. Positive staining (green) was apparent for each (Figure 3.5d).

Live-cell tracking in MNs was initiated following a 2-hour starvation period with a 10 min simultaneous pulse of 5 ng/ml BDNF and 40 µg/ml of the pH- sensitive fluorescent dye pHrodo, linked to dextran. MNs were rinsed in media and replenishment with warmed MN starvation media for imaging (exact parameters can be found in section 2.5). pHrodo does not fluoresce in neutral pH of the media, however upon endocytosis into a more acidic environment the fluorophore becomes active and more intense as acidity increases. The simultaneous stimulation was deliberately used to increase the endosomal pool. Due to the non-specificity of pHrodo for RTKs however, the data collected is not solely representative of RTK transport, but of global retrograde transport in these cells.

The range of velocities observed in MN tracking experiments were similar to those in the MEF cells, from -1.36 μms^{-1} (anterograde) to > 2 μms^{-1} (retrograde) and equally, there were fewer endosomes moving at speeds in excess of 1μms^{-1} in +/*Loa* compared to wild-type at both 10 and 30 min chase (40% less at 10 min and 80% less at 30 min) (Figure 3.6b).

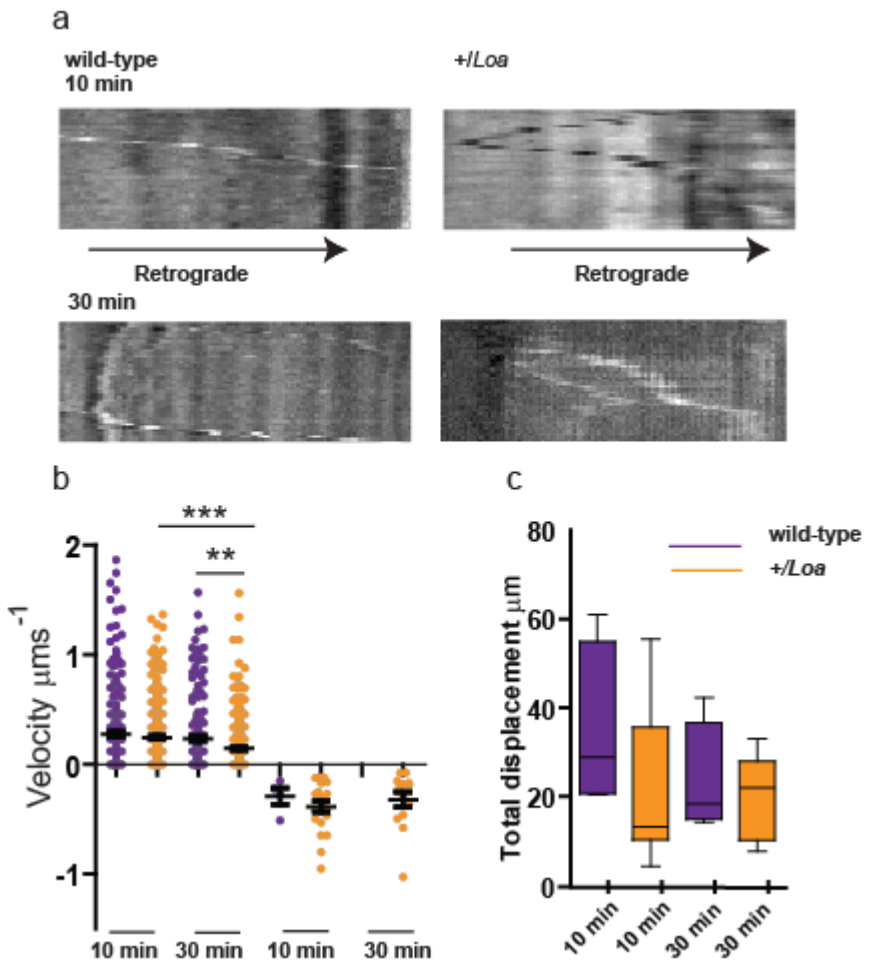

Figure 3.6: Transport is aberrant in +/*Loa* MNs. a) Kymographs of MN trafficking in wild-type and +/*Loa* MNs. b) Retrograde and anterograde velocities in wild-type and +***/Loa.*** d) Track displacement at 10 and 30 min chase. For each chase time analysed 'n' values were as follows; at 10 min, wild-type n = 257 movements from 8 tracks (5 cells) and n = 373 frame displacements from 8 tracks (7 cells) for +/*Loa*. At 30 min wild-type n = 194 movements from 7 tracks (3 cells) and +/*Loa* n = 314 movements from 8 tracks (3 cells).

Retrograde velocities identified a trend for slower velocities in +/Loa at 10 min, which reached significance at 30 min chase (P = 0.0090**) Figure 3.6b and Table 3.2.

	minimum	median	maximum
wild-type	0.05	0.12	1.87
Loa/Loa	0.05	0.12	1.37
wild-type	0.05	0.12	1.57
Loa/Loa	0.05	0.05	1.57

Table 3.2: Minimum, median and maximum retrograde velocities in wild-type and *+/Loa* MNs. 10 min (dark pink) and 30 min (pink) chase. Units = μms^{-1}.

Retrograde velocity decreased in +Loa between 10 and 30 min chase (P = <0.0001***), perhaps due to increased endosome size, producing an increased challenge to remain associated with mutant dynein and/or MTs (Figure 3.6b).

Interestingly, although anterograde speed was not significantly different between the genotypes, there was an increased propensity towards anterograde movements in +/*Loa* compared to wild-type MNs, which had a distinct lack of such movements during the 30 min chase (Figure 3.6b).

Upper and lower ranges of track displacement in +/*Loa* compared to wild-type were distinctly different at 10 min (20.4 µm to 61.0 µm in wild-type and 4.2 µm to 55.4 µm in +/*Loa*) and at 30 min chase (14.1 µm to 42.2 µm for wild-type and 7.6 µm to 33 µm for +/*Loa*) (Figure 3.6c).

3.5 Chapter 3 summary

Data in this chapter has shown that the *Loa* mutation impairs retrograde velocity in two very different cell types. MEFs are more resilient in nature than MNs and it is likely that the susceptibility of MN to degeneration comes from the vast axonal distances that are difficult to overcome, hence the neurological phenotype observed. In the next chapter I have investigated the effect of the delayed GF-receptor transport on intracellular signalling.

Chapter 4

Impaired retrograde trafficking affects cell signalling

4.1 Introduction

Chapter 3 showed impaired transport of GFs and their receptors in *Loa* when compared to wild-type. Here, I will report the effect of delayed transport on ERK and JNK signalling.

Endocytosis of receptor-ligand complexes creates a signalling endosome that can initiate signalling pathways until such time that the receptor-ligand complex is sorted for recycling or degradation. Due to the delayed transport in *Loa*, I hypothesised that, as a result, intracellular signalling would be prolonged in *Loa*.

4.2 Activation of ERK 1/2 is prolonged in *Loa* MEFs following EGF stimulation

To investigate the effect of delayed endosome sorting and degradation on intracellular signalling, the ERK 1/2 pathway was explored. Wild-type and *Loa/Loa* MEFs were starved for 2 hours before stimulation with 20 ng/ml EGF. Cells were lysed to ensure disruption of all cellular sub-fractions at 10, 30, 60, 120, and 180 min post application of the ligand.

As shown in Figure 4.1, a peak of phosphorylated (active) ERK 1/2 (pERK 1/2) was apparent at 10 min post stimulation and, as expected [154] was transient such that by 60 min the wild-type levels were nearing those of the starved control. In contrast pERK 1/2 activation was found to be prolonged in *Loa/Loa* such that at 30 min post stimulation there was a 1.5 fold increase in pERK 1/2 levels in *Loa/Loa.* At 60, 120, and 180 min the fold increases were 1.4, 1.2, and 5.3, respectively, when compared to wild-type (Figure 4.1a-b).

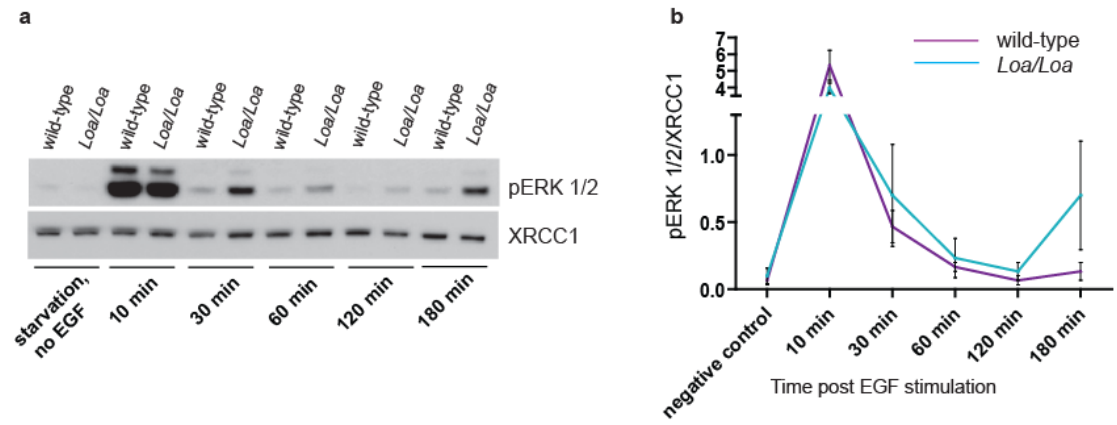

Figure 4.1: ERK 1/2 activation is prolonged in *Loa* MEFs. a) Following starvation, continuous stimulation with EGF produces a marked increase in pERK 1/2 activation, which is prolonged in *Loa/Loa* up to and including 180 min, n=3. b) Quantification of ERK 1/2 signalling in (a).

It has been noted that at the 180 min time point, ERK 1/2 activation appears to be increasing in *Loa/Loa.* pERK 1/2 is known to translocate and cycle between the cytosol and nucleus [197] and thus it would be interesting to see if nuclear

translocation was affected in *Loa*, perhaps contributing to the elevated and apparent cyclic nature of pERK 1/2 in *Loa.*

4.3 pERK 1/2 translocation is not affected in *Loa*

To determine whether pERK 1/2 translocation was affected in *Loa*, subcellular fractions from wild-type and *Loa/Loa* MEFs were probed. For these experiments cells were subjected to a 10 min pulse of EGF prior to the chase periods of 10 and 30 min. A pulse was deemed to be most appropriate to distinguish between pERK 1/2 that was unable to translocate to the nucleus and that of either newly activated pERK 1/2 from continuous ligand stimulation or that which is cycling between the nucleus and cytoplasm.

Increased pERK 1/2 levels in *Loa/Loa* were consistently observed in each of the sub-cellular fractions at 0 min chase (Figure 4.2a-b).

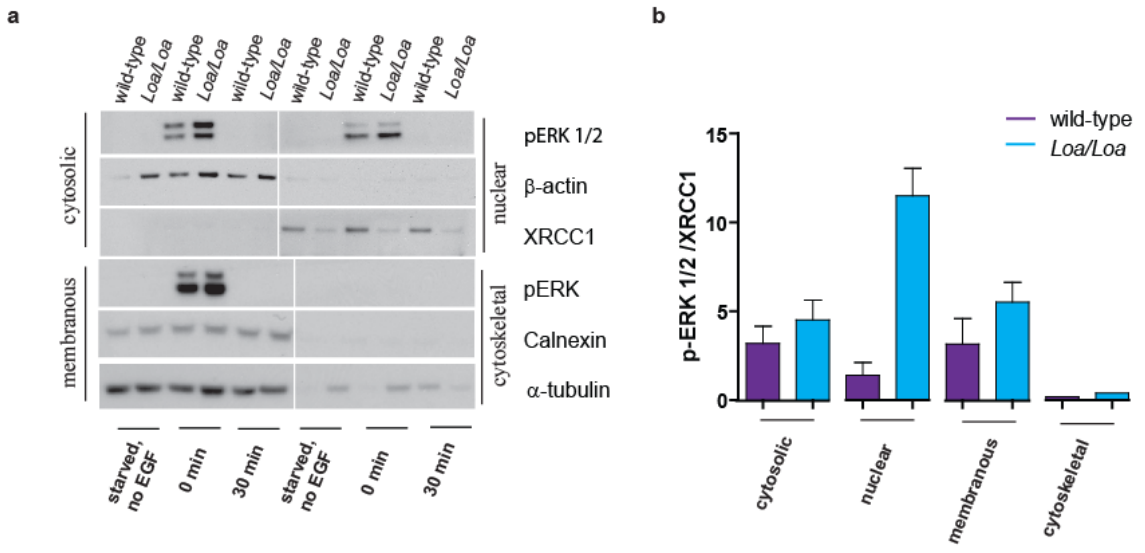

Figure 4.2: pERK 1/2 nuclear translocation is not affected by *Loa.* a) pERK 1/2 levels in cytosolic (upper left), nuclear (upper right), membranous (lower left) and cytoskeletal (lower right) sub-cellular fractions isolated from MEFs. β-actin, XRCC1, calnexin and α-tubulin were used as loading controls for respective fractions. b) Graph shows quantifications of pERK 1/2 levels in subcellular fractionations at 0 min chase (or 10 min stimulation), n=3.

Cytosolic, nuclear and membranous fractions, had 1.4, 8.2, and 1.7-fold increases in pERK 1/2 levels, respectively, compared to wild-type (Figure 4.2a-b). Only one of three experiments had detectable p-ERK 1/2 in the cytoskeletal fractions, however this did show the same trend with a 2-fold increase in *Loa/Loa* compared to wild-type.

To enable comparison of this result to that of the previous experiment (Figure 4.1), it is important to recall that the current experiment is one of pulse-chase whereas the former is one of continuous stimulation. For this reason the 0 min chase time point would be reflective of 10 min in the previous experiment. A second and important difference is the method of sample collection. In the original experiment, sample collection was instantaneous at the time points indicated by application of a lysis buffer. In comparison, sub-cellular fractionation required many ice washing steps and incubation with several extraction buffers, taking ~60 min to complete. It is therefore likely that the increase in pERK 1/2 observed in *Loa/Loa* is actually a reflection of prolonged ERK 1/2 activation rather than an increase in response.

It is tempting to conclude from the graph that the majority of p-ERK 1/2 is located in the nucleus following stimulation, this, although likely to be true, would be an assumption, for the following reason; the method used to collect sub-cellular fractions resulted in low protein concentrations that could not be measure by conventional means, I therefore loaded equal volumes for western blot analysis, regardless of the volume in which the sample had been collected. However, one would predict an increase in p-ERK in the nuclear fraction following EGF stimulation as, pERK 1/2 is known to locate to the nucleus to phosphorylate downstream effectors [197]. One would also predict a high level of p-ERK 1/2 in the cytosolic fraction due to the origin of activation. Also, activation occurs from membranous compartments, resulting in detectable levels there. It is therefore likely, that the trends in the graph are representative of the relative quantities of pERK 1/2 in the subcellular compartments. A conclusion that can be drawn from this data is that nuclear translocation of p-ERK 1/2 is not affected as levels are increased across all fractions rather than, for example, the cytosolic fraction having an increase and the nuclear fraction a decrease in comparison to the wild-type. The lack of p-ERK 1/2 observed at the

later time point is likely due to low protein concentration in all samples due to limitations of the extraction technique and the return of p-ERK 1/2 levels towards baseline.

4.4 pERK activation is not a result of starvation

It was important to clarify that increased levels of pERK were not due to prolonged starvation, as ERK 1/2 is known to become active in response to starvation to induced autophagy in some cell types for cell survival (reviewed in [175]. To test this, MEFs were starved for up to 4 hours and pERK 1/2 levels detected. pERK 1/2 was not detectable in the starved MEFs when compared to the un-starved control cells (Figure 4.3).

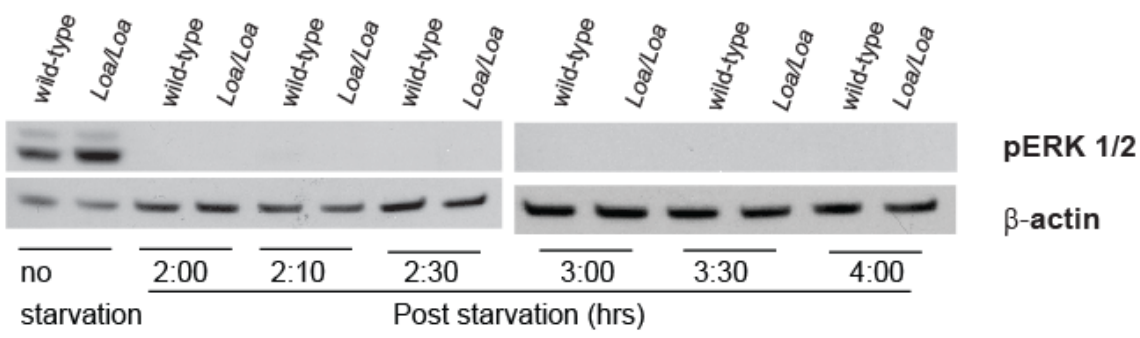

Figure 4.3: Starvation does not activate ERK 1/2 in MEFs. pERK 1/2 is undetectable in comparison to un-starved controls.

4.5 Aberrant pERK 1/2 activation in motor neurons

Following 2 hours starvation and subsequent stimulation with 5 ng/ml BDNF, whole cell, MN fractions were collected from wild-type and *Loa* heterozygotes (+/*Loa*) at 10, 30, 60, and 180 min post stimulation.

pERK 1/2 levels were found to be similar between wild type and +/*Loa* in untreated cells (Figure 4.4).

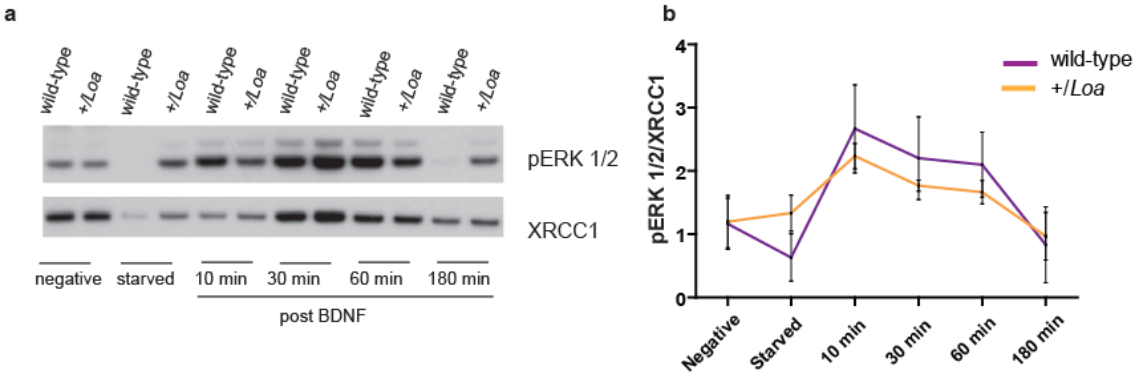

Figure 4.4: Starvation activates ERK 1/2 in *Loa* MNs. a) pERK 1/2 levels in +/*Loa* MNs are higher than wild-type following starvation. +/*Loa* does respond to BDNF activation but not to the same extent as wild-type, which has higher levels of pERK 1/2 at 10, 30 and 60 min post BDNF stimulation. b) Quantification of pERK 1/2 in (a).

After 2 hours starvation pERK 1/2 levels in +/*Loa* are >2-fold higher than those of wild-type. As ERK 1/2 is known to induce autophagy for promotion of cell survival, increased levels of pERK 1/2 may indicate increased susceptibility of neurons to stress in +/*Loa.*

Following BDNF stimulation, wild-type cells have a clear increase in pERK 1/2 activity at 10 min, which, declines gradually over the course of time. However, levels are still >3-fold higher at 60 min than they were prior to stimulation.

+/*Loa* responds to BDNF stimulation and follows the same trajectory as wild-type over time, however, the overall amount is ~0.8-fold less than wild-type. At 180 min wild-type pERK 1/2 levels drop below those of +/*Loa*, perhaps indicating prolongation of the signal in +/*Loa* after this point

4.6 p c-Fos levels are increased and prolonged in MEFs following EGF stimulation

Having identified prolonged activation of ERK 1/2 in *Loa/Loa* MEFs attention was shifted to the effect this would have on the down-stream immediate early gene, c-Fos.

Initial attempts to detect c-Fos revealed many bands on western blot and so it was essential to establish the identity of the bands.

The predicted size of c-Fos is ~41 kDa, according to ExPASy, Bioinformatics Research Portal. A band of this size can be seen (Figure 4.5, lane 1), as can bands of ~49 KDa, ~62-65 KDa, and ~98 KDa. The ~49 KDa bands were predicted to be phosphorylated c-Fos (p c-Fos) and the ~98 KDa, p c-Fos/c-Jun dimers. However, the identity of the predominant bands at ~62-65 KDa, was not clear.

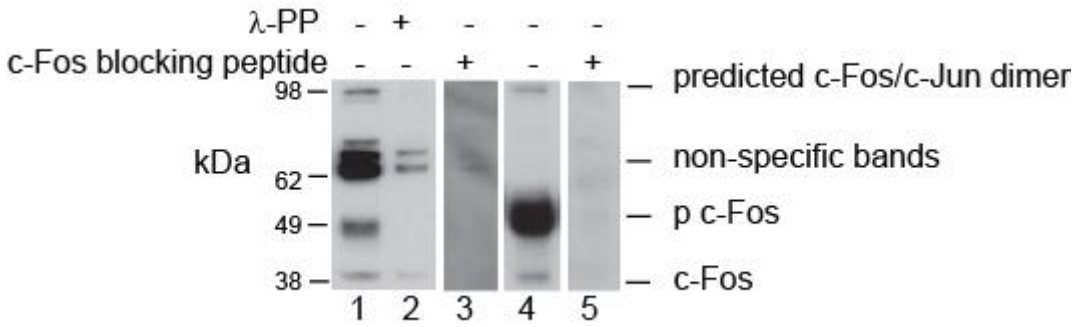

Figure 4.5: Elucidation of c-Fos on western blot. Lanes 1-3 are lysates from MEFs stimulated with 20 ng/ml EGF, lanes 4 and 5 are motor neuron lysates stimulated with 5 ng/ml BDNF. Samples are treated with λ-protein phosphatase (λ-PP) or c-Fos blocking peptide as indicated to determine the identity of the bands. c-Fos, p c-Fos, non-specific bands and c-Fos/c-Jun dimers were identified at 41 KDa, 49 KDa, 62-65 KDa and 98 KDa respectively.

To confirm the predictions and reveal the identity of additional bands, whole cell lysates from MEFs simulated with 20 ng/ml EGF and lysed at 60 min post stimulation were treated with λ-protein phosphatase (λ-PP). Phosphatase inhibitors were omitted from the sample to be treated with λ-PP so as not to inhibit the phosphatase activity.

Following λ-PP treatment the ~98 kDa and ~49 kDa bands disappeared (Figure 4.5, lane 2), confirming these bands as phosphorylated proteins. Due to their size and the antibody used I am confident that they are p c-Fos/c-Jun dimers and p c-fos respectively. The ~41 KDa band remained as expected for the unphosphorylated form of c-Fos. The intense bands ~62-65 KDa also remained, however a c-Fos blocking peptide showed these bands to be non-specific (Figure 4.5, lane 3).

A similar band pattern was observed in MNs but interestingly the non-specific doublet was not always present these samples (Figure 4.5, lane 4, 5), indicating detection of cell type specific proteins that are not c-Fos.

Once the identities of the bands were determined, samples described in section 4.1, which showed prolonged pERK 1/2 in *Loa/Loa*, were probed for c-Fos.

My hypothesis was that prolonged activity of pERK 1/2 in *Loa/Loa* would result in an increase in c-Fos expression.

There was 0.9-fold less c-Fos in *Loa/Loa* compared to wild-type following starvation (Figure 4.6a-b). However, following EGF stimulation c-Fos levels were increased in *Loa/Loa* by 1.5, 1.6, 1.6, 1.1 and 2.1-fold at 10, 30, 60, 120, and 180 min respectively (Figure 4.6a-b).

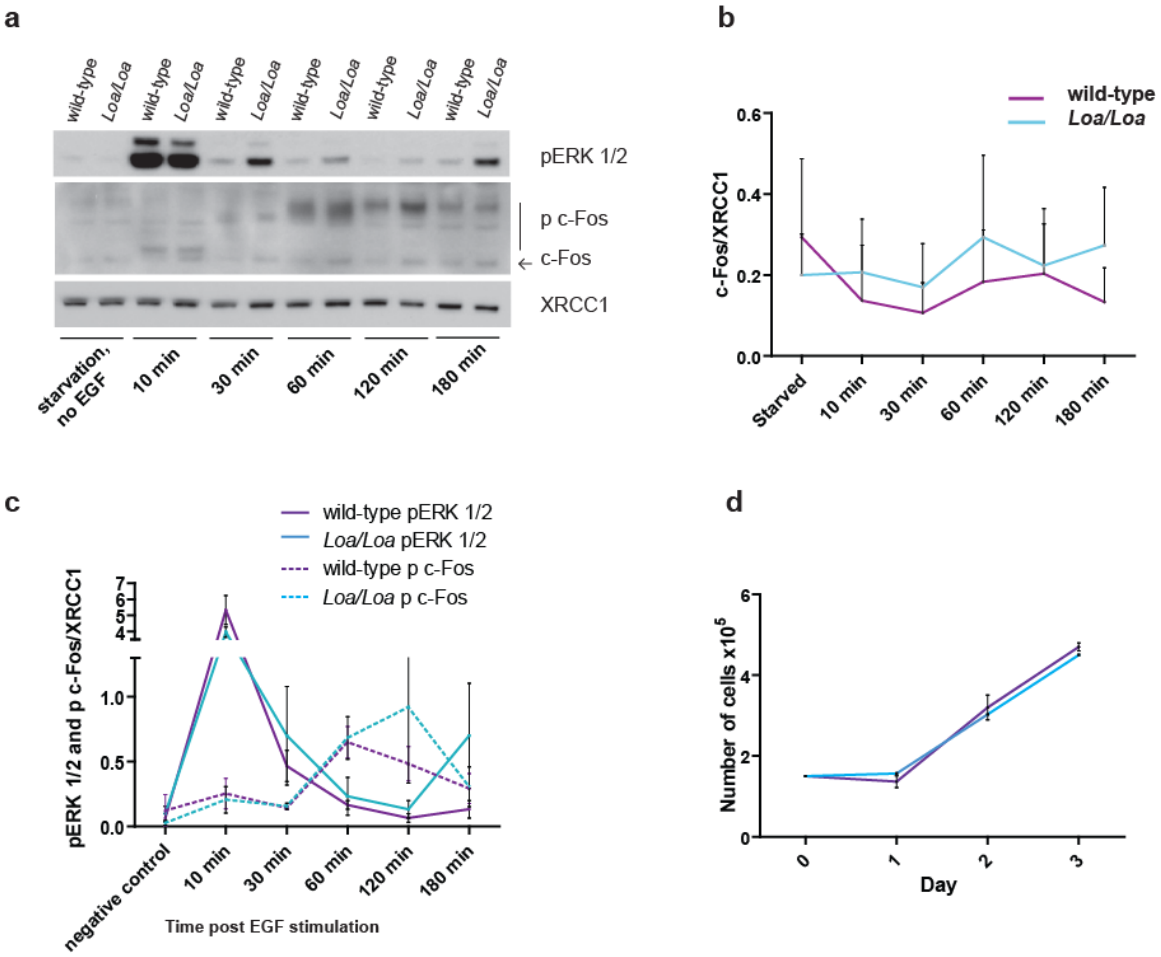

Figure 4.6: Levels of c-Fos and p c-Fos are increased in *Loa* MEFs. a) pERK 1/2, c-Fos and p c-Fos levels are increased and prolonged in *Loa/Loa* compared to wild-type. b) Quantification of c-Fos levels in *Loa/Loa* and wild-type. c) *Loa/Loa* p c-Fos peaks 60 min later than wild-type, at the120 min time point. pERK 1/2 is overlaid to show the relationship between the two, pERK 1/2 declines before there is an increase in p c-Fos. d) Cell proliferation rates were the same in wild-type and *Loa/Loa.*

Levels of p c-Fos were, as expected, found to be low following starvation, however, although low in quantity there was ~4-fold less p c-fos in *Loa/Loa* than wild-type (Figure 4.6c).

After stimulation with 20 ng/ml EGF a delay of around 30 min was observed, before the Ras/Raf/ERK pathway resulted in c-Fos translation and phosphorylation on Ser-362 and Ser-374. This can be observed between the 30 and 60 min time points (Figure 4,6c).

The c-Fos phosphorylation curve in *Loa/Loa* was similar to wild-type until 60 min. After which time wild-type levels of p c-Fos began to reduce back to basal levels whereas *Loa/Loa* p c-Fos levels continued to increase, peaking, higher than wild-type levels, at 120 min post EGF stimulation (Figure 4.6c). As EGF-induced ERK 1/2 activation is transient, pERK 1/2 typically declines before additional c-Fos phosphorylation at Thr-325 and Thr-331 can occur. Phosphorylation at these latter two residues would produce hyperphosphorylated, stable p c-Fos which, would have greater impact on cell fate [154]. Due to prolonged activation of ERK 1/2 in *Loa/Loa* it would have been interesting to see if the hyperphosphorylated, stable c-Fos was present in *Loa/Loa*. Using size alone it was difficult to determine if there was a presence of hyperphosphorylated c-Fos. Attempts were made to detect hyperphosphorylated c-Fos using an antibody specific to phosphorylated Thr-325 however, the antibody was inadequate to conclude either way (data not shown).

It would be plausible to hypothesise that the altered levels of pERK 1/2 and p c-Fos would result in increased proliferation rates in *Loa/Loa.* Surprisingly this was not found to be the case shown through regulated experiments (Figure 4.6d). However, working with the cells over-time, left the impression that *Loa/Loa* MEFs proliferated at a slower rate than the wild-type, and that differences in proliferations rates between wild-type and *Loa/Loa* were highly dependent on the confluency of the cells.

4.7. p c-Fos and JNK are increased in *Loa* MNs following starvation

Data in section 4.5 showed a 2-fold increase in pERK 1/2 levels in +/*Loa* compared to wild-type MNs following starvation and I suggested that this may initiate autophagy to promote cell survival. Following on from this finding it was important to determine if starvation-induced cell stress was sufficient to activate JNK. Similar to ERK1/2, following acute starvation, JNK can act as an activator of autophagy to promote cell survival. If however, starvation is prolonged such that autophagic attempts to rescue the cell fail, the cell may enter class II programmed cell death, or autophagy-induced cell death pathway. Entry into apoptosis has been shown to be preceded by heightened, sustained levels of c-Fos (see sections 1.5.1-1.5.3).

Marked JNK activation was found in +/*Loa* following starvation, which declined with time following BDNF stimulation (Figure 4.7a-b). Wild-type did not show a distinct activation but did fluctuate between the 10 min and 60 min time points.

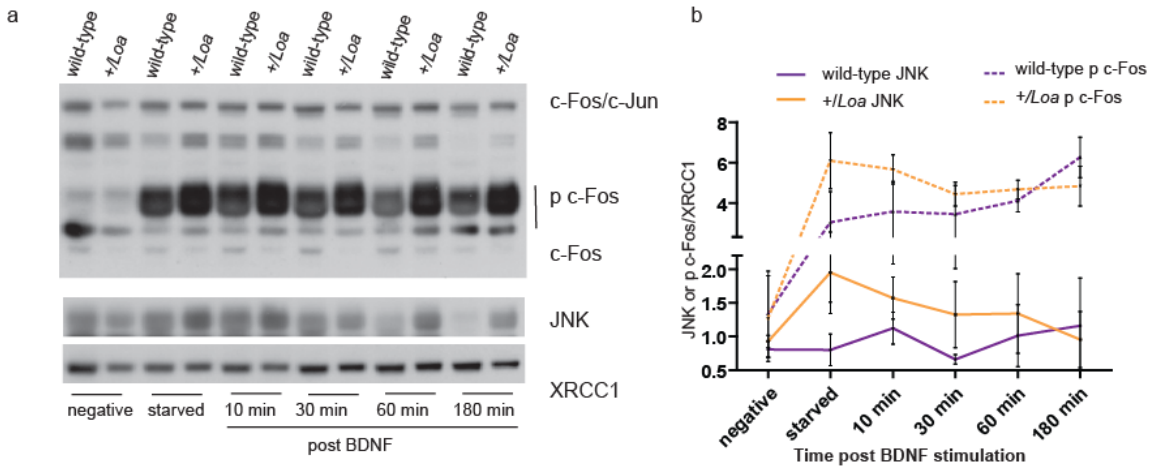

Figure 4.7: JNK and p c-Fos is activated in *Loa* MNs following starvation. a) A peak of JNK activity is observed following starvation in +/*Loa* MNs, which, declines following BDNF stimulation. p c-Fos is dramatically induced by starvation in +/*Loa* MNs whereas a gradual incline is apparent in wild-type following starvation and subsequent stimulation with BDNF. b) Quantification of p c-Fos and JNK in (a)

When looking at c-Fos expression, starvation increased c-Fos in both genotypes however, +/*Loa* levels were 2-fold higher than those of wild-type, following the pattern seen with JNK (Figure 4.7a-b). c-Fos levels, like JNK reduced by 30 min post stimulation to a level that was maintained until the end of the experiment. In contrast wild-type MNs had a gradual increase in c-Fos levels over the course of time, following a pattern expected from pERK 1/2 activation (Figure 4.4a-b and 4.7a-b).

4.8 Chapter 4 summary

EGF stimulation of MEF cells highlighted prolonged activation of ERK 1/2, which in turn resulted in increased levels of both c-Fos and active p c-Fos in *Loa/Loa* when compared to wild-type. Starvation did not appear to play a significant role in these signalling events. In contrast, starvation in MNs activated ERK 1/2, JNK and c-Fos in +/*Loa* to a much greater extent than wild-type. It is plausible that *Loa* inflicts increased susceptibility to stressors such as nutrient deprivation and as a result pERK and JNK are activated at a faster rate and to a greater extent than in healthy, wild-type cells. The purpose of which may be to induce autophagy and promote cell survival. If autophagic processing is hindered due to *Loa* the cell may be pushed towards cells death.

Chapter 5

Differential expression of TCF25 and KLC1 in *Loa*

5.1 Introduction

Chapter 3 and 4 demonstrate how *Loa* affects dynein processivity, which in turn leads to alterations in cell signalling. This current chapter arose from a prediction of multiple differentially expressed genes in *Loa,* and has resulted in some interesting findings, particularly with regards to transcription factor 25 (*Tcf25*) and kinesin light chain 1 (*Klc1*).

5.2 TCF25 is up-regulated during *Loa* brain development

Microarray analysis was carried out by Dr Marcel van der Brug, Department of Neuroscience, Scripps Research Institute, Jupiter, Florida 33458. Briefly, RNA was collected from two wild-type, +/*Loa* and *Loa/Loa* E13 mouse brains using a trizol-based protocol, (and by Dr Violeta Soura). Illumina mouse oligonucleotide arrays (Mouse-6_V1) and Illumina Beadstudio software suite were used to determine differential expression. Reproducibility across the samples was good to excellent among the majority, as confirmed by their 'diff' scores [82]. Of the 94 genes identified as being differentially expressed in *Loa/Loa* compared to wild-type, 79 were up-regulated whilst 15 were down-regulated. Comparisons between +/*Loa* vs wild-type, and +/*Loa* vs *Loa/Loa* were also made. A full list of genes, expression values and Diff. scores can be found in the appendix. There were two genes identified as being of particular interest due to their relationship with dynein and the signalling pathways discussed in chapter 4. They are the genes encoding TCF25 and KLC1, which were shown to have a *Loa,* dose dependent up or down regulation respectively (Table 5.1).

Gene	wild-type average signal	+/*Loa* average signal	*Loa/Loa* average signal
Tcf25	747.0996	1063.559	1172.774
Klc1	7438.797	6275.124	2454.743

Table 5.1: *Klc1* and *Tcf25* are differentially expressed in *Loa.* Microarray analysis indicates up-regulation (green) and down-regulation (purple) in +/*Loa* and *Loa/Loa,* respectively, compared to wild-type. n=2.

To confirm the microarray data, mRNA was extracted from 3 wild-type, +/*Loa* and *Loa/Loa* E13 brains. Reverse transcription reactions produced cDNA to be used for quantitative real-time polymerase chain reaction (qPCR) analysis. qPCR did not revealed a significant difference between expression of *Tcf25* in +/*Loa* compared to wild-type (triplicate, mean cycle thresholds (CT) were 24.26 and 23.41, respectively) , however there was a 1.5 and 1.7-fold up-regulation of *Tcf25* in *Loa/Loa* (CT = 22.82), compared to wild-type and +/*Loa* respectively (P = 0.0006*** and P = 0.0018**, respectively, according to a Mann-Whitney U test of significance) (Figure 5.1a-b).

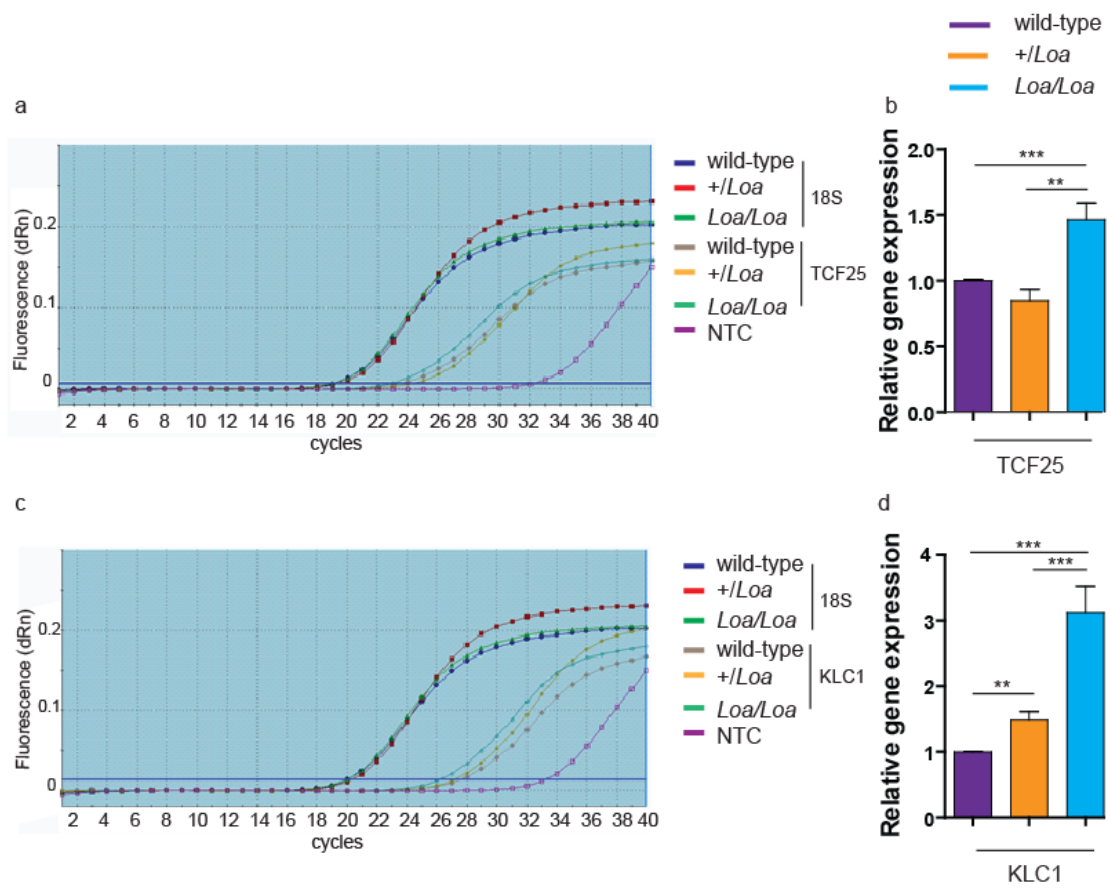

Figure 5.1: *Tcf25* and *Klc1* are up-regulated in *Loa.* a) TCF25 is up-regulated in *Loa/Loa* compared to +/*Loa* and wild-type, as determined by qPCR. b) Graph shows quantification of the data in (a). c) Kinesin light chain 1 is up-regulated in +/*Loa* and *Loa/Loa* compared to wild-type, and in *Loa/Loa* compared to +/*Loa*. d) Graph shows quantification of the data in (c). n = 3 E13 brains from each genotype, repeated in triplicate. NTC = no template control.

Interestingly, quantification of KLC1 revealed differences to that of the microarray data. Compared to wild-type *Klc1* was found to be 1.5-fold up-regulated in +/*Loa* (CTs were 27.6 and 27.2 for wild-type and +/*Loa* respectively and P = 0.0061**) and 3.1-fold up-regulated in *Loa/Loa* (CT = 26.22) compared to wild-type (P = <0.0001***). The difference between +/*Loa* and *Loa/Loa* was also significantly different at 2.1-fold increase (P = 0.0003***) (Figure 5.1c-d).

These findings were interesting both from the relevance of the genes involved but also due to the discrepancies between the different techniques used. To address this and to identify whether an increase in messenger RNA actually translated to an increase in protein expression, protein from E13 brains was extracted for western blot analysis. Each gene will be discussed separately, along with subsequent experimental findings, beginning with *Tcf25*.

5.3 TCF25 protein expression is altered in E13 *Loa* brains and MEF cells

Western blot analysis confirmed the significant up-regulation of TCF25 in *Loa/Loa* compared to wild-type, by 2.8-fold (Figure 5.2a) (P = 0.0317*, Mann-Whitney U), confirming both the microarray and qRT-PCR data (Figure 5.1a-b, Table 5.1). TCF25 has 5 known isoforms, four between 68-72 kDa and one larger isoform at ~77 kDa. Two distinct bands can be seen on western blot and the expression difference between the genotypes is significant only in the smaller of the isoforms (P = 0.0159*, Mann-Whitney U) (Figure 5.2a-b).

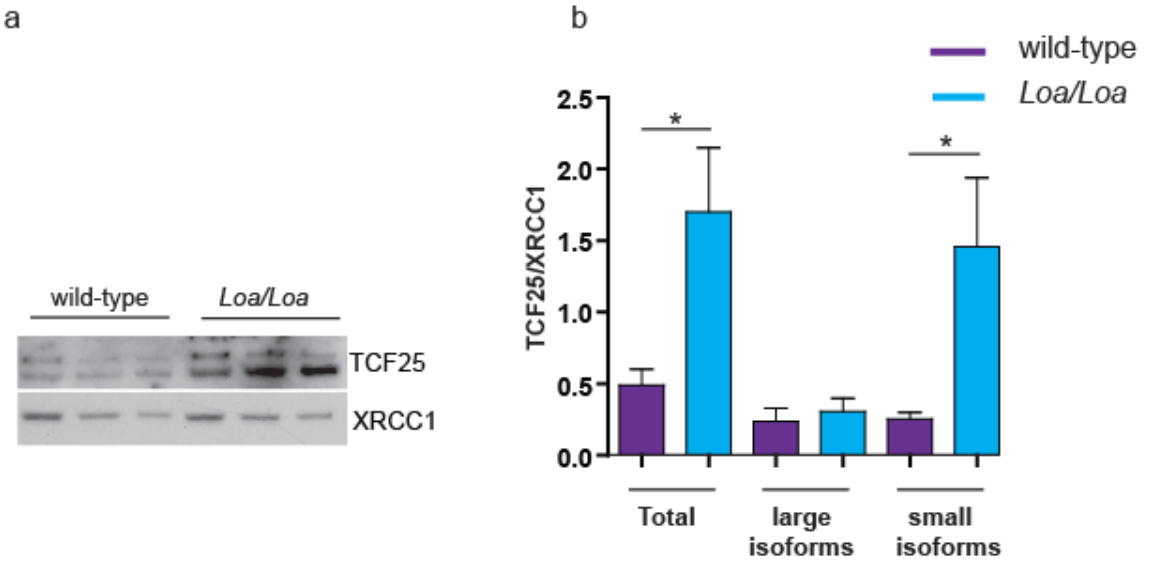

Figure 5.2: TCF25 protein expression is up-regulated in *Loa* E13 brains. a) Western blot showing the 68-72 kDa (lower band) and ~77 kDa (upper band) isoforms of TCF25. The smaller isoforms are significantly up-regulated in *Loa/Loa* compared to wild-type. b) Quantification of the data in (a) showing that TCF25 up-regulation is specific to the smaller, 68-72kDa TCF25 isoforms, n = 3.

TCF25 controls the transcription of c-Fos by regulating the expression of SRF(see section 1.4.6). Due to the observed alteration in ERK 1/2 and c-Fos expression in MEFs (chapter 4), it would be interesting to explore any alterations of TCF25 in MEFs. Thus, cells were starved for 2 hours and then pulsed for 10 min with 20 ng/ml EGF. Whole cell lysates were collected for

detection of TCF25 and untreated/un-starved cells were used as a negative control.

There was a distinct lack of the ~77 kDa isoform in all of the *Loa/Loa* samples, which was significantly different from 0 min to 120 min post EGF stimulation (P = 0.0134* according to two-way ANOVA) (Figure 5.3 a-d).

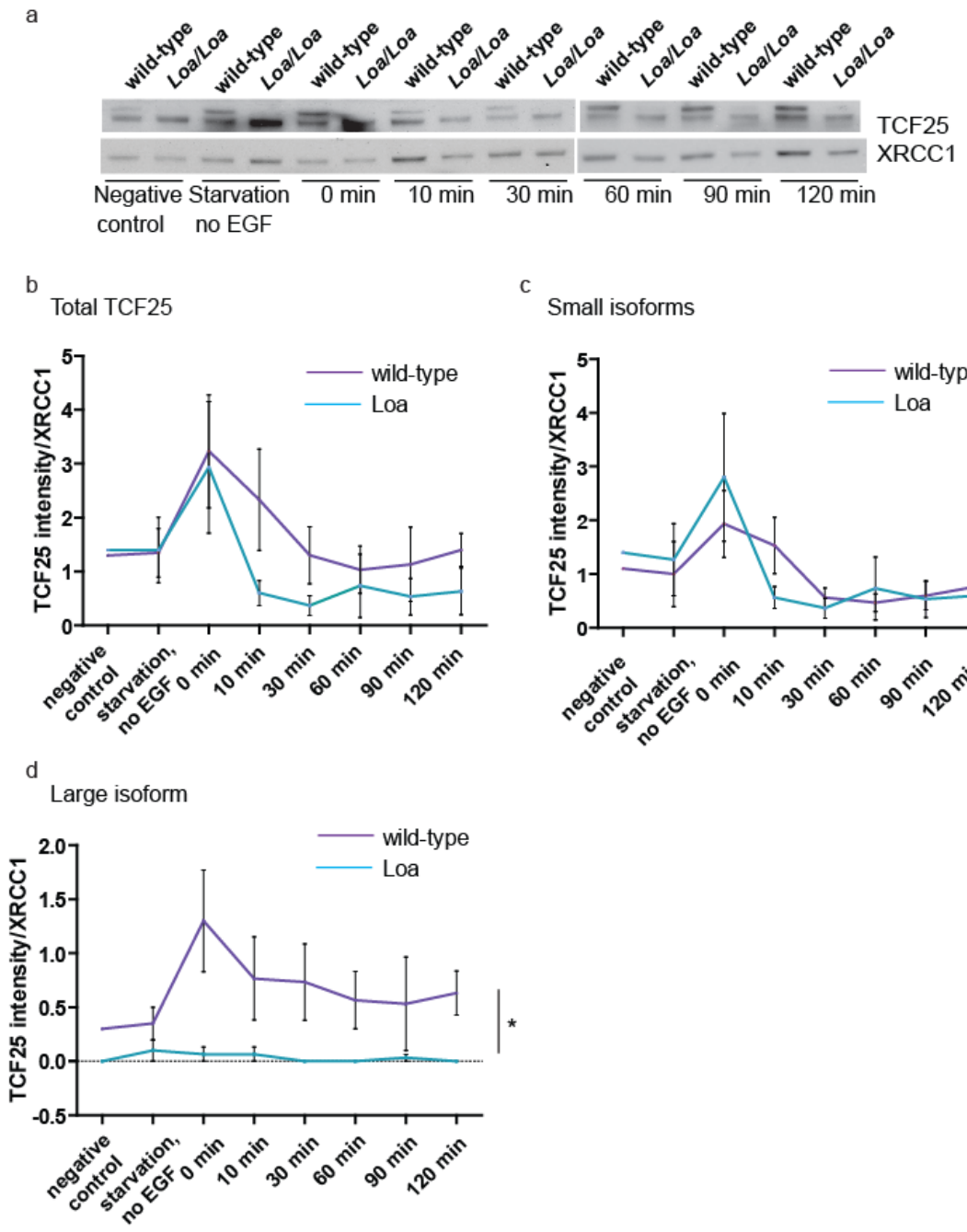

Figure 5.3: TCF25 expression is aberrant in *Loa* MEFs. a) Large, ~77 kDa isoforms of TCF25 are lacking in *Loa/Loa* MEFs. b) Quantification of total TCF25 revealed a reduction in *Loa/Loa* compared to wild-type. This reduction was not due to significant changes in the smaller, 88-72 kDa isoforms (c), but was specific to the larger ~77 kDa isoforms (d). n = 3.

EGF stimulation increased the expression of the smaller isoforms of TCF25 in both genotypes at 0 min chase, however, there was a 1.4-fold increase in *Loa/Loa* expression compared to wild-type (Figure 5.3c).

5.4 KLC1 protein expression is up-regulated in *Loa*

Microarray data revealed down-regulation of KLC1 in *Loa/Loa* when compared to wild-type. In contrast qRT-PCR showed a significant up-regulation. As kinesin is the opposing motor to dynein, KLC1 was of great interest even though there were some discrepancies in the data. Thus, I decided to check whether increased mRNA translated to an increase in protein levels. Western blot analysis revealed a 1.4 and 1.3-fold increase in KLC1 expression in +/*Loa* and *Loa/Loa* respectively, compared to wild-type (Figure 5.4a-b).

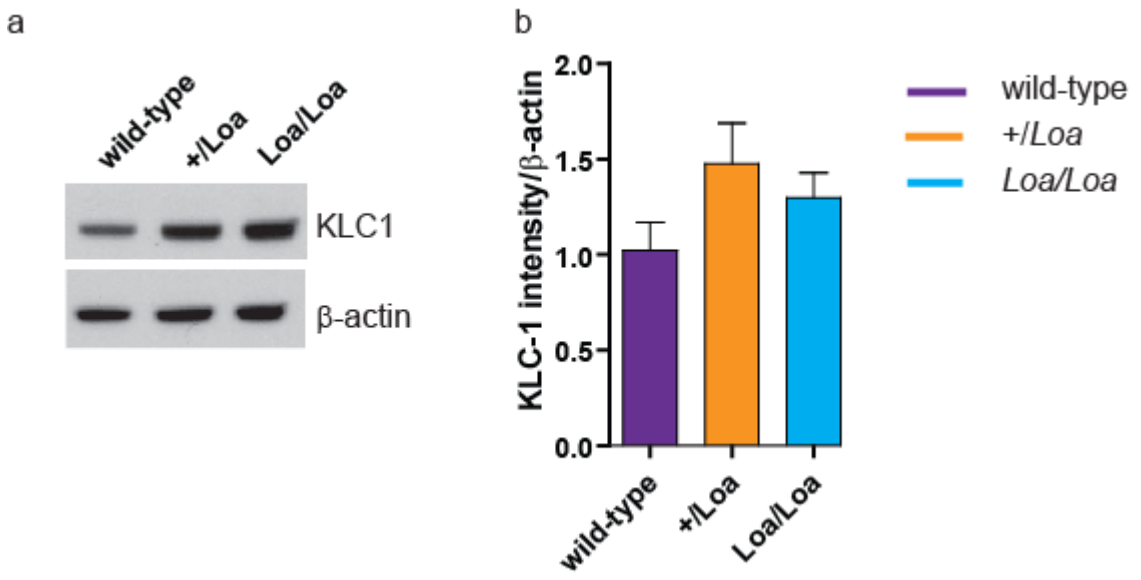

Figure 5.4: KLC1 protein expression is increased in *Loa* MEFs. a) KLC1 protein levels are increased in +/*Loa* and *Loa/Loa* when compared to wild-type. b) Graph showing quantification of the western blots, n = 3.

KLC1 has been shown to have a regulatory effect on KHC by holding it in a closed and inactive conformation, unbound from MTs. Upon cargo binding it is suggested that the conformation of the kinesin complex alters, to be in a more open complex for binding and transport along MTs (see Figure 1.5). For this reason it would be interesting to determine if the elevated levels of KLC1 in *Loa* were present in the soluble or MT-bound fraction of the cell. To test this, a MT pull-down assay was performed by Dr Wenhan Deng, University of Sussex,

followed by western blot analysis of MT-bound KLC1. Briefly, newborn mouse brains were homogenised, followed by high-speed centrifugation and recovery of cytosolic supernatants. Taxol and adenylyl-imidodiphosphate (AMP-PNP) were added to stabilise MTs and bind kinesin respectively before separation of MT-bound proteins and soluble fractions by further centrifugation [82]. I then proceeded with western blot analysis of the MT-bound and soluble fractions.

There was a 70% increase of KLC1 in the supernatant of *Loa/Loa* when compared to wild-type (Figure 5.5a-b) and a 50% reduction in that bound to MTs (Figure 5.5c-d), which reached significance according to a Mann-Whitney U test of significant (P = 0.0294*).

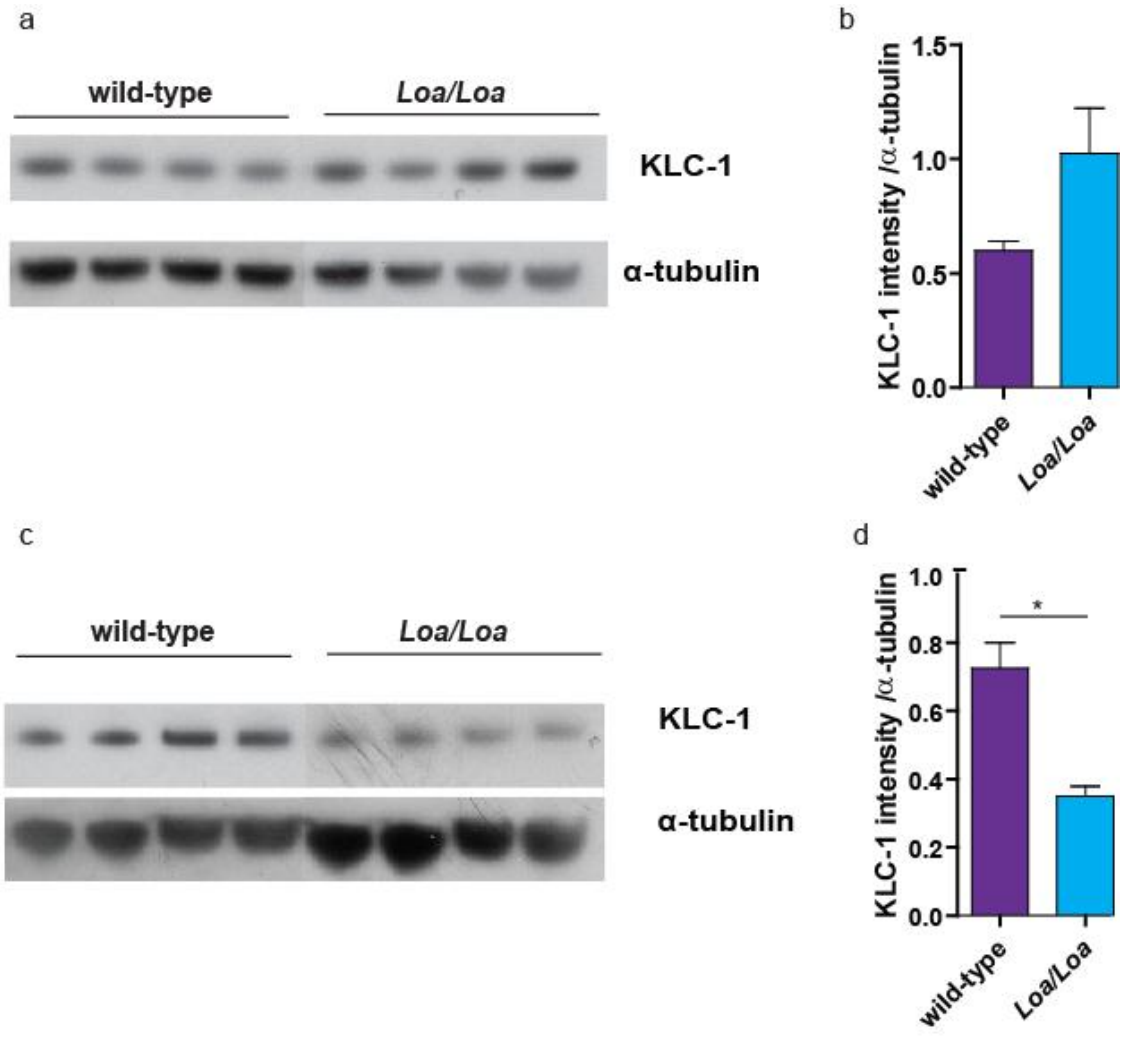

Figure 5.5: Soluble KLC1 is increased in *Loa* while there is less KLC1 bound to MTs. a) *Loa/Loa* has more KLC1 in the supernatant than wild-type following a microtubule (MT) pull-down assay. b) Quantification of the data in (a). c) *Loa/Loa* has less KLC1 associated with MTs than wild-type. d) Quantificaition of the data in (c), P = 0.0294*.

Dynein is a known cargo of kinesin. For this reason DIC was used for immuno-precipitation to identify whether there were alterations in dynein-kinesin association. KLC1 was found to associate with DIC 6.8-fold more strongly in *Loa/Loa* than in wild-type brain samples (Figure 5.6a-b).

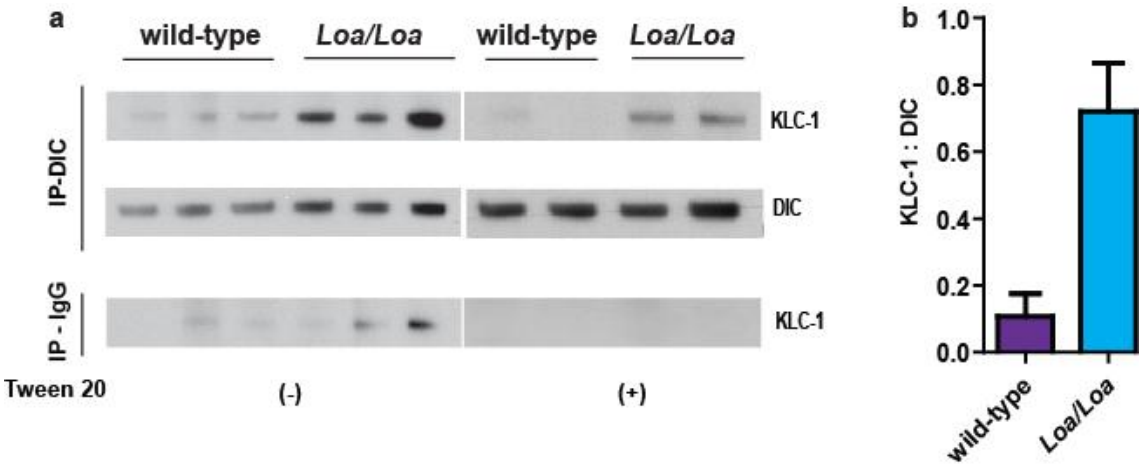

Figure 5.6: KLC1 associates more strongly with DIC in *Loa.* a) Immunoprecipitation of the dynein complex with the 74.1 antibody to DIC revealed and increased association of KLC1 with DIC in *Loa/Loa* compared to wild-type. Washing the sepharose beads with detergent (bottom right panel) eliminated the non-specific binding KLC-1 to the beads in the IP-IgG negative controls, which was apparent in the non-detergent washes (bottom left panel). b) Quantification of the western blots revealed a 6.8-fold increase in association between KLC1 and DIC in *Loa/Loa* compared to wild-type.

5.5 Chapter 5 summary

Chapter 5 has identified aberrant expression of TCF25 and KLC1 in *Loa.* Altered regulation of specific TCF25 isoforms may identify compensatory pathways to rescue impaired cell development in neurons.

Up-regulation of KLC1 provokes an interesting model of dynein-kinesin, motor-cooperation, which will be discussed further in chapter 6, but is likely an attempt to restore homeostasis within the cell.

Chapter 6

Discussion

6.1 Introduction

Throughout this thesis significant changes have been identified as consequences of a single point mutation (*Loa*) in *Dync1h1*. These changes are not cell-type specific in their origin but are more so in their response. As an example, chapter 3 identified aberrant but comparable, intracellular trafficking in both MEF cells and MNs. Both cell types showed reduced retrograde speeds and increased numbers of anterograde movements in *Loa*, however, it was chapter 4 and 5 that began to show how the cell types differ in their responses through intracellular signalling pathways. There are some findings from each of the results chapters (3-5) that I would like to discuss in further detail.

6.2 Dynein kinetics

Chapter 3 (Figure 3.1a-b) identifies an increased number of EGF-containing vesicles in *Loa/Loa* compared to wild-type across the time course and with greatest significance at 10 min chase. This is the time during which EEs fuse together for sorting in the emerging MVB. The increased number of particles remaining in *Loa/Loa* at this time may be representative of altered EE morphology and delayed MVB formation. This observation is intriguing due to previous work in our lab that showed an increased affinity between DHC, DIC and DLIC, and a reduced affinity for the p150 subunit of dynactin, in *Loa* [82]. As DIC, DLIC and dynactin are regulators of cargo attachment, this finding may be indicative of impaired cargo docking to the dynein complex, delaying subsequent transport along MTs. At later timepoints an increased number of EGF-containing vesicles remain in *Loa/Loa* compared to wild-type. This may indicate delayed degradation of EGFR at this point.

Live cell imaging of EGF-Alexafluor546 identified a couple of interesting findings. The first was the increased number but reduced speed and distance of side-steps made in *Loa* compared to wild-type. Dynein is known to make side-steps, probably from one MT to another to enable navigation through a crowded cytoplasm. The movements observed in *Loa/Loa* however, may not be representative of an energy-dependent ‘step’, rather, they may indicate that the dynein complex is either dissociating from MTs [20], or, as suggested from our previous work [82] from the cargo it is carrying.

Dynein processivity is reliant on co-operation between dynein heads (see section 1.1.5). Due to the location of *Loa* in the homodimerisation domain of the two heavy chains, *Loa* may alter the force applied to both the leading and lagging heads, resulting in increased bidirectional movement. Multiple motors are required for cargo transport and it is possible that reductions in dynein-MT [20] and/or dynein-cargo associations [82] brought about by *Loa* would result in reduced numbers of full-functional dynein complexes associated simultaneously with both cargo and MTs for transport to occur, thus resulting in the aberrant track velocities and premature run terminations observed [20, 199, 200].

In addition cooperation between the two motors has been well established [23] however inhibition of one motor does not necessarily result in inhibition of the other [201]. It is therefore plausible that, in *Loa,* any tug-of-war between kinesin and mutant dynein is balanced more favourably towards the anterograde movement of kinesin than it is towards the dynein mediated retrograde movement.

6.3 *Loa* influences on cell signalling

Chapter 4 demonstrates well the difference in activation between EGF and BDNF. The former activates the transient Ras/Raf pathway, whilst the latter incorporates the Rap1 pathway for sustained activation (section 1.4.3 and 1.4.4, and Figure 4.1 and 4.4).

In MEF cells *Loa* induced prolonged ERK 1/2 activation. Moreover, activation of the IEG c-Fos was increased. As consequence of this, it would be reasonable for one to predict that cell proliferation would be increased in *Loa/Loa* cells compared to wild-type however, interestingly no statistical difference in cell proliferation was found between *Loa/Loa* and wild-type (Figure 4.6d). An explanation for this may lie in evidence that a constitutively active Ras/Raf/ERK 1/2 pathway is sufficient for a cell to enter senescence or even apoptosis (reviewed in [198]). Although not investigated here, the study of senescence and/or apoptosis in *Loa* MEFs would be interesting work for the future.

In MNs pERK 1/2 levels were reduced compared to wild-type following GF stimulation. This difference may be due to the prior response of MNs to

starvation. It would be informative to repeat the GF stimulation on MNs that are not already in a stressed state as I would predict a similar response to that of the MEF cells. If my hypotheses were correct, prolonged activation of ERK 1/2 and increased levels of c-Fos, may, in a terminally differentiated cell such as a MN, stress the cell to such an extent that it is pushed into programmed cell death.

ERK 1/2 and JNK can both initiate autophagy to promote cell survival during nutrient deprivation. Since autophagy is dependent on dynein transport, impairment of autophagosome transport that mirrors endosome transport in *Loa* may result in a stalling of autophagosomes in the cytosol, rendering the neuroprotective aspect of this pathway redundant. The stress of prolonged starvation, coupled to impaired autophagosome processing for nutrient recycling would likely switch the JNK signal from one of protector to one of class II, autophagy- induced cell death, as the volume of the stalled autophagosomes overtakes the volume of the cytosol. In support of this theory is the previously reported increase in accumulation of autophagosomes in *Loa* [196] and the observed ERK 1/2 and JNK elevation compared to wild-type following 2 hours starvation (Figure 4.4a-b and 4.7a-b). Furthermore, the peak in c-Fos activation observed in +/*Loa* MNs following starvation is consistent with activation via JNK as opposed to ERK 1/2 and entry into apoptosis (Figure 4.7) [187].

In my experiments GF stimulation after 2 hours starvation coincided with a decrease in JNK levels and an increased pERK 1/2. This may indicate that GFs have the ability to salvage the cell from its autophagy-induced apoptotic fate. However the patterns observed following starvation and previous evidence that JNK is the overriding factor to ERK 1/2 [203] is more suggestive that apoptosis has been initiated. Cell survival assays and the use of autophagic and apoptotic markers would help to determine the mechanisms and pathways leading to cell fate. Signalling effects in MNs and MEFs are summarised in Figure 6.1.

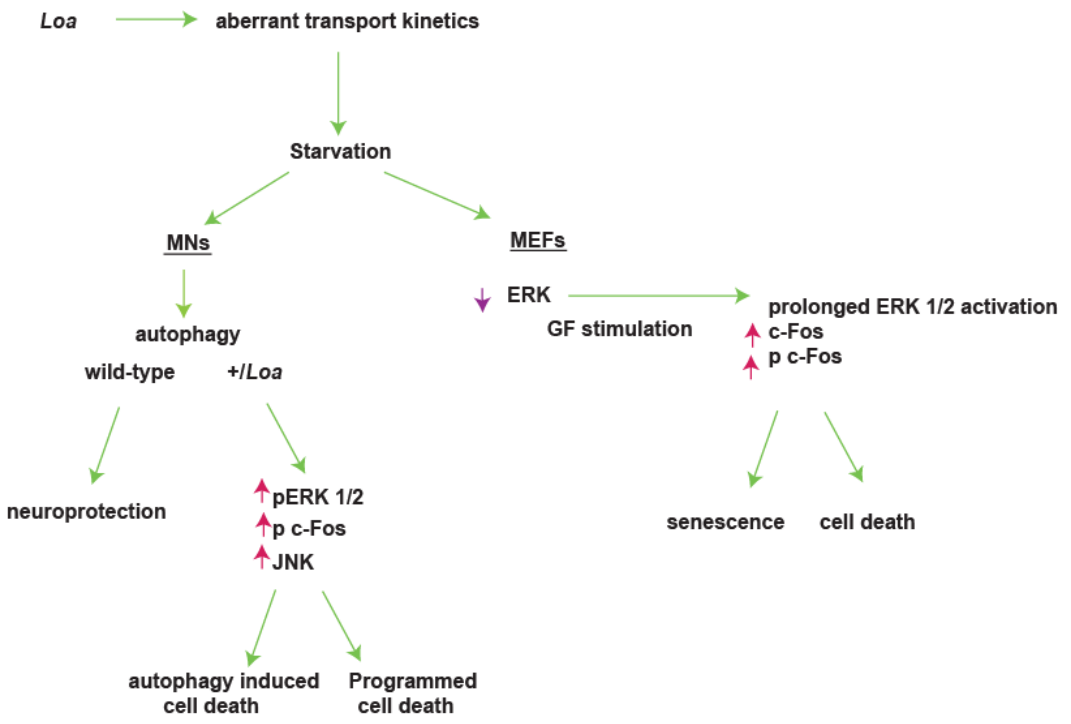

Figure 6.1 Summary of signalling in *Loa* MNs and MEFs. *Loa* results in aberrant transport kinetics, which influence cell-type specific responses. +/*Loa* MNs appear to be more susceptible to starvation, indicated by increased pERK 1/2, p c-Fos and JNK following a 2 hour starvation period. This is perhaps due to delayed processing of autophagosomes and will push the cell towards cell death. In contrast starvation does not initiate these signals in MEFs. GF stimulation in MEFs results in prolonged pERK 1/2, and increased levels of c-Fos. This is not reflected by an increase in cell proliferation and thus may be indicative of entry into senescence.

6.4 TCF25 identified as a potential biomarker of disease

The up-regulation of TCF25 identified in E13 *Loa/Loa* brains (Table 5.1, Figure 5.1a-b, and 5.2a-b) is an interesting finding for two reasons: TCF25 is expressed intensely in developing DRGs and to a lesser but significant extent, in the adult brain [165]. It is therefore possible that up-regulation of TCF25 in *Loa/Loa* may be indicative of an attempt to compensate for impaired neuronal migration and developmental morphology, identified in *Loa* (see section 1.2.10). Due to the minimal knowledge surrounding TCF25 in any pathway other than that of SRF regulation, these mechanisms would need to be elucidated through further work.

Alternatively, there are reports that overexpression of isoform b (71 kDa) is linked to an increase in cell death [202]. As the 68-72 kDa isoforms were prominent in *Loa/Loa* E13 embryos, it would be useful to identify which of the 68-72 kDa isoforms are up-regulated as they may reveal novel protein functions and may produce a useful biomarker of neurological disease, potentially for diseases such as SMA-LED, which, in some cases harbours a mutation just 2 nucleotides away from *Loa* and thus potentially may show the same alteration in gene expression (see section 1.2.4).

Loa/Loa MEFs revealed the absence of the ~77 kDa TCF25 isoform (Figure 5.3a-d), which is interesting because in humans the ~77 kDa isoform of nulp/TCF25 has been shown to be a negative regulator of SRF [164]. The data presented here is therefore suggestive that the distinctive lack of the ~77 kDa in *Loa/Loa* MEFs may, render the cell unable to regulate aberrant activation of ERK 1/2 through this pathway (Figure 4.1a-b) and therefore an increase in c-Fos is observed (Figure 4.6a-c).

6.5 Cooperation between motors to restore homeostasis

Impaired retrograde kinetics in *Loa,* likely leads to an increase in dynein at the plus end of MTs, along with an imbalance of cargo and organelle positioning within the cell. Up-regulation of KLC1 (Figure 5.1c-d and 5.4a-b) may be a compensatory mechanism to hold KHC inactive, thus inhibiting further plus-end transport of cargos. Data from the MT-binding assays support this theory as more soluble KLC1 is present in *Loa/Loa* brain homogenate compared to wild-type (Figure 5.5a-b), and there is more KLC1 bound to MTs in wild-type (Figure 5.5c-d). KLC1 isoforms have been shown to determine specificity for cargos, and dynein has been shown to interact with KLC1, through DIC [204, 205]. Immunoprecipitation revealed a greater association of KLC1 with DIC in *Loa/Loa* compared to wild-type (Figure 5.6). Thus, at the local level in *Loa,* detection of reduced retrograde transport may signal for the cell to send more dynein to the cell periphery in preparation of retrograde transport. The interaction between KLC1 and DIC would enable kinesin complex activation for this to occur. A wider regulatory mechanism may prevent the anterograde transport of further cargo to the cell periphery to try and restore the global balance across the cell as a whole (Figure 6.2).

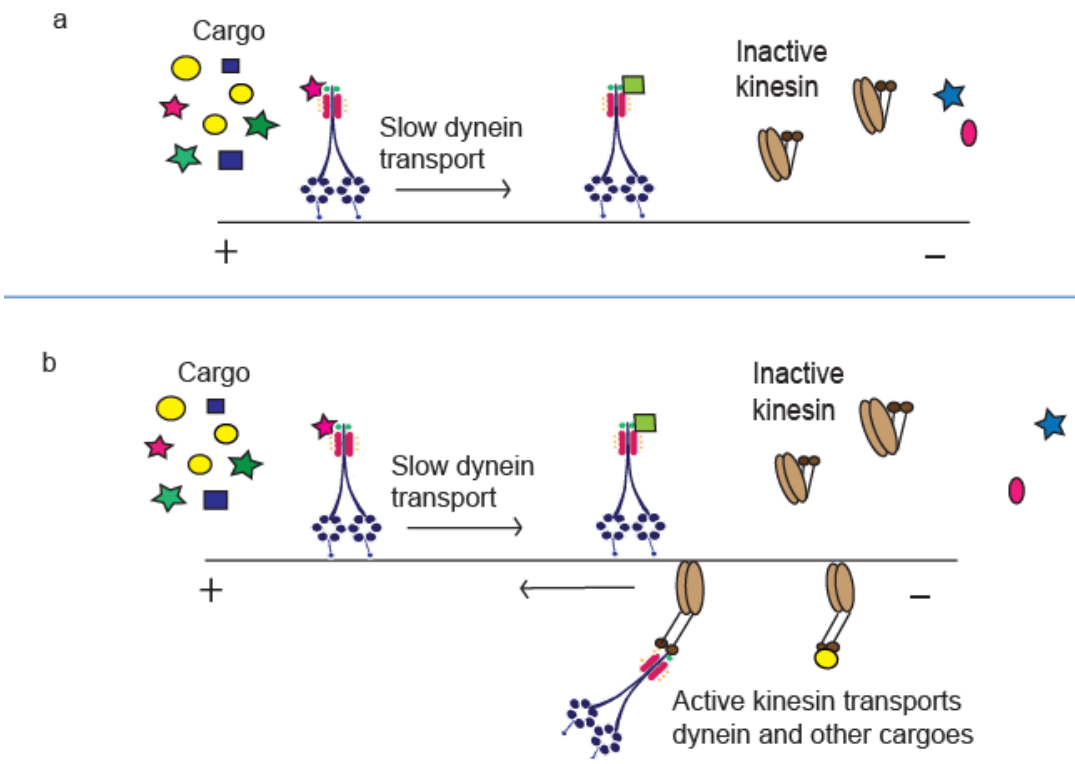

Figure 6.2: Model of KLC1's role in regulation of cargo transport in the dynein deficient *Loa* mouse. a) Global effect of increased KLC-1 in *Loa/Loa* cells. Retrograde transport of cargos via dynein is slow. An imbalance of organelles, neurotrophic factors and motor proteins is detected by the cell. The cell responds by increasing KLC-1 expression, which holds kinesin inactive, preventing further transport of cargos to the periphery of the cell. b) Local effect of increased KLC-1 in *Loa/Loa* cells. KLC-1 binds to more DIC in *Loa/Loa* cells than wild-type. Binding activates kinesin to transport dynein and other cargos to the periphery of the cell. Preferential transport of dynein and a reduction in transport of other cargoes will increase the quantity of available dynein motors for retrograde trafficking.

6.6 Conclusion

The data presented in this thesis demonstrate kinetics of dynein mediated transport in both MEF cells and MNs. Comparisons of wild-type cells and those expressing mutant dynein (*Loa)* have produced intriguing results with regard to direct effects on kinetics and indirect effects on cell signalling and gene expression. These data have advanced our understanding of dynein's role in endocytic trafficking and signalling and may help us to establish causal pathways leading to neurodegeneration and neuropathies. Through understanding comes advancement towards therapeutic targets for reduction and/or elimination of the severe physical and mental phenotypes associated with such diseases. This work has identified TCF25 as one such possibility and GF induced increases in cell signalling are suggestive that GF antagonists may be another.

The lack of resilience in neuronal cells likely comes from the intrinsic post-mitotic nature and immense size of these remarkable cells. Finding a cure for neurological diseases is arguably the greatest challenge facing the scientific world today, however I hope that data provided here is a step in the right direction.

Appendix

Section 1: wild-type v *Loa/Loa*

Gene	wild-type	+/*Loa*	*Loa/Loa*	Difference	rank	DiffScore	rank
1110033K02Rik	299.7043	446.701	490.4942	190.7899	117	15.2402	88
1700001C14Rik	606.3853	835.638	1036.026	429.6407	63	336.687	1
2310021P13Rik	3056.875	4235.99	4646.516	1589.641	12	13.9501	92
3110037B15Rik	734.1217	989.026	1169.834	435.7123	62	50.0171	37
4731420N21	811.3674	1139.31	1256.109	444.7416	59	58.437	30
4833414E09Rik	1326.167	1912.92	2255.813	929.646	23	32.0577	56
4930453J04Rik	520.0317	825.538	931.2266	411.1949	66	69.7107	23
5330432J10Rik	480.5189	664.47	843.3755	362.8566	78	53.0645	33
5830407P18Rik	399.3127	608.566	664.9161	265.6034	95	68.6584	24
5830417I10Rik	767.9138	1094.19	1214.533	446.6192	58	59.2835	27
6030432P03Rik	1113.585	1504.99	1678.134	564.549	44	34.6564	50
6720454L07Rik	309.5771	429.248	483.2011	173.624	123	21.4227	72
8430401P03Rik	440.2191	594.196	681.1563	240.9372	107	51.2713	34
9430047F21Rik	440.1024	632.859	694.6588	254.5564	100	59.2835	27
9530014D17Rik	744.2233	1068.31	1126.951	382.7277	72	20.901	75
9530018D06Rik	360.5136	621.356	651.3539	290.8403	89	32.4838	54
9630013P03Rik	1006.005	1163.71	1551.673	545.668	46	13.3467	93
9630032J03Rik	663.9113	917.229	1041.446	377.5347	75	26.4065	64
9830166E18Rik	496.7465	723.582	822.1331	325.3866	84	74.0551	20
9845300_4289	1225.763	895.876	740.4278	-485.335	55	-73.441	21
A130017C09Rik	337.4109	514.532	602.6982	265.2873	94	32.4838	54
A430103B12Rik	783.9323	1299.09	1520.167	736.2347	34	115.288	12
A530083M17Rik	709.1996	957.445	1237.907	528.7074	49	49.9902	38
A630076E03Rik	599.74	897.883	976.7273	376.9873	76	26.4065	64
A730021C13Rik	673.0079	864.588	1169.08	496.0721	53	17.7985	77
A730058G16Rik	316.0765	443.98	482.7279	166.6514	126	21.2349	73
A830029A02Rik	386.3829	596.629	636.8015	250.4186	102	28.6847	58
A930004J17Rik	590.6741	782.98	950.929	360.2549	79	94.8222	18
A930019L04Rik	486.7676	781.841	750.7315	263.9639	96	27.7802	61
A930104B17Rik	292.7176	355.415	471.2229	178.5053	121	26.5706	63
Acat3	2819.561	2333.98	1691.049	-1128.51	20	-17.084	79
Acvr1b	1959.145	1400.95	1175.916	-783.229	30	-125.15	10
AI605517	756.8443	1011.03	1160.179	403.3347	69	34.4666	51
Ankrd11	749.5829	1076.73	1249.005	499.4221	51	25.3871	67
Atp6ap2	1632.037	1369.61	1054.399	-577.638	41	-17.672	78
B130020M22Rik	607.6091	1013.71	1179.1	571.4909	43	336.687	1
B130047N10Rik	315.5312	495.975	485.5807	170.0495	124	26.7048	62
B230208H17Rik	708.1891	1080.04	1072.018	363.8289	77	90.1765	19
C130002K18Rik	354.4715	461.704	623.4166	268.9451	92	43.8329	42
C130045F17Rik	353.6219	537.828	608.0193	254.3974	101	23.868	70
C130064E22Rik	471.4221	631.384	720.0695	248.6474	104	21.1806	74
C330006D17Rik	351.4017	485.573	543.8321	192.4304	116	24.2849	69
C530036F05Rik	964.4423	1335.62	1564.357	599.9147	37	24.9076	68
C530040B18Rik	384.4811	529.288	581.4246	196.9435	114	16.5209	81
C79267	388.7869	637.239	638.6948	249.9079	103	55.6839	32
Chd1	312.8964	450.732	502.9508	190.0544	118	15.6768	83
Clasp1	786.2283	1176.6	1247.348	461.1197	57	336.687	1
Clspn	352.4508	472.391	608.5924	256.1416	99	26.2175	66
Csnk1e	5784.711	5941.49	8724.002	2939.291	6	23.4589	71
D030064C08Rik	493.6785	683.019	834.3757	340.6972	81	57.474	31

D230005E09Rik	359.535	531.947	626.7526	267.2176	93	47.8395	39
D230017C05Rik	1527.57	1886.89	2437.518	909.948	26	69.8255	22
D230034L24Rik	730.958	1004.9	1169.044	438.086	61	336.687	1
D430007A19Rik	1805.916	2353	2910.541	1104.625	21	44.1363	41
D930044I17Rik	503.8788	739.279	911.0601	407.1813	67	111.609	13
E130318A13Rik	207.0589	271.215	361.6896	154.6307	128	16.7565	80
E430033B07Rik	955.5	1134.48	1722.673	767.173	31	110.428	14
EG633692	2088.418	1671.67	1343.883	-744.535	32	-13.006	94
Eif2s3y	165.0472	517.901	800.116	635.0688	36	20.2864	76
Enah	564.2087	732.42	1007.616	443.4073	60	29.0874	57
Golga2	764.8349	1101.29	1568.636	803.8011	29	336.687	1
Gtl2	695.7593	1017.66	1233.999	538.2397	47	15.6065	84
Gukmi1	409.3028	620.794	625.0294	215.7266	110	36.7335	48
Jarid1d	160.5449	308.627	396.0511	235.5062	108	41.0403	43
Jph4	344.2819	441.828	521.3304	177.0485	122	28.0761	60
Klc1	7438.797	6275.12	2454.743	-4984.05	3	-45.904	40
LOC100039786	4105.797	3393.41	2602.609	-1503.19	13	-28.43	59
LOC100045054	502.2799	807.898	883.488	381.2081	73	16.2594	82
LOC100046744	2319.667	3180.27	4433.915	2114.248	11	14.9726	89
LOC100047082	1916.344	2476.57	3136.012	1219.668	17	67.5043	25
LOC386124	584.102	710.671	924.6829	340.5809	82	14.4001	91
LOC641366	430.9122	776.694	678.3563	247.4441	106	35.7454	49
Mtap2	519.0618	893.484	919.5319	400.4701	70	62.6883	26
Mtch2	6759.886	5602.26	4458.917	-2300.97	10	-121.16	11
Nipbl	2230.627	3141.73	3437.668	1207.041	18	39.7463	45
Nrk	765.6023	1346.22	1264.095	498.4927	52	336.687	1
Nsmce2	3368.11	2652.1	2224.824	-1143.29	19	-40.548	44
Pcmt1	1998.705	1639.68	1257.261	-741.444	33	-15.463	85
Ppp1r12a	1170.69	1517.88	2446.846	1276.156	15	336.687	1
Ppp1r13b	1347.261	1032.68	791.0375	-556.224	45	-37.863	47
Prdm2	1662.745	2198.37	2547.745	885	28	59.2835	27
Psmd5	1557.549	1187.63	1024.593	-532.956	48	-106.57	16
Purb	711.3504	972.354	1134.929	423.5786	65	33.3361	52
Rrm2	895.1329	603.57	515.8557	-379.277	74	-14.971	89
scl0001487.1_50	1318.808	1231.8	837.1353	-481.673	56	-50.914	36
scl000972.1_0	456.4228	715.201	794.9742	338.5514	83	108.35	15
Slit2	340.4627	477.252	511.2849	170.8222	125	15.4202	87
Stxbp3	269.1633	367.459	422.5476	153.3843	129	15.4222	86
Tcf25	747.0996	1063.56	1172.774	425.6744	64	99.3109	17
Tmem63b	2207.706	2985	3446.837	1239.131	16	50.9301	35
Tssc8	738.8944	1131.16	1313.397	574.5026	42	33.0558	53
Ttn	471.2359	773.904	959.9691	488.7332	54	336.687	1
Xist	3145.592	3236.25	292.1439	-2853.45	7	-334.19	9
Zfp326	538.4688	793.265	817.4946	279.0258	91	38.4322	46

Section 2: wild-type v *+/Loa*

4930453J04Rik	520.0317	825.538	931.2266	305.5064	86	69.7107	6
5830407P18Rik	399.3127	608.566	664.9161	209.2537	112	68.6584	7
9530018D06Rik	360.5136	621.356	651.3539	260.8425	97	32.4838	11
A430103B12Rik	783.9323	1299.09	1520.167	515.1567	50	115.288	4
A930019L04Rik	486.7676	781.841	750.7315	295.0736	88	27.7802	12
Adam33	372.1302	596.789	533.3846	224.6584	109	10.9142	20

B130020M22Rik	607.6091	1013.71	1179.1	406.0979	68	336.687	1
B130047N10Rik	315.5312	495.975	485.5807	180.4441	120	26.7048	13
Bst2	1777.211	1184.26	1479.183	-592.952	38	#######	24
C130045F17Rik	353.6219	537.828	608.0193	184.2058	119	23.868	14
C230048N02Rik	273.0325	434.837	297.3929	161.8042	127	#######	24
C79267	388.7869	637.239	638.6948	248.4521	105	55.6839	9
D430006A07Rik	349.3383	545.037	520.7577	195.6987	115	16.1778	17
Ddx6	1553.528	2469.47	2642.629	915.941	25	2.44077	22
Gukmi1	409.3028	620.794	625.0294	211.4911	111	36.7335	10
Hmox1	1366.73	460.719	1181.924	-906.011	27	#######	24
Jmjd2a	456.9127	257.482	381.7981	-199.431	113	#######	24
LOC100045405	632.4607	1016.55	1212.991	384.0883	71	12.0585	18
Mtap6	2416.568	3740.87	3498.963	1324.301	14	18.8519	16
Nfic	471.4015	824.266	920.268	352.8641	80	10.9582	19
Nrk	765.6023	1346.22	1264.095	580.6197	40	336.687	1
Peg3	1230.301	1881.76	1620.805	651.461	35	22.122	15
Pop4	8059.39	5361.2	6662.532	-2698.19	8	-1.4376	23
Prmt1	24504.9	9644.31	21487.24	-14860.6	1	#######	24
Rn18s	8297.79	14056.5	13853.01	5758.67	2	9.9987	21
scl000972.1_0	456.4228	715.201	794.9742	258.7779	98	108.35	5
Ttn	471.2359	773.904	959.9691	302.6682	87	336.687	1
Usp40	572.353	879.668	845.3895	307.3151	85	58.2364	8
Section 3: *+/Loa* v *Loa/Loa*							
Dcn	6771.753	7185.81	4609.991	-2575.81	9	-30.054	5
E430033B07Rik	955.5	1134.48	1722.673	588.189	39	110.428	3
Eif2s3y	165.0472	517.901	800.116	282.2151	90	20.2864	7
Klc1	7438.797	6275.12	2454.743	-3820.38	4	-45.904	4
Ppp1r12a	1170.69	1517.88	2446.846	928.968	24	336.687	1
Slc4a1	2067.334	1661.36	2624.223	962.866	22	24.4116	6
Xist	3145.592	3236.25	292.1439	-2944.1	5	-334.19	2

Appendix: Microarray data from wild-type, +/*Loa* and *Loa/Loa* E13 brains. Genes identified as up or down-regulated in +/*Loa* and *Loa/Loa* when compared to wild-type are listed (left). Gene expression readings are listed for wild-type (purple), +/*Loa* (peach) and Loa/Loa (blue). Difference in signal from wild-type is shown in yellow for *Loa/Loa* (section 1), +/*Loa* (section 2) and +/*Loa* v *Loa/Loa* (section 3). Positive numbers indicate up-regulation whilst negative numbers indicate down-regulation. Ranks were allocated (green) depending on the difference in signal between the genotypes. Diff. scores indicating reproducibility across samples are shown. Scores above 30 indicate good reproducibility (pink) whereas below 30 is poor (light blue). Ranks based on diff. scores are shown far right.

References

1. Hook, P. and R.B. Vallee, *The dynein family at a glance.* J Cell Sci, 2006. **119**(Pt 21): p. 4369-71.

2. Pfister, K.K., et al., *Genetic analysis of the cytoplasmic dynein subunit families.* PLoS Genet, 2006. **2**(1): p. 0022-0026.

3. Porter, M.E., et al., *Cytoplasmic dynein heavy chain 1b is required for flagellar assembly in Chlamydomonas.* Mol Biol Cell, 1999. **10**(3): p. 693-712.

4. Perrone, C.A., et al., *A novel dynein light intermediate chain colocalizes with the retrograde motor for intraflagellar transport at sites of axoneme assembly in chlamydomonas and Mammalian cells.* Mol Biol Cell, 2003. **14**(5): p. 2041-56.

5. DeWitt, M.A., et al., *Cytoplasmic dynein moves through uncoordinated stepping of the AAA+ ring domains.* Science, 2012.**335**(6065): p. 221-5.

6. King, S.M., *AAA domains and organization of the dynein motor unit.* J Cell Sci, 2000. **113 (Pt 14)**: p. 2521-6.

7. Kon, T., et al., *Distinct functions of nucleotide-binding/hydrolysis sites in the four AAA modules of cytoplasmic dynein.* Biochemistry, 2004. **43**(35): p. 11266-74.

8. Cho, C., S.L. Reck-Peterson, and R.D. Vale, *Regulatory ATPase sites of cytoplasmic dynein affect processivity and force generation.* J Biol Chem, 2008. **283**(38): p. 25839-45.

9. Silvanovich, A., et al., *The third P-loop domain in cytoplasmic dynein heavy chain is essential for dynein motor function and ATP-sensitive microtubule binding.* Mol Biol Cell, 2003. **14**(4): p. 1355-65.

10. Gee, M.A., J.E. Heuser, and R.B. Vallee, *An extended microtubule-binding structure within the dynein motor domain.* Nature, 1997. **390**(6660): p. 636-9.

11. Kon, T., K. Sutoh, and G. Kurisu, *X-ray structure of a functional full-length dynein motor domain.* Nat Struct Mol Biol, 2011 **18**(6): p. 638-42.

12. Burgess, S.A., et al., *Dynein structure and power stroke.* Nature, 2003. **421**(6924): p. 715-8.

13. Roberts, A.J., et al., *AAA+ Ring and linker swing mechanism in the dynein motor.* Cell, 2009. **136**(3): p. 485-95.

14. Willemsen, M.H., et al., *Mutations in DYNC1H1 cause severe intellectual disability with neuronal migration defects.* J Med Gen, 2012. **49**(3): p. 179-83.

15. Imamula, K., et al., *The coordination of cyclic microtubule association/dissociation and tail swing of cytoplasmic dynein.* PNAS U S A, 2007. **104**(41): p. 16134-9.

16. Reck-Peterson, S.L., et al., *Single-molecule analysis of dynein processivity and stepping behaviour.* Cell, 2006. **126**(2): p. 335-48.

17. Qiu, W., et al., *Dynein achieves processive motion using both stochastic and coordinated stepping.* Nat Struct Mol Biol, 2012. **19**(2): p. 193-200.

18. Gennerich, A and Vale, R., *Walking the walk: How kinesin and dynein coordinate their steps.* Curr Opin Cell Biol, 2009. **21**(1): p. 59-67.

19. Gennerich, A., et al., *Force-induced bidirectional stepping of cytoplasmic dynein.* Cell, 2007. **131**(5): p. 952-965.

20. Ori-McKenney, K.M., et al., *A cytoplasmic dynein tail mutation impairs motor processivity.* Nat Cell Biol, 2010. **12**(12): p. 1228-34.

21. Ross, J.L., et al., *Processive bidirectional motion of dynein-dynactin complexes in vitro.* Nat Cell Biol, 2006. **8**(6): p. 562-70.

22. Hendricks, A.G., J.E. Lazarus, and E.L. Holzbaur, *Dynein at odd angles?* Nat Cell Biol, 2010. **12**(12): p. 1126-8.

23. Ally, S., et al., *Opposite-polarity motors activate one another to trigger cargo transport in live cells.* J Cell Biol, 2009. **187**(7): p. 1071-82.

24. Kuta, A., et al., *Mouse cytoplasmic dynein intermediate chains: identification of new isoforms, alternative splicing and tissue distribution of transcripts.* PLoS One, 2010. **5**(7): p. e11682.

25. Dillman, J.F., 3rd and K.K. Pfister, *Differential phosphorylation in vivo of cytoplasmic dynein associated with anterogradely moving organelles.* J Cell Biol, 1994. **127**(6 Pt 1): p. 1671-81.

26. Nurminsky, D.I., et al., *Cytoplasmic dynein intermediate-chain isoforms with different targeting properties created by tissue-specific alternative splicing.* Mol Cell Biol, 1998. **18**(11): p. 6816-25.

27. Ha, J., et al., *A neuron-specific cytoplasmic dynein isoform preferentially transports TrkB signaling endosomes.* J Cell Biol, 2008. **181**(6): p. 1027-39.

28. Steffen, W., et al., *The involvement of the intermediate chain of cytoplasmic dynein in binding the motor complex to membranous organelles of Xenopus oocytes.* Mol Biol Cell, 1997. **8**(10): p. 2077-88.

29. Tynan, S.H., M.A. Gee, and R.B. Vallee, *Distinct but overlapping sites within the cytoplasmic dynein heavy chain for dimerization and for intermediate chain and light intermediate chain binding.* J Biol Chem, 2000. **275**(42): p. 32769-74.

30. Tan, S.C., J. Scherer, and R.B. Vallee, *Recruitment of dynein to late endosomes and lysosomes through light intermediate chains.* Mol Biol Cell, 2011. **22**(4): p. 467-77.

31. Lo, K.W., H.M. Kan, and K.K. Pfister, *Identification of a novel region of the cytoplasmic Dynein intermediate chain important for dimerization in the absence of the light chains.* J Biol Chem, 2006. **281**(14): p. 9552-9.

32. Lo, K.W., et al., *Interaction of the DYNLT (TCTEX1/RP3) light chains and the intermediate chains reveals novel intersubunit regulation during assembly of the dynein complex.* J Biol Chem, 2007. **282**(51): p. 36871-8.

33. Brill, L.B., 2nd and K.K. Pfister, *Biochemical and molecular analysis of the mammalian cytoplasmic dynein intermediate chain.* Methods, 2000. **22**(4): p. 307-16.

34. Schnorrer, F., K. Bohmann, and C. Nusslein-Volhard, *The molecular motor dynein is involved in targeting swallow and bicoid RNA to the anterior pole of Drosophila oocytes.* Nat Cell Biol, 2000. **2**(4): p. 185-90.

35. Fejtova, A., et al., *Dynein light chain regulates axonal trafficking and synaptic levels of Bassoon.* J Cell Biol, 2009. **185**(2): p. 341-55.

36. Niclas, J., V.J. Allan, and R.D. Vale, *Cell cycle regulation of dynein association with membranes modulates microtubule-based organelle transport.* J Cell Biol, 1996. **133**(3): p. 585-93.

37. Dell, K.R., C.W. Turck, and R.D. Vale, *Mitotic phosphorylation of the dynein light intermediate chain is mediated by cdc2 kinase.* Traffic, 2000. **1**(1): p. 38-44.

38. Whyte, J., et al., *Phosphorylation regulates targeting of cytoplasmic dynein to kinetochores during mitosis.* J Cell Biol, 2008. **183**(5): p. 819-34.

39. Gill, S.R., et al., *Dynactin, a conserved, ubiquitously expressed component of an activator of vesicle motility mediated by cytoplasmic dynein.* J Cell Biol, 1991. **115**(6): p. 1639-50.

40. Deacon, S.W., et al., *Dynactin is required for bidirectional organelle transport.* J Cell Biol, 2003. **160**(3): p. 297-301.

41. Karki, S. and E.L. Holzbaur, *Affinity chromatography demonstrates a direct binding between cytoplasmic dynein and the dynactin complex.* J Biol Chem, 1995. **270**(48): p. 28806-11.

42. Vaughan, K.T. and R.B. Vallee, *Cytoplasmic dynein binds dynactin through a direct interaction between the intermediate chains and p150Glued.* J Cell Biol, 1995. **131**(6 Pt 1): p. 1507-16.

43. Flores-Rodriguez, N., et al., *Roles of dynein and dynactin in early endosome dynamics revealed using automated tracking and global analysis.* PLoS One, 2011. **6**(9): p. e24479.

44. Melkonian, K.A., et al., *Mechanism of dynamitin-mediated disruption of dynactin.* J Biol Chem, 2007. **282**(27): p. 19355-64.

45. Hoogenraad, C.C., et al., *Mammalian Golgi-associated Bicaudal-D2 functions in the dynein-dynactin pathway by interacting with these complexes.* EMBO J, 2001. **20**(15): p. 4041-54.

46. Jordens, I., et al., *The Rab7 effector protein RILP controls lysosomal transport by inducing the recruitment of dynein-dynactin motors.* Curr Biol, 2001. **11**(21): p. 1680-5.

47. Howell, B.J., et al., *Cytoplasmic dynein/dynactin drives kinetochore protein transport to the spindle poles and has a role in mitotic spindle checkpoint inactivation.* J Cell Biol, 2001. **155**(7): p. 1159-72.

48. King, J.M., T.S. Hays, and R.B. Nicklas, *Dynein is a transient kinetochore component whose binding is regulated by microtubule attachment, not tension.* J Cell Biol, 2000. **151**(4): p. 739-48.

49. Yamada, M., et al., *LIS1 and NDEL1 coordinate the plus-end-directed transport of cytoplasmic dynein.* EMBO 2008. **27**(19). p. 2471-2483.

50. Sasaki, S., et al., *A LIS1/NUDEL/Cytoplasmic dynein heavy chain complex in the developing and adult nervous system.* Neuron, 2000. **28**. p. 681-696.

51. Tanaka, T., et al., *Lis1 and doublecortin function with dynein to mediate the coupling of the nucleus to the centrosome in neuronal migration.* J Cell Biol, 2004. **165**(5). p. 709-721.

52. Stehman, S., et al., *NudE and NudEL are required for mitotic progression and are involved in dynein recruitment to kinetochores.* J Cell Biol, 2007. **178**(4). p. 583-594.

53. Liang, Y., et al., *Nudel functions in membrane traffic mainly through association with Lis1 and cytoplasmic dynein.* J Cell Biol, 2004. **164**(4): p. 557-66.

54. Lam, C. et al., *Functional interplay between LIS1, NDE1 and NDEL1 in dynein-dependent organelle positioning.*J Cell Sci, 2009. **123**. p. 202-212.

55. Kardon, J.R. and R.D. Vale, *Regulators of the cytoplasmic dynein motor.* Nat Rev Mol Cell Biol, 2009. **10**(12): p. 854-65.

56. Verhey, K.J. and J.W. Hammond, *Traffic control: regulation of kinesin motors.* Nature reviews. Mol Cell Biol, 2009. **10**(11): p. 765-77.

57. Hirokawa, N., et al., *Kinesin superfamily motor proteins and intracellular transport.* Nature reviews. Mol Cell Biol, 2009. **10**(10): p. 682-96.

58. Hackney, D.D., N. Baek, and A.C. Snyder, *Half-site inhibition of dimeric kinesin head domains by monomeric tail domains.* J Biochem, 2009. **48**(15): p. 3448-56.

59. Cai, D., et al., *Kinesin-1 structural organization and conformational changes revealed by FRET stoichiometry in live cells.* J Cell Biol, 2007. **176**(1): p. 51-63.

60. Seiler, S., et al., *Cargo binding and regulatory sites in the tail of fungal conventional kinesin.* Nat Cell Biol, 2000. **2**(6): p. 333-8.

61. Rahman, A., D.S. Friedman, and L.S. Goldstein, *Two kinesin light chain genes in mice. Identification and characterization of the encoded proteins.* J Biol Chem, 1998. **273**(25): p. 15395-403.

62. Wozniak, M.J. and V.J. Allan, *Cargo selection by specific kinesin light chain 1 isoforms.* EMBO J, 2006. **25**(23): p. 5457-68.

63. Ligon, L.A., et al., *A direct interaction between cytoplasmic dynein and kinesin I may coordinate motor activity.* J Biol Chem, 2004. **279**(18): p. 19201-8.

64. Dietrich, K.A., et al., *The kinesin-1 motor protein is regulated by a direct interaction of its head and tail.* Proc Natl Acad Sci U S A, 2008. **105**(26): p. 8938-43.

65. Verhey, K.J., et al., *Light chain-dependent regulation of Kinesin's interaction with microtubules.* J Cell Biol, 1998. **143**(4): p. 1053-66.

66. Gindhart, J.G., Jr., et al., *Kinesin light chains are essential for axonal transport in Drosophila.* J Cell Biol, 1998. **141**(2): p. 443-54.

67. Weedon, M.N., et al., *Exome sequencing identifies a DYNC1H1 mutation in a large pedigree with dominant axonal Charcot-Marie-Tooth disease.* Am J Hum Genet, 2011. **89**(2): p. 308-12.

68. Harms, M.B., et al., *Mutations in the tail domain of DYNC1H1 cause dominant spinal muscular atrophy.* Neurology, 2012. **78**(22): p. 1714-20.

69. Puls, I., et al., *Mutant dynactin in motor neuron disease.* Nat Genet, 2003. **33**(4): p. 455-6.

70. LaMonte, B., et al., *Disruption of dynein/dynactin inhibits axonal transport in motor neurons causing late-onset progressive degeneration.* Neuron, 2002. **34**. p. 715-727.

71. Pilz, D.T., et al., *LIS1 and XLIS (DCX) mutations cause most classical lissencephaly, but different patterns of malformation.* Hum Mol Genet, 1998. **7**(13): p. 2029-37.

72. Wynshaw-Boris, A. and M.J. Gambello, *LIS1 and dynein motor function in neuronal migration and development.* Genes Dev, 2001. **15**(6): p. 639-51.

73. Hrabe de Angelis, M.H., et al., *Genome-wide, large-scale production of mutant mice by ENU mutagenesis.* Nat Genet, 2000. **25**(4): p. 444-7.

74. Witherden, A.S., et al., *An integrated genetic, radiation hybrid, physical and transcription map of a region of distal mouse chromosome 12, including an imprinted locus and the 'Legs at odd angles' (Loa) mutation.* Gene, 2002. **283**(1-2): p. 71-82.

75. Hafezparast, M., et al., *Mutations in dynein link motor neuron degeneration to defects in retrograde transport.* Science, 2003. **300**(5620): p. 808-12.

76. Dupuis, L., et al., *Mice with a mutation in the dynein heavy chain 1 gene display sensory neuropathy but lack motor neuron disease.* Exp Neurol, 2009. **215**(1): p. 146-52.

77. Chen, X.J., et al., *Proprioceptive sensory neuropathy in mice with a mutation in the cytoplasmic Dynein heavy chain 1 gene.* J Neurosci, 2007. **27**(52): p. 14515-24.

78. Rogers, D.C., et al., *SHIRPA, a protocol for behavioral assessment: validation for longitudinal study of neurological dysfunction in mice.* Neurosci Lett, 2001. **306**(1-2): p. 89-92.

79. Ilieva, H.S., et al., *Mutant dynein (Loa) triggers proprioceptive axon loss that extends survival only in the SOD1 ALS model with highest motor neuron death.* PNAS, 2008. **105**(34): p. 12599-604.

80. Chen, X.J., et al., *Proprioceptive sensory neuropathy in mice with a mutation in the cytoplasmic Dynein heavy chain 1 gene.* J Neurosci, 2007. **27**(52): p. 14515-24.

81. Ori-McKenney, K.M. and R.B. Vallee, *Neuronal migration defects in the Loa dynein mutant mouse.* Neural Dev, 2011. **6**: p. 26.

82. Deng, W., et al., *Neurodegenerative mutation in cytoplasmic dynein alters its organization and dynein-dynactin and dynein-kinesin interactions.* J Biol Chem, 2010. **285**(51): p. 39922-34.

83. Banks, G.T., et al., *Behavioral and other phenotypes in a cytoplasmic Dynein light intermediate chain 1 mutant mouse.* J Neurosci. **31**(14): p. 5483-94.

84. Kumari, S., S. Mg, and S. Mayor, *Endocytosis unplugged: multiple ways to enter the cell.* Cell Res, 2010. **20**(3): p. 256-75.

85. Swanson, J.A., *Shaping cups into phagosomes and macropinosomes.* Nat Rev Mol Cell Biol, 2008. **9**(8): p. 639-49.

86. Scott, C.C., R.J. Botelho, and S. Grinstein, *Phagosome maturation: a few bugs in the system.* J Membr Biol, 2003. **193**(3): p. 137-52.

87. Mercanti, V., et al., *Selective membrane exclusion in phagocytic and macropinocytic cups.* J Cell Sci, 2006. **119**(Pt 19): p. 4079-87.

88. Hansen, C.G., et al., *SDPR induces membrane curvature and functions in the formation of caveolae.* Nat Cell Biol, 2009. **11**(7): p. 807-14.

89. Williams, T.M. and M.P. Lisanti, *The caveolin proteins.* Genome Biol, 2004. **5**(3): p. 214.

90. Singh, R.D., et al., *Caveolar endocytosis and microdomain association of a glycosphingolipid analog is dependent on its sphingosine stereochemistry.* J Biol Chem, 2006. **281**(41): p. 30660-8.

91. Pearse, B.M., *Coated vesicles from pig brain: purification and biochemical characterization.* J Mol Biol, 1975. **97**(1): p. 93-8.

92. Ybe, J.A., et al., *Clathrin self-assembly is regulated by three light-chain residues controlling the formation of critical salt bridges.* EMBO J, 1998. **17**(5): p. 1297-303.

93. Chen, C.Y., et al., *Clathrin light and heavy chain interface: alpha-helix binding superhelix loops via critical tryptophans.* EMBO J, 2002. **21**(22): p. 6072-82.

94. Kirchhausen, T., *Clathrin.* Annu Rev Biochem, 2000. **69**: p. 699-727.

95. Ohno, H., *Physiological roles of clathrin adaptor AP complexes: lessons from mutant animals.* J Biochem, 2006. **139**(6): p. 943-8.

96. Morgan, J.R., et al., *A conserved clathrin assembly motif essential for synaptic vesicle endocytosis.* J Neurosci, 2000. **20**(23): p. 8667-76.

97. Aguilar, R.C., et al., *Functional domain mapping of the clathrin-associated adaptor medium chains mu1 and mu2.* J Biol Chem, 1997. **272**(43): p. 27160-6.

98. Sorkin, A. and G. Carpenter, *Interaction of activated EGF receptors with coated pit adaptins.* Science, 1993. **261**(5121): p. 612-5.

99. Doherty, G.J. and H.T. McMahon, *Mechanisms of endocytosis.* Annu Rev Biochem, 2009. **78**: p. 857-902.

100. Ungewickell, E., et al., *Role of auxilin in uncoating clathrin-coated vesicles.* Nature, 1995. **378**(6557): p. 632-5.

101. Newmyer, S.L., A. Christensen, and S. Sever, *Auxilin-dynamin interactions link the uncoating ATPase chaperone machinery with vesicle formation.* Dev Cell, 2003. **4**(6): p. 929-40.

102. Rapoport, I., et al., *A motif in the clathrin heavy chain required for the Hsc70/auxilin uncoating reaction.* Mol Biol Cell, 2008. **19**(1): p. 405-13.

103. Schmid, S.L. and J.E. Rothman, *Two classes of binding sites for uncoating protein in clathrin triskelions.* J Biol Chem, 1985. **260**(18): p. 10050-6.

104. Bock, J.B., et al., *A genomic perspective on membrane compartment organization.* Nature, 2001. **409**(6822): p. 839-41.

105. Stenmark, H. and V.M. Olkkonen, *The Rab GTPase family.* Genome Biol, 2001. **2**(5): p. REVIEWS3007.

106. Desnoyers, L., Anant, J.S., and Seabra, M.C., *Geranylgeranylation of Rab proteins.* Biochem Soc Trans, 1996. **24**(3): p. 699-701.

107. Horgan, C. P. and McCaffrey, M.W., *Rab GTPases and microtubule motors.* Biochem Soc Trans, 2011. **39**(5): p. 1202-1206.

108. Bielli, A., et al., *The small GTPase Rab4a interacts with the central region of cytoplasmic dynein light intermediate chain-1.*Biochem Biophys Res Commun, 2001. **281**(5): p. 1141-1153.

109. Jordens, I., et al., *The Rab7 effector protein RILP controls lysosomal transport by inducing the recruitment of dynein-dynactin motors.* Cur Biol, 2001. **11**: p. 1680-1685.

110. Horgan, C. P., et al., *Rab11-FIP3 links the Rab11 GTPase and cytoplasmic dynein to mediate transport to the endosomal-recycling compartment.* J Cell Sci, 2010. **123**(2): p. 181-191.

110. Hutagalung, A.H. and Novick, P.J., *Role of Rab GTPases in membrane traffic and cell physiology*. Physiol Rev, 2011. **91**: p. 119-149.

111. Wilson, J.M., et al., *EEA1, a tethering protein of the early sorting endosome, shows a polarised distribution in hippocampal neurons, epithelial cells, and fibroblasts.* Mol Biol Cell, 2000. **11**: p. 2657-2671.

112. Trischler, M., W. Stoorvogel, and O. Ullrich, *Biochemical analysis of distinct Rab5- and Rab11-positive endosomes along the transferrin pathway.* J Cell Sci, 1999. **112 (Pt 24)**: p. 4773-83.

113. Woodman, P. *ESCRT proteins, endosome organisation and mitogenic receptor down-regulation.* Biochem Soc Trans, **37**(1): p. 146-150.

114. Matsuo, H., et al., *Role of LBPA and Alix in multivesicular liposome formation and endosome organization.* Science, 2004. **303**(5657): p. 531-4.

115. White, I.J., et al., *EGF stimulates annexin 1-dependent inward vesiculation in a multivesicular endosome subpopulation.* EMBO J, 2006. **25**(1): p. 1-12.

116. Marsh, M., et al., *Three-dimensional structure of endosomes in BHK-21 cells.* PNAS U S A, 1986. **83**(9): p. 2899-903.

117. Chen, B., et al., *Endocytic sorting and recycling require membrane phosphatidylserine asymmetry maintained by TAT-1/CHAT-1.* PLoS Genet. **6**(12): p. e1001235.

118. Feng, Y., B. Press, and A. Wandinger-Ness, *Rab 7: an important regulator of late endocytic membrane traffic.* J Cell Biol, 1995. **131**(6 Pt 1): p. 1435-52.

119. Piper, R.C. and J.P. Luzio, *Late endosomes: sorting and partitioning in multivesicular bodies.* Traffic, 2001. **2**(9): p. 612-21.

120. Bright, N.A., Gratian, M.J., Luzio, J.P., *Endocytic delivery to lysosomes mediated by concurrent fusion and kissing events in living cells.* Curr Biol, 2005. **15**(4): p. 360-365.

121. Peplowska, K., et al., *The CORVET tethering complex interacts with the yeast Rab5 homolog Vps21 and is involved in endo-lysosomal biogenesis.* Dev Cell, 2007. **12**: p. 739-750.

122. Luzio, J.P., Pryor, P.R., and Bright, N.A., *Lysosomes: fusion and function.* Nat Rev Mol Cell Biol, 2007. **8**: p. 622-632.

123. Ganley, I.G., et al., *Rab9 GTPase regulates late endosome size and requires effector interaction for its stability.* Mol Biol Cell, 2004. **15**(12): p. 5420-30.

124. McKanna, J.A., H.T. Haigler, and S. Cohen, *Hormone receptor topology and dynamics: morphological analysis using ferritin-labeled epidermal growth factor.* PNAS USA, 1979. **76**(11): p. 5689-93.

125. Driskell, O.J., et al., *Dynein is required for receptor sorting and the morphogenesis of early endosomes.* Nat Cell Biol, 2007. **9**(1): p. 113-20.

126. Schuster, M., et al., *Transient binding of dynein controls bidirectional long-range motility of early endosomes.* PNAS U S A, 2011. **108**(9): p. 3618-23.

127. Ceresa, B.P. and S.J. Bahr, *rab7 activity affects epidermal growth factor:epidermal growth factor receptor degradation by regulating endocytic trafficking from the late endosome.* J Biol Chem, 2006. **281**(2): p. 1099-106.

128. McKay, S.E., et al., *The expression of trkB and p75 and the role of BDNF in the developing neuromuscular system of the chick embryo.* Development, 1996. **122**(2): p. 715-24.

129. Fayard, B., et al., *The secreted brain-derived neurotrophic factor precursor pro-BDNF binds to TrkB and p75NTR but not to TrkA or TrkC.* J Neurosci Res, 2005. **80**(1): p. 18-28.

130. Boyd, J.G. and T. Gordon, *The neurotrophin receptors, trkB and p75, differentially regulate motor axonal regeneration.* J Neurobiol, 2001. **49**(4): p. 314-25.

131. York, R.D., et al., *Rap1 mediates sustained MAP kinase activation induced by nerve growth factor.* Nature, 1998. **392**(6676): p. 622-6.

132. Howe, C.L., et al., *NGF signaling from clathrin-coated vesicles: evidence that signaling endosomes serve as a platform for the Ras-MAPK pathway.* Neuron, 2001. **32**(5): p. 801-14.

133. Burke, P., K. Schooler, and H.S. Wiley, *Regulation of epidermal growth factor receptor signaling by endocytosis and intracellular trafficking.* Mol Biol Cell, 2001. **12**(6): p. 1897-910.

134. Taub, N., et al., *Late endosomal traffic of the epidermal growth factor receptor ensures spatial and temporal fidelity of mitogen-activated protein kinase signaling.* Mol Biol Cell, 2007. **18**(12): p. 4698-710.

135. Sorkin, A., et al., *Recycling of epidermal growth factor-receptor complexes in A431 cells: identification of dual pathways.* J Cell Biol, 1991. **112**(1): p. 55-63.

136. Carpenter, G. and S. Cohen, *Epidermal growth factor.* Annu Rev Biochem, 1979. **48**: p. 193-216.

137. Madshus, I.H. and E. Stang, *Internalization and intracellular sorting of the EGF receptor: a model for understanding the mechanisms of receptor trafficking.* J Cell Sci, 2009. **122**(Pt 19): p. 3433-9.

138. Cohen, S., G. Carpenter, and L. King, Jr., *Epidermal growth factor-receptor-protein kinase interactions. Co-purification of receptor and epidermal growth factor-enhanced phosphorylation activity.* J Biol Chem, 1980. **255**(10): p. 4834-42.

139. Avraham, R. and Y. Yarden, *Feedback regulation of EGFR signalling: decision making by early and delayed loops.* Nat Rev Mol Cell Biol, 2011. **12**(2): p. 104-17.

140. Schuster, N., N. Dunker, and K. Krieglstein, *Transforming growth factor-beta induced cell death in the developing chick retina is mediated via activation of c-jun N-terminal kinase and downregulation of the anti-apoptotic protein Bcl-X(L).* Neuroscience letters, 2002. **330**(3): p. 239-42.

141. Nguyen, T.T., et al., *Co-regulation of the mitogen-activated protein kinase, extracellular signal-regulated kinase 1, and the 90-kDa ribosomal S6 kinase in PC12 cells. Distinct effects of the neurotrophic factor, nerve growth factor, and the mitogenic factor, epidermal growth factor.* J Biol Chem, 1993. **268**(13): p. 9803-10.

142. Huang, E.J. and L.F. Reichardt, *Trk receptors: roles in neuronal signal transduction.* Annu Rev Biochem, 2003. **72**: p. 609-42.

143. Tanaka, S., et al., *Both the SH2 and SH3 domains of human CRK protein are required for neuronal differentiation of PC12 cells.* Mol Cell Biol, 1993. **13**(7): p. 4409-15.

144. Hirata, T., et al., *Amplification, up-regulation and over-expression of C3G (CRK SH3 domain-binding guanine nucleotide-releasing factor) in non-small cell lung cancers.* J Hum Genet, 2004. **49**(6): p. 290-5.

145. Thiele, C.J., Z. Li, and A.E. McKee, *On Trk--the TrkB signal transduction pathway is an increasingly important target in cancer biology.* Clin Cancer Res, 2009. **15**(19): p. 5962-7.

146. Shaw, P.E., H. Schroter, and A. Nordheim, *The ability of a ternary complex to form over the serum response element correlates with serum inducibility of the human c-fos promoter.* Cell, 1989. **56**(4): p. 563-72.

147. Treisman, R., *The serum response element.* Trends Biochem Sci, 1992. **17**(10): p. 423-6.

148. Treisman, R., *Identification and purification of a polypeptide that binds to the c-fos serum response element.* EMBO J, 1987. **6**(9): p. 2711-7.

149. Schroter, H., et al., *Synergism in ternary complex formation between the dimeric glycoprotein p67SRF, polypeptide p62TCF and the c-fos serum response element.* EMBO J, 1990. **9**(4): p. 1123-30.

150. Treisman, R., *Ternary complex factors: growth factor regulated transcriptional activators.* Curr Opin Genet Dev, 1994. **4**(1): p. 96-101.

151. Karim, F.D., et al., *The ETS-domain: a new DNA-binding motif that recognizes a purine-rich core DNA sequence.* Genes Dev, 1990. **4**(9): p. 1451-3.

152. Halazonetis, T.D., et al., *c-Jun dimerizes with itself and with c-Fos, forming complexes of different DNA binding affinities.* Cell, 1988. **55**(5): p. 917-24.

153. Monje, P., M.J. Marinissen, and J.S. Gutkind, *Phosphorylation of the carboxyl-terminal transactivation domain of c-Fos by extracellular signal-regulated kinase mediates the transcriptional activation of AP-1 and cellular transformation induced by platelet-derived growth factor.* Mol Cell Biol, 2003. **23**(19): p. 7030-43.

154. Murphy, L.O., et al., *Molecular interpretation of ERK signal duration by immediate early gene products.* Nat Cell Biol, 2002. **4**(8): p. 556-64.

155. Vouret-Craviari, V., et al., *Differential activation of p44mapk (ERK1) by alpha-thrombin and thrombin-receptor peptide agonist.* J Biochem, 1993. **289 (Pt 1)**: p. 209-14.

156. Ji, Y., et al., *Acute and gradual increases in BDNF concentration elicit distinct signaling and functions in neurons.* Nat Neurosci, 2010. **13**(3): p. 302-9.

157. Noordman, Y.E., P.A. Jansen, and W.J. Hendriks, *Tyrosine-specific MAPK phosphatases and the control of ERK signaling in PC12 cells.* J Mol Signal, 2006. **1**: p. 4.

158. Kermorgant, S. and P.J. Parker, *Receptor trafficking controls weak signal delivery: a strategy used by c-Met for STAT3 nuclear accumulation.* J Cell Biol, 2008. **182**(5): p. 855-63.

159. Dhanasekeran, D.N., et al. *Scaffold proteins of MAP-kinase modules*. Oncogene, 2007. **26**: p. 3185-3202.

160. Teis, D., Wunderlich, W., and Huber, L.A., *Localisation of the MP1-MAPK scaffold complex to endosomes is mediated by p14 and required for signal transduction.* Dev Cell, 2002. **3**: p. 803-814.

161. Hanafusa, H., et al., *Sprouty1 and sprouty2 provide a control mechanism for the Ras/MAPK signalling pathway.* Nat Cell Biol, 2002. **11**: p. 850-858.

162. Farooq, A., *Structure and regulation of MAPK phosphatases.* Cell Signal, 2004. **16**(7): p. 769-779.

163. Muda, M., et al., *The dual specificity phosphatases M3/6 and MKP-3 are highly selective for inactivation of distinct mitogen-activated protein kinases.* J Biol Chem, 1996. **271**(44): p. 27205-8.

164. Cai, Z., et al., *hnulp1, a basic helix-loop-helix protein with a novel transcriptional repressive domain, inhibits transcriptional activity of serum response factor.* Biochem and Biophys Res Commun, 2006. **343**(3): p. 973-81.

165. Olsson, M., et al., *Nulp1, a novel basic helix-loop-helix protein expressed broadly during early embryonic organogenesis and prominently in developing dorsal root ganglia.* Cell Tissue Res, 2002. **308**(3): p. 361-70.

166. Tsukada, M. and Y. Ohsumi, *Isolation and characterization of autophagy-defective mutants of Saccharomyces cerevisiae.* FEBS letters, 1993. **333**(1-2): p. 169-74.

167. Klionsky, D.J., et al., *A unified nomenclature for yeast autophagy-related genes.* Developmental cell, 2003. **5**(4): p. 539-45.

168. Noda, T. and Y. Ohsumi, *Tor, a phosphatidylinositol kinase homologue, controls autophagy in yeast.* J Biol Chem, 1998. **273**(7): p. 3963-6.

169. Cook, S. J., Morley, S.J., *Nutrient-responsive mTOR signalling grows on sterile ground.* Biochem J, 2007. **403**: p. e1-e3.

170. Jung, C.H., et al., *mTOR regulation of autophagy.* FEBS letters, 2010. **584**(7): p. 1287-95.

171. Findlay, G.M., et al. *A MAP4 kinase related to Ste20 is a nutrient-sensitive regulator of mTOR signalling.* Biochem J, 2007. **403**: p. 13-20.

172. Scott, R.C., O. Schuldiner, and T.P. Neufeld, *Role and regulation of starvation-induced autophagy in the Drosophila fat body.* Dev Cell, 2004. **7**(2): p. 167-78.

173. Fox, H.L., et al., *Amino acids stimulate phosphorylation of p70S6k and organization of rat adipocytes into multicellular clusters.* Am J Physiol, 1998. **274**(1 Pt 1): p. C206-13.

174. Chang, Y.Y., et al., *Nutrient-dependent regulation of autophagy through the target of rapamycin pathway.* Bioch Soc Trans, 2009. **37**(Pt 1): p. 232-6.

175. Sridharan, S., et al., *Regulation of autophagy by kinases.* Cancers, 2011. **3**: p. 2630-2654

176. Byfield, M.P., J.T. Murray, and J.M. Backer, *hVps34 is a nutrient-regulated lipid kinase required for activation of p70 S6 kinase.* J Biol Chem, 2005. **280**(38): p. 33076-82.

177. Jung, C.H., et al., *ULK-Atg13-FIP200 complexes mediate mTOR signaling to the autophagy machinery.* Mol Biol Cell, 2009. **20**(7): p. 1992-2003.

178. Mammucari, C., et al., *FoxO3 Controls Autophagy in Skeletal Muscle in Vivo.* Cell, 2007. **6**:p. 458-471.

179. Derijard, B., et al., *Independent human MAP-kinase signal transduction pathways defined by MEK and MKK isoforms.* Science, 1995. **267**(5198): p. 682-5.

180. Russell, M., C.A. Lange-Carter, and G.L. Johnson, *Direct interaction between Ras and the kinase domain of mitogen-activated protein kinase kinase kinase (MEKK1).* J Biol Chem, 1995. **270**(20): p. 11757-60.

181. Pattingre, S., et al., *Bcl-2 antiapoptotic proteins inhibit Beclin 1-dependent autophagy.* Cell, 2005. **122**(6): p. 927-39.

182. Wei, Y., et al., *Dual Role of JNK-mediated Phosphorylation of Bcl-2 in Autophagy and Apoptosis regulation.* Autophagy, 2008. **4**(7): 949-951.

183. Biswas, S.C., et al., *Pro-apoptotic Bim induction in response to nerve growth factor deprivation requires simultaneous activation of three different death signaling pathways.* J Biol Chem, 2007. **282**(40): p. 29368-74.

184. Xu, P., et al., *JNK regulates FoxO-dependent autophagy in neurons.* Genes Dev, 2011. **25**(4): p. 310-22.

185. Lei, K. and R.J. Davis, *JNK phosphorylation of Bim-related members of the Bcl2 family induces Bax-dependent apoptosis.* PNAS USA, 2003. **100**(5): p. 2432-7.

186. Tsai, M.S., et al., *Abolishing Bax-dependent apoptosis shows beneficial effects on spinal muscular atrophy model mice.* ASGT J, 2006. **13**(6): p. 1149-55.

187. Colotta, F., et al., *Expression and involvement of c-fos and c-jun protooncogenes in programmed cell death induced by growth factor deprivation in lymphoid cell lines.* J Biol Chem, 1992. **267**(26): p. 18278-83.

188. Banerjee, R., M.F. Beal, and B. Thomas, *Autophagy in neurodegenerative disorders: pathogenic roles and therapeutic implications.* Trends Neurosci, 2010. **33**(12): p. 541-9.

189. Yu, W.H., et al., *Macroautophagy--a novel Beta-amyloid peptide-generating pathway activated in Alzheimer's disease.* J Cell Biol, 2005. **171**(1): p. 87-98.

190. Caccamo, A., et al., *Rapamycin rescues TDP-43 mislocalization and the associated low molecular mass neurofilament instability.* J Biol Chem, 2009. **284**(40): p. 27416-24.

191. Kabuta, T., Y. Suzuki, and K. Wada, *Degradation of amyotrophic lateral sclerosis-linked mutant Cu,Zn-superoxide dismutase proteins by macroautophagy and the proteasome.* J Biol Chem, 2006. **281**(41): p. 30524-33.

192. Li, L., X. Zhang, and W. Le, *Altered macroautophagy in the spinal cord of SOD1 mutant mice.* Autophagy, 2008. **4**(3): p. 290-3.

193. Maday, S., K.E. Wallace, and E.L. Holzbaur, *Autophagosomes initiate distally and mature during transport toward the cell soma in primary neurons.* J Cell Biol, 2012. **196**(4): p. 407-17.

194. Kimura, S., T. Noda, and T. Yoshimori, *Dynein-dependent movement of autophagosomes mediates efficient encounters with lysosomes.* Cell Struct Funct, 2008. **33**(1): p. 109-22.

195. Batlevi, Y., et al., *Dynein light chain 1 is required for autophagy, protein clearance, and cell death in Drosophila.* PNAS USA, 2010. **107**(2): p. 742-7.

196. Ravikumar, B., et al., *Dynein mutations impair autophagic clearance of aggregate-prone proteins.* Nat Genet, 2005. **37**(7): p. 771-6.

197. Lidke, D.S., et al., *ERK nuclear translocation is dimerization-independent but controlled by the rate of phosphorylation.* J Biol Chem, 2010. **285**(5): p. 3092-102.

198. Cagnol, S. and J.C. Chambard, *ERK and cell death: mechanisms of ERK-induced cell death--apoptosis, autophagy and senescence.* FEBS J, 2010. **277**(1): p. 2-21.

199. Gennerich, A. and Vale, R, D., *Walking the walk: how kinesin and dynein coordinate their steps*. Curr Opin Cell Biol, 2009. **21**(1): p. 59-67.

200. Gennerich, A., et al., *Force-induced bidirectional stepping of cytoplasmic dynein.* Cell, 2007. **131**(5): p. 952-965.

201. Flores-Rodriguez, N., et al., *Roles of dynein and dynactin in early endosome dynamics revealed using automated tracking and global analysis.* PLoS, 2011. **6**(9): p. e24479.

202. Steen, H. and D. Lindholm, *Nuclear localized protein-1 (Nulp1) increases cell death of human osteosarcoma cells and binds the X-linked inhibitor of apoptosis protein.* Biochem Biophys Res Comm, 2008. **366**(2): p. 432-7.

203. Cavigelli, M., et al., *Induction of c-fos expression through JNK-mediated TCF/Elk-1 phosphorylation.* EMBO J, 1995. **14**(23): p. 5957-64.

204. Wozniak, M.J. and V.J. Allan, *Cargo selection by specific kinesin light chain 1 isoforms.* EMBO J, 2006. **25**(23): p. 5457-68

205. Ligon, L.A., et al., *A direct interaction between cytoplasmic dynein and kinesin I may coordinate motor activity.* J Biol Chem, 2004. **279**(18): p. 19201-8.